Mohsen M. Baligh
Amr S. Azzouz
Robert T. Martin

Cone Penetration Tests Offshore the Venezuelan Coast

MIT Sea Grant College Program

Massachusetts Institute of Technology
Cambridge, Massachusetts 02139

MITSG 80-21
December 1980

CONE PENETRATION TESTS

OFFSHORE THE VENEZUELAN COAST

by

Mohsen M. Baligh

Amr S. Azzouz

Robert T. Martin

Sea Grant College Program
Massachusetts Institute of Technology
Cambridge, Massachusetts 02139

Report No. MITSG 80-21
Index No. 80-321-Cim

ABSTRACT

In situ tests have recently attracted considerable increased interest among the geotechnical profession as a means of complementing laboratory tests in offshore soil exploration.

This report describes in situ measurements in marine sediments offshore the Venezuelan coast obtained by means of the FUGRO electrical cone penetrometer capable of measuring the cone penetration resistance, q_c, and the relatively new conical piezometer probes which measure the pore pressures, u. Continuous measurements of q_c and u are particularly attractive in offshore exploration because of their efficiency and reliability, capability in identifying soil conditions for proposed structures and detecting small changes in stratification, and similarity with pile foundations, especially regarding the strain (or stress) path they cause in the soil.

Cone penetration results are correlated to soil properties obtained from laboratory tests using existing theoretical and empirical procedures.

FOREWORD

A three-year research program entitled, "In Situ Evaluation of Geotechnical Properties of Marine Sediments," sponsored primarily by the National Oceanic and Atmospheric Administration through its MIT Sea Grant Program, was initiated in July, 1978 by the Constructed Facilities Division of MIT. Matching funds for this research were provided by FUGRO, Inc., Consulting Engineers, and by Instituto Tecnologico Venezolano del Petroleo. The final objective of the program was to improve the present capabilities of the geotechnical profession in the area of offshore site investigation through evaluating existing in situ tests and, whenever possible, to develop new more reliable methods and devices to determine the necessary soil parameters for foundation design.

The electric (Dutch) cone penetrometer and the conical piezometer probe represent a new generation of in situ testing devices which are particularly valuable offshore because of their simplicity, consistency, and economy. However, for applications in medium to soft clays they lack a solid evaluated experience by the profession and a well defined common basis for analysis, especially in the U.S. Hence, this research concentrated on:

1. Performing Dutch cone and pore pressure probe tests on several representative onshore and offshore soil types for which there already exist extensive information about their in situ undrained stress-strain-strength behavior;

2. Developing improved theoretical models for interpreting the results of the measured cone penetration and pore pressure data and preparing guidelines for using cone penetrometers to estimate in situ properties for foundation design.

This report is one of a series of MIT reports published as a result of this research program. It presents cone penetration measurements performed offshore the Venezuelan coast and uses developed theoretical and empirical procedures to correlate these cone penetration data to soil properties from laboratory tests. Other reports and unpublished theses related to this project are listed below.

RELATED REPORTS

Levadoux, J.N. and M.M. Baligh. PORE PRESSURES DURING CONE PENETRATION IN CLAYS. MITSG 80-12. 310 pp. $8.00.

Baligh, M.M. and J.N. Levadoux. PORE PRESSURE DISSIPATION AFTER CONE PENETRATION. MITSG 80-13. 368 pp. $8.00.

Baligh, M.M., V. Vivatrat, and C.C. Ladd. EXPLORATION AND EVALUATION OF ENGINEERING PROPERTIES FOR FOUNDATION DESIGN OF OFFSHORE STRUCTURES. MITSG 79-8. 268 pp. $8.00.

MIT/Marine Industry Collegium. TOWARDS IMPROVED TECHNIQUES FOR PREDICTING SOIL STRENGTH: OPPORTUNITY BRIEF #16. MITSG 79-17. 19 pp. $3.50.

Levadoux, J.N. "Pore Pressures due to Cone Penetration." Thesis, Department of Civil Engineering, Massachusetts Institute of Technology, 1980.

Kevvadas, M. "Stress-Strain Models for Soils Based on Plasticity Theory." Thesis, Department of Civil Engineering, Massachusetts Institute of Technology, 1980.

Vivatrat, V. "Cone Penetration in Clays." Thesis, Department of Civil Engineering, Massachusetts Institute of Technology, 1978.

The MIT Sea Grant Marine Resources Information Center maintains an inventory of technical publications. We invite orders and inquiries to:

Marine Resources Information Center
MIT Sea Grant College Program
Building E38-302
Massachusetts Institute of Technology
Cambridge, Massachusetts 02139
(617) 253-5944

ACKNOWLEDGMENTS

The authors are indebted to Jack Germaine, Instructor at MIT, for his invaluable help during the field work; Juan Rodriguez, Eli Schwartz, Instituto Tecnologico Venezolano Del Petroleo, and Hugo Perez for the planning and coordination of the project; Fugro Consulting Engineers for conducting the field work, providing cone resistance and routine laboratory test data; Professor Charles C. Ladd for sophisticated laboratory soil engineering data; Anwar Wissa, Geotechniques Int., for providing the pore pressure probes used in this study; and Mike Morrison, Research Assistant, for his critical review of the manuscript.

The field offshore work conducted in this study was funded by the Instituto Tecnologico Venezolano Del Petroleo (INTERVEP). The research program on the "In Situ Evaluation of Geotechnical Properties of Marine Sediments" at MIT is sponsored primarily by the National Oceanic and Atmospheric Administration through its MIT Sea Grant Program, grant number NA79AA-D-00101. Matching Funds are also provided by Fugro Consulting Engineers and INTERVEP.

TABLE OF CONTENTS

	PAGE
ABSTRACT	2
FOREWORD	3
ACKNOWLEDGMENTS	6
TABLE OF CONTENTS	7
LIST OF TABLES	9
LIST OF FIGURES	10
CHAPTER 1: INTRODUCTION	15
CHAPTER 2: BACKGROUND	18
2.1 TEST EQUIPMENT	18
2.1.1 The FUGRO Cone Penetrometers	18
2.1.2 The Conical Piezometer Probes	19
2.2 TYPICAL RESULTS IN ONSHORE DEPOSITS	20
2.2.1 Penetration Data	20
2.2.2 Dissipation Data	21
CHAPTER 3: INTERPRETATION OF CONE PENETRATION RESULTS IN CLAYS	30
3.1 THE COMPLICATED UNDRAINED BEHAVIOR OF SATURATED CLAYS	31
3.2 EXISTING SIMPLE SOLUTIONS	32
3.3 STRAIN-PATH SOLUTIONS	39
3.4 EMPIRICAL CORRELATIONS	44
3.4.1 Correlations between the FUGRO Cone Resistance and the Field Vane Strength	44
3.4.2 Penetration Pore Pressures	53

PAGE

CHAPTER 4: OFFSHORE CONE PENETRATION RESULTS 102

4.1 INTRODUCTION 102

4.2 SOIL STRATIFICATION 104

4.3 CORRELATIONS 112

4.3.1 General 112

4.3.2 General Correlations at Site E1 115

4.3.3 General Correlations at Site F1 117

4.3.4 Correlations in the Orinoco Clays 118

CHAPTER 5: CONCLUSIONS 148

REFERENCES 150

APPENDIX A: CONE PENETRATION DATA 157

LIST OF TABLES

TABLE		PAGE
3.1	Summary of existing theories of cone penetration in clays.	59
3.2	Tabulation of correlations between cone resistance and the field vane strengths at NGI-Fugro sites.	60
3.3	Tabulation of correlations between cone resistance and the field vane strengths at MIT test sites.	61
4.1	Soil layering data at site E1.	126
4.2	Unit weights, pore pressure, effective and total stresses.	127

LIST OF FIGURES

FIGURE		PAGE
2.1	The Fugro drillstring anchor and Wison cone jacking device for offshore work.	23
2.2	Diagram of the Fugro electrical cone with friction sleeve	24
2.3	Conical piezometer probes used at MIT (after Wissa et al., 1975; Baligh et al., 1978)	25
2.4	Typical pore pressure recorded at the tip of an 18° conical probe.	26
2.5	Cone penetration in soil profiling.	26
2.6	Cone resistance and pore pressure during penetration.	27
2.7	Cone penetration data in Atchafalaya clay, Louisiana.	28
2.8	Pore pressure dissipation at the tip of an 18° conical probe.	29
3.1a	Normalized stress strain relations from $\overline{CK_oU}$ tests on normally consolidated Boston Blue Clay.	62
3.1b	Normalized stress-strain relations from $\overline{CK_oU}$ tests on Boston Blue Clay (OCR = 4).	63
3.2	Assumed failure patterns for deep penetration.	64
3.3	Model for cone penetration mechanism according to Baligh (1975).	65
3.4	Sharp rough wedge resistance factors for steady penetration in anisotropic clays.	66
3.5	Comparison of stress path and strain path methods.	67
3.6.	Application of the strain path method to deep steady cone penetration: flow chart.	68
3.7	Predicted deformation pattern around a 60° cone.	69

FIGURE		PAGE
3.8	Strain paths of selected elements during penetration of a 60° cone.	70
3.9	Contours of octahedral shear strain, γ_{oct} .	71
3.10	Contours of octahedral shear strain rate, $\dot{\gamma}_{oct}$.	72
3.11	Predicted three-dimensional deviatoric stress path during steady penetration of a 60° cone in normally consolidated Boston Blue Clay.	73
3.12	Predicted deviatoric stress paths along two streamlines during steady penetration of a 60° cone in normally consolidated Boston Blue Clay.	74
3.13	Predicted contours of normalized octahedral shear stress, τ_{oct}, and extent of failure during steady cone penetration in normally consolidated Boston Blue Clay (18° and 60° tips).	75
3.14	Predicted contours of normalized excess pore pressure, Δu, during steady cone penetration in normally consolidated Boston Blue Clay (18° and 60° tips).	76
3.15	Predicted vs. measured longitudinal distributions of normalized excess pore pressures along 18° and 60° cones during steady penetration in Boston Blue Clay.	77
3.16	Comparison of predicted and measured cone resistances in Boston Blue Clay.	78
3.17	Predicted and measured point resistance in Boston Blue Clay (18° and 60° tips) at Station 246, Saugus, Massachusetts.	79
3.18	Empirical Cone Factor, $N_c(FV) = [q_c-\sigma_{vo}]/s_u(FV)$, at the Saugus, MA, test site.	80
3.19	Empirical cone factor, $N_c(FV) = [q_c-\sigma_{vo}]/s_u(FV)$, at EABPL, LA.	81
3.20	Empirical cone factor, $N_c(FV) = [q_c-\sigma_{vo}]/s_u(FV)$, at Amherst, MA.	82

FIGURE		PAGE
3.21	Average field vane strength profiles at MIT and NGI-Fugro test sites.	83
3.22	Empirical cone factor $N_c(FV)$ vs. depth for nine clay deposits.	84
3.23	Empirical cone factors $N_c(FV)$ and $N_c'(FV)$ for very soft to medium clays.	85
3.24	Empirical cone factor $N_c'(FV)$ vs. depth for nine clay deposits.	86
3.25	Empirical cone factors for stiff clays.	87
3.26	Pore pressures measured along an 18° unenlarged cone during steady penetration.	88
3.27	Pore pressures measured along an 18° enlarged cone during steady penetration.	89
3.28	Pore pressures measured along a 60° unenlarged cone during steady penetration.	90
3.29	Pore pressures measured along a 60° enlarged cone during steady penetration.	91
3.30	Cone resistance and pore pressures for an 18° unenlarged cone (2δ = 18°, D/d = 1) in Boston Blue Clay.	92
3.31	Cone resistance and pore pressures for a 60° unenlarged cone (2δ = 60°, D/d = 1) in Boston Blue Clay.	93
3.32	Penetration pore pressure to cone resistance in Boston Blue Clay.	94
3.33	Cone resistance and pore pressure for an 18° unenlarged cone (2δ = 18°, D/d = 1) in EABPL Clay.	95
3.34	Cone resistance and pore pressure for a 60° unenlarged cone (2δ = 60°, D/d = 1) in EABPL clay.	96
3.35	Penetration pore pressure to cone resistance ratio in EABPL clay.	97
3.36	Soil conditions at the Amherst, MA, test site.	98

FIGURE		PAGE
3.37	Cone resistance and pore pressure for an 18° unenlarged cone (2δ = 18°, D/d = 1) in Connecticut Valley Varved Clay.	99
3.38	Cone resistance and pore pressure for a 60° unenlarged cone (2δ = 60°, D/d = 1) in Connecticut Valley Varved Clay.	100
3.39	Pore pressure to cone resistance ratios in Connecticut Valley Varved Clay.	101
4.1	Boring locations.	128
4.2	Soil profile and stratification data at site E1.	129
4.3	Cone resistance and pore pressure at site E1.	130
4.4	Soil profile and stratification data at site F1.	131
4.5	Pore pressure to cone resistance ratios at site E1.	132
4.6	$\Delta q_c/\bar{\sigma}_{vo}$ at site E1.	133
4.7	$(u-u_o)/\bar{\sigma}_{vo}$ at site E1.	134
4.8	$\Delta q_c/\bar{\sigma}_{vo}$ at site F1.	135
4.9	Plasticity chart: Orinoco clay.	136
4.10	Stress history: Orinoco clay.	137
4.11	Compressibility and coefficient of consolidation: Orinoco clay.	138
4.12	Normalized stress vs. strain from direct simple shear tests: N.C. Orinoco clay.	139
4.13	Undrained shear strength data at site E1.	140
4.14	Undrained shear strength data at site F1.	141
4.15	Effect of OCR on $s_u(DSS)/\bar{\sigma}_{vc}$: Orinoco clay.	142
4.16	Penetration pore pressure data at site E1.	143

		PAGE
4.17	Penetration pore pressure data at site F1.	144
4.18	$(u-u_o)/\bar{\sigma}_{vo}$ data: Orinoco clay.	145
4.19	$\Delta q_c/s_u$ data: Orinoco clay.	146
4.20	$(u-u_o)/s_u$ data: Orinoco clay.	147
A-1	Δq_c data for Site E1.	158
A-2	Δq_c data for Site F1.	159
A-3	Δq_c data for Site D1.	160
A-4	u data for Site E1.	161
A-5	u data for Site F1.	162
A-6	u data for Site D1.	163

CHAPTER 1

INTRODUCTION

The objectives of soil investigation at the site of a proposed structure are to estimate stratigraphy (i.e., the extent, thickness and location of different layers) and to determine the engineering properties of the layers pertinent to foundation design (strength, permeability, compressibility). The most common procedure used in soil exploration consists of making borings from which samples are recovered for the purposes of soil identification and subsequent laboratory testing. Laboratory tests generally provide well defined controllable boundary and drainage conditions, uniform stresses (or strains) within the sample, and hence, enable easy interpretation of test results. The major disadvantages of laboratory tests are the disturbance of soil samples (leading to properties different from the foundations soils) and the uncertainty in estimating the spatial variation of soil parameters from the very small volume of soil normally tested.

The behavior of offshore sediments follows the same fundamentals as onshore soils (effective stress principle, Darcy's law, ...etc.), but offshore geotechnical investigations pose special problems (Hedberg et al., 1978; Sullivan, 1978; Sangrey, 1977; de Ruiter, 1976; Dn V, 1976; Hoeg, 1976; and NGI, 1973).

Some of the problems are:

1. Hydrostatic stress relief. When retrieved to the surface, deep offshore samples are subjected to a hydrostatic stress

relief that can exceed 20 times the values normally encountered onshore. This, together with the practical difficulties of deep sampling, cause severe disturbance of the soil structure (Sangrey, 1977).

2. Stability during sampling. Geotechnical drilling in deep waters is usually performed from floating vessels. The movement of these vessels during drilling and sampling produces lower quality samples.

3. The cost of field offshore work is roughly 10 to 15 times higher than onshore sites. This restricts offshore geotechnical research, limits the scope of typical exploration programs and prohibits comprehensive correlations between various offshore measurements.

In situ tests have recently attracted considerable increased interest among the geotechnical profession as a means of complementing laboratory tests in soil exploration. In situ tests avoid disturbances caused by the stress relief associated with retrieving samples to the surface and can provide a more detailed description of the vertical variation of soil properties. However, in situ tests generally have complicated boundary conditions, involve significant stress (and strain) variations within the soil, and uncontrollable drainage conditions; interpretation is more difficult and requires varying degrees of empiricism in estimating soil parameters for design purposes. Undesirable soil disturbances seriously affect test results in some in situ tests and require as much scrutiny as sampling disturbances (e.g., in the pressuremeter test).

New challenges in offshore work stimulated research in re-evaluating existing in situ tests and developing more reliable techniques and devices. Leading offshore in situ tests are:

1. The field (remote) vane shear test routinely used in the Gulf of Mexico (Doyle et al., 1971 and Kraft et al., 1976) and is applicable to soft to stiff clays only.

2. Cone penetrometers extensively used in the North Sea (Zuidberg, 1974).

This report describes in situ measurements in marine sediments offshore the Venezuelan coast obtained by means of the Fugro electrical cone penetrometer which is capable of providing the cone penetration resistance, q_c, and the relatively new conical piezometer probes (Wissa et al., 1975) which are capable of measuring the pore pressures, u. Measurements of q_c and u during cone penetration are particularly attractive in offshore exploration because of: 1) efficiency, reliability and other capabilities discussed later; 2) applicability in a variety of soils ranging from sands to soft clays; and, 3) similarity with pile foundations, especially regarding the strain (or stress) path they cause in the soil.

Finally, cone penetration results are correlated to soil properties obtained from laboratory tests using existing theoretical and empirical procedures.

CHAPTER 2

BACKGROUND

2.1 TEST EQUIPMENT

Offshore drilling for this research was conducted from the North-Sea vessel M/S SURVEYOR operated by the Heerema Marine Contractors under the supervision of FUGRO personnel acting as the geotechnical consultants. Offshore cone penetrometer equipment including the drillstring anchor, the "Wison" downhole hydraulic jack and related devices, (Fig. 2.1), the Fugro electrical cone to measure the cone resistance, q_c, and recording equipment were owned and operated by FUGRO Consulting Engineers. The conical piezometer probes were manufactured by Geotechniques, Int. to be compatible with FUGRO jacking devices and were operated by MIT using FUGRO offshore equipment (jacks, recorders, ... etc).

2.1.1 The FUGRO Cone Penetrometers. Offshore measurements of cone resistance, q_c, (representing the force per unit area required to push the cone tip) presented subsequently were conducted by means of the well-known FUGRO electrical cone (de Ruiter, 1971, Fig. 2.2) and supporting equipment (signal recorder and pushing devices). The cone has a 60° apex angle, a $10cm^2$ base area and is pushed at a rate of 2cm/sec. Continuous q_c measurements are taken by a strain-gauge load cell located behind the tip and recorded on a strip chart onship. Measurements of the sleeve friction, f_s, are routinely obtained, but f_s readings were disregarded

in this study.

2.1.2 The Conical Piezometer Probes. The piezometer probe was developed by Wissa et al., (1975)* to measure pore water pressures. The probe basically consists of a fine porous element located on a conical tip connected hydraulically to an electro-mechanical pressure transducer which transmits the signal to the recording equipment at the surface. In the original design, the porous stone was located at the tip of an 18° cone as described by Wissa et al., (1975). Subsequent designs enabled measurements of pore pressures at different locations on the cone and the shaft behind it to be obtained, Fig. 2.3 (Baligh et al., 1978). Compared to existing piezometers, these probes have a much shorter response time (essentially instantaneous) and hence provide wider capabilities. In addition to cone penetration measurements (described below), these probes have been successfully used in establishing the flow pattern and detecting problem areas in dams, determining wave effects on pore pressures in offshore soil deposits (Wissa et al., 1975), for measuring pore pressures in the foundation soils under a runway due to plane traffic and in monitoring consolidation of industrial wastes (MIT).

Offshore pore pressure measurements described subsequently represent the first attempt to measure pore pressures during cone penetration in deep offshore sediments. These measurements

* A similar device was also developed by Torstensson (1975), but was not tested by MIT.

were performed by means of a special 60° cone where pore pressures are measured at the tip, Fig. 2.3.

2.2 TYPICAL RESULTS IN ONSHORE DEPOSITS

Figure 2.4 shows a typical record of pore pressure measurements at the tip of an 18° conical probe in a deposit of Boston Blue Clay (BBC) at Saugus, Mass. When steady penetration starts at a depth of 43.5 ft (say), the pore pressure increases rapidly and reaches the so-called penetration value, u, in less than 3 inches. Steady penetration at a rate of about 2cm/sec continues to a depth of 47 ft (indicated by the arrow), when another push rod (1m long) is required. The installation of the rod takes 45 sec and the pore pressure during this time decreases due to soil consolidation. Penetration is then resumed and the process repeated. Note the unmistakable sudden decrease in u at depths 47.2, 49.3 and 58.6 ft which suggests the presence of dense sandy layers. Cone resistance measurements, q_c, show a significant increase in q_c at these locations.

2.2.1 Penetration Data. Figure 2.5 shows the cone resistance, q_c and the penetration pore pressure, u, (after eliminating the decay that takes place during push-rod installation) obtained from two separate tests 45 ft apart in a deposit consisting of peat, sand and heavily desiccated clay which contains sandy lenses. Individually, q_c and u records detect major changes in soil strata, but jointly, they have an excellent potential for soil identification as well. For example, in the peat, q_c is low and u is high, whereas in the relatively

clean sand, q_c is high and u is very close to the hydrostatic values, u_o. Small excess pore pressures during penetration $(u - u_o)$ were also measured by Schmertmann (1978a) when he attempted to assess the liquifaction potential of sands by means of similar probes.

Figures 2.6 and 2.7 show penetration data consisting of the cone resistance, q_c, and penetration pore pressures, u, in two clay deposits. The first, Fig. 2.6, consists of a lean medium to stiff deposit of the marine illitic Boston Blue Clay (BBC) having a medium sensitivity. The second, Fig. 2.7, consists of a plastic, soft to medium deposit of the East Atchafalaya Basin Protection Levee (EABPL) clay having a low sensitivity. Clearly, both q_c and u are very consistent and repeatable. Furthermore, due to the continuous nature of penetration data, results can: 1) Detect the presence of thin soft and hard layers which might affect stability and drainage; 2) distinguish between strata even in difficult cases of consecutive layers having slightly different properties; and 3) provide a good measure of soil variability (scatter) affecting design reliability. For further information on the use of cone penetration data in soil profiling, the reader is referred to Baligh et al., 1980.

2.2.2 Dissipation Data. Figure 2.8 shows the pore pressure u(t) at the tip of an 18° probe after a time t when penetration stopped at four elevations in the BBC deposits described in Fig. 2.6. u(t) decays from the penetration value, u, to the

hydrostatic value, u_o, at different rates depending on the coefficient of consolidation, c, of the clay. Results in Fig. 2.8 obtained at depths 37, 57 and 96.5 ft indicate slower dissipation rates (lower c) with depth. On the other hand, results at a depth of 27 ft illustrate one of the many problems encountered in interpretating dissipation results. u(t) remains constant (and in a few cases increases slightly) for a short period (17 sec in Fig. 2.8) after cone penetration stops. This is believed to result from inherent soil variability causing the initial pore pressures in the soil at t = 0 to have an inconsistent non-uniform distribution (see u in Fig. 2.6).

Baligh and Levadoux (1980) present a consolidation theory for interpreting pore pressure dissipation records in order to estimate the consolidation and permeability characteristics of soils. Unfortunately, dissipation rates in the Venezuelan offshore clays described subsequently were so slow, that the necessary waiting time to achieve meaningful degrees of dissipation was too long. Therefore, no dissipation analyses could be performed in the offshore Venezuelan clays.

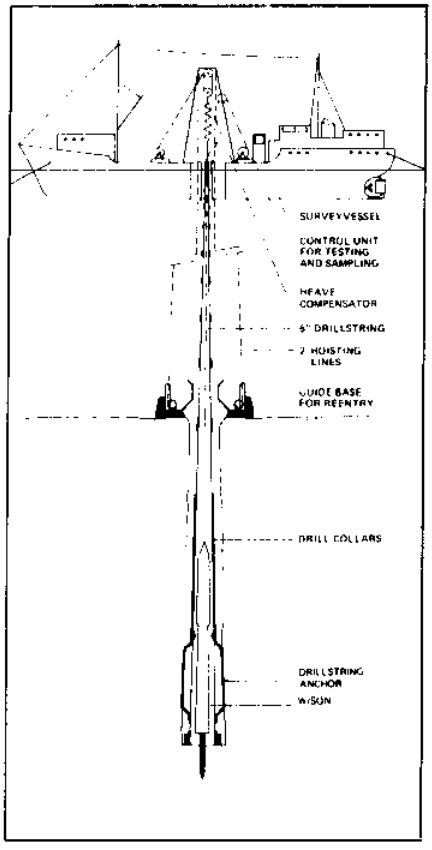

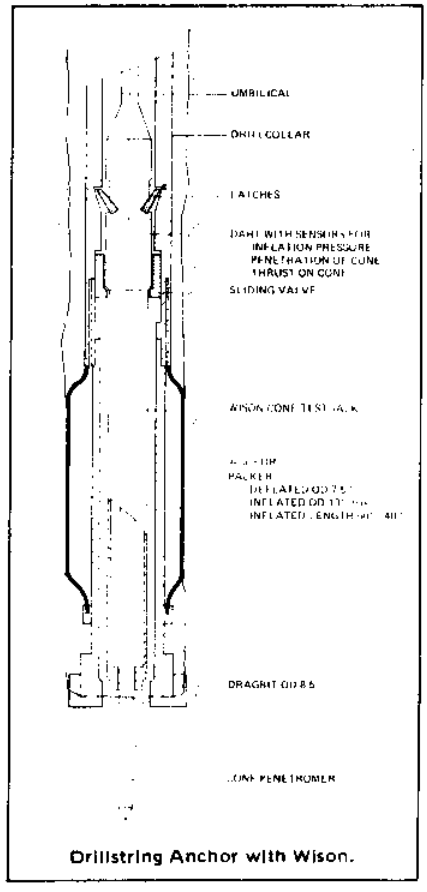

Figure 2.1 The Fugro drill string anchor and Wison cone jacking device for offshore work.

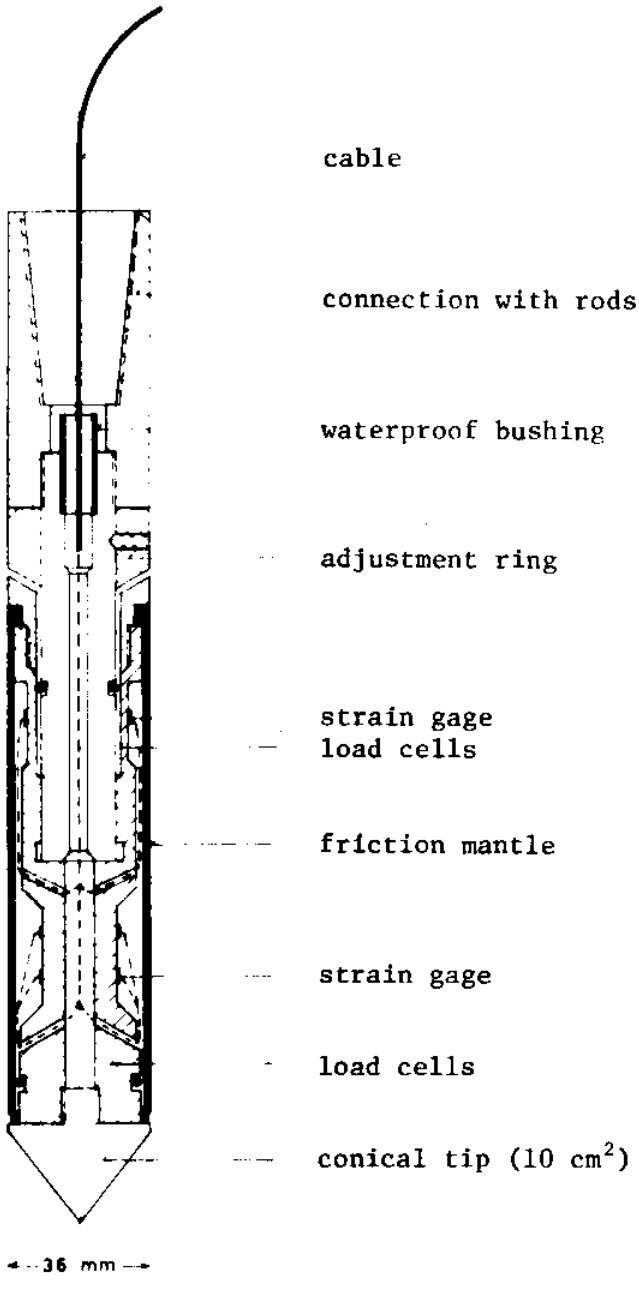

Figure 2.2 Diagram of the Fugro electrical cone with friction sleeve (from Sanglerat (1972)).

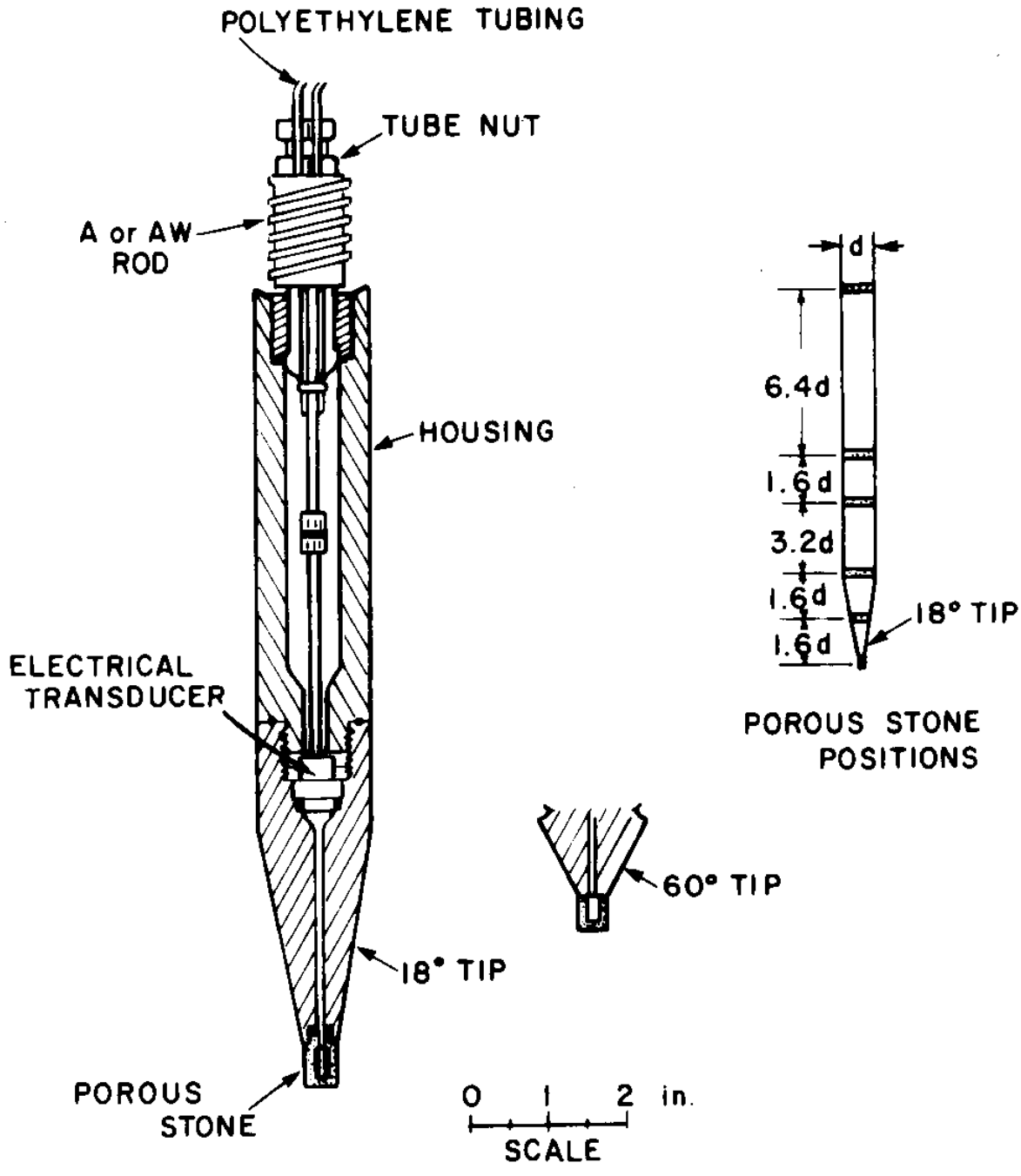

Figure 2.3 Conical piezometer probes used at MIT (after Wissa et al., 1975; Baligh et al., 1978).

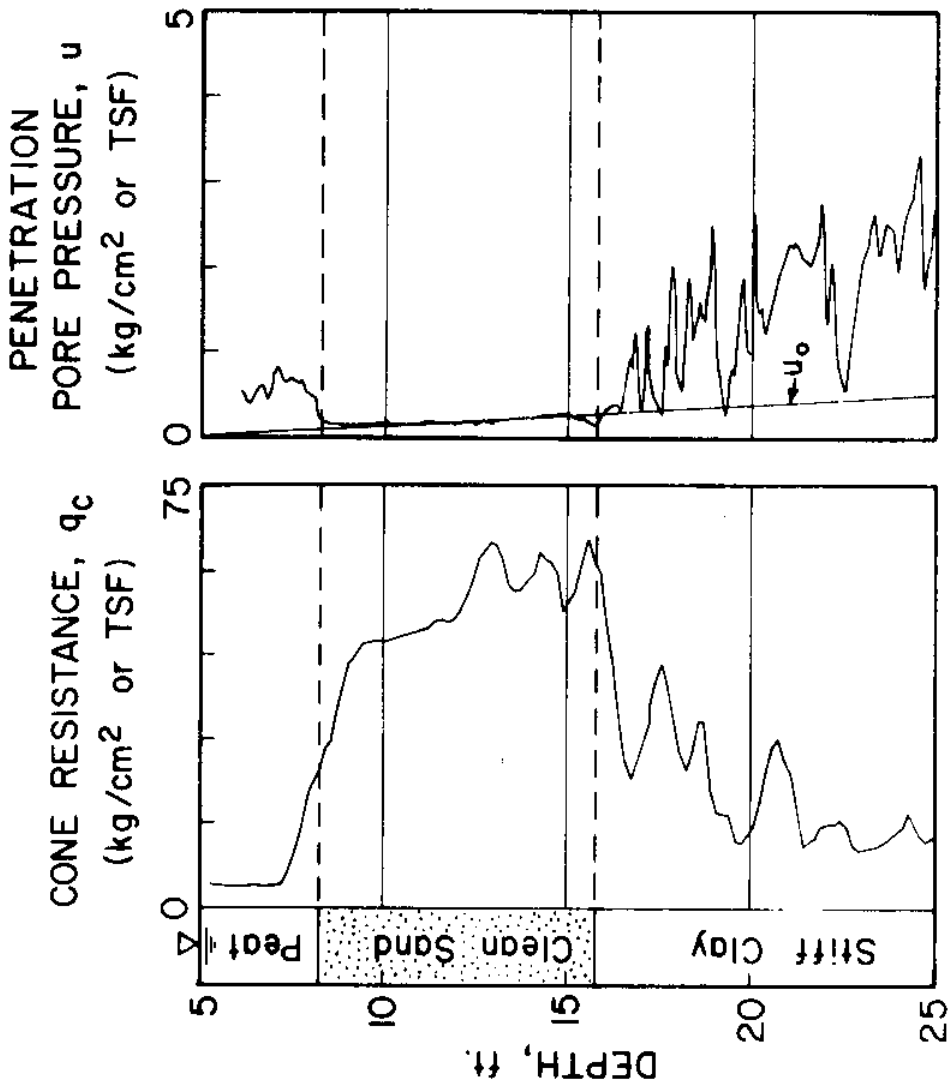

Figure 2.5 Cone penetration in soil profiling.

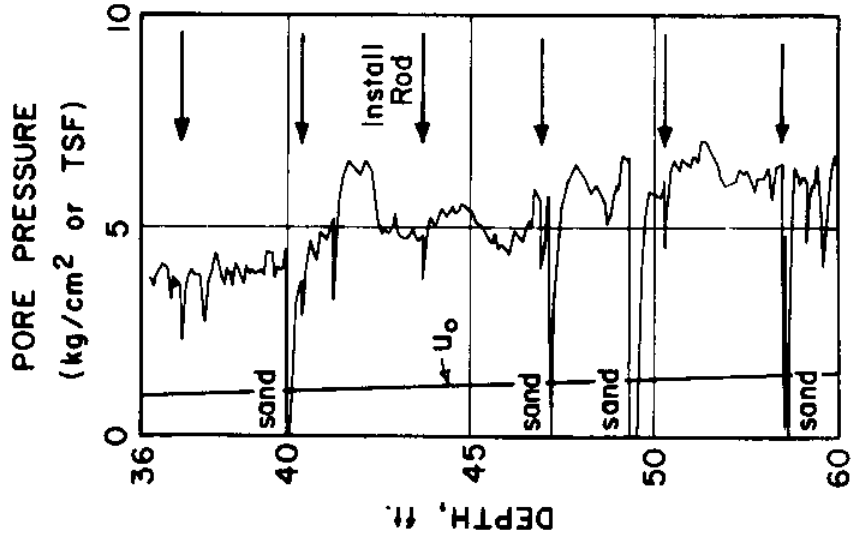

Figure 2.4 Typical pore pressure recorded at the tip of an 18° conical probe.

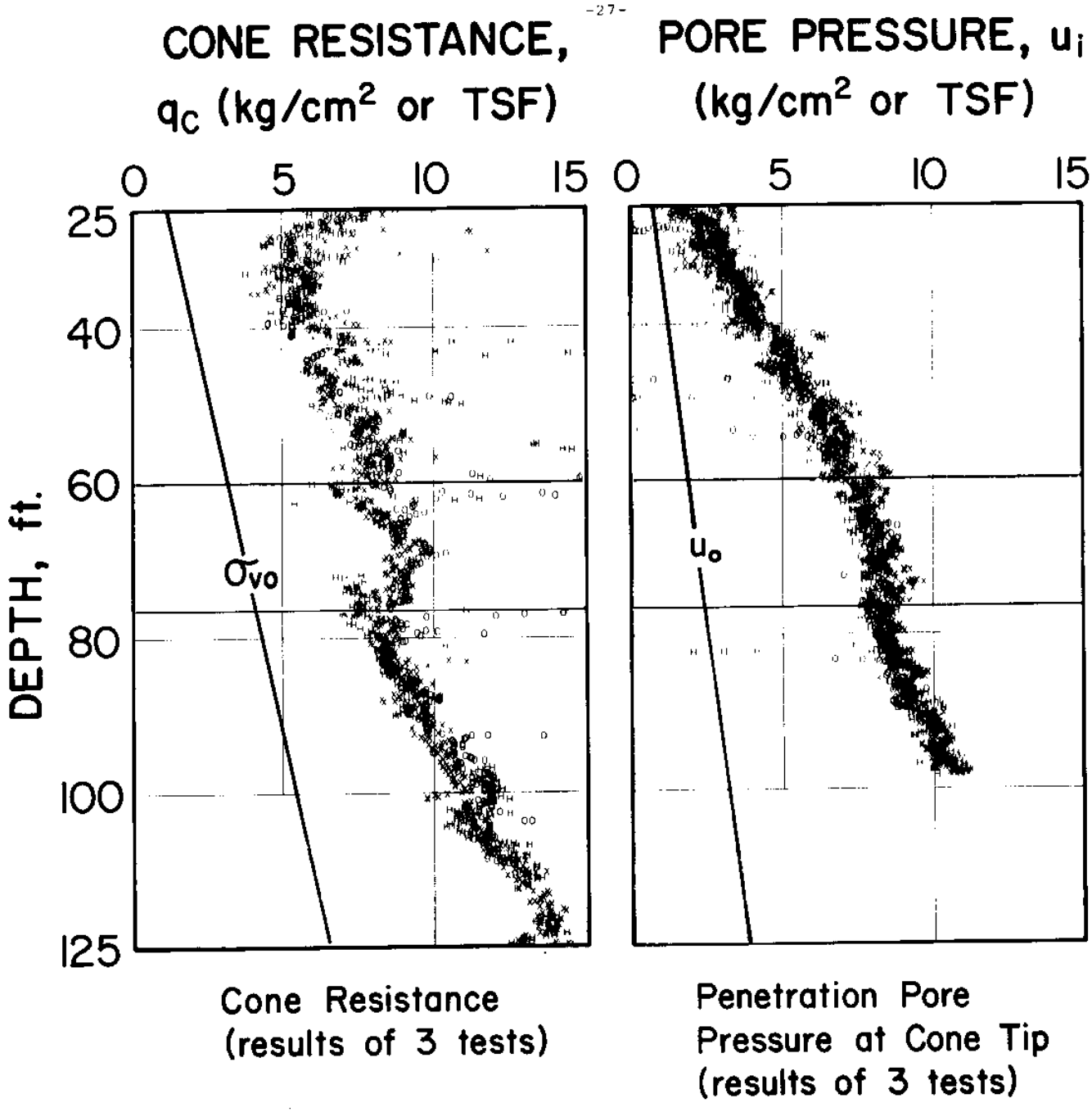

Figure 2.6 Cone resistance and pore pressure during penetration.

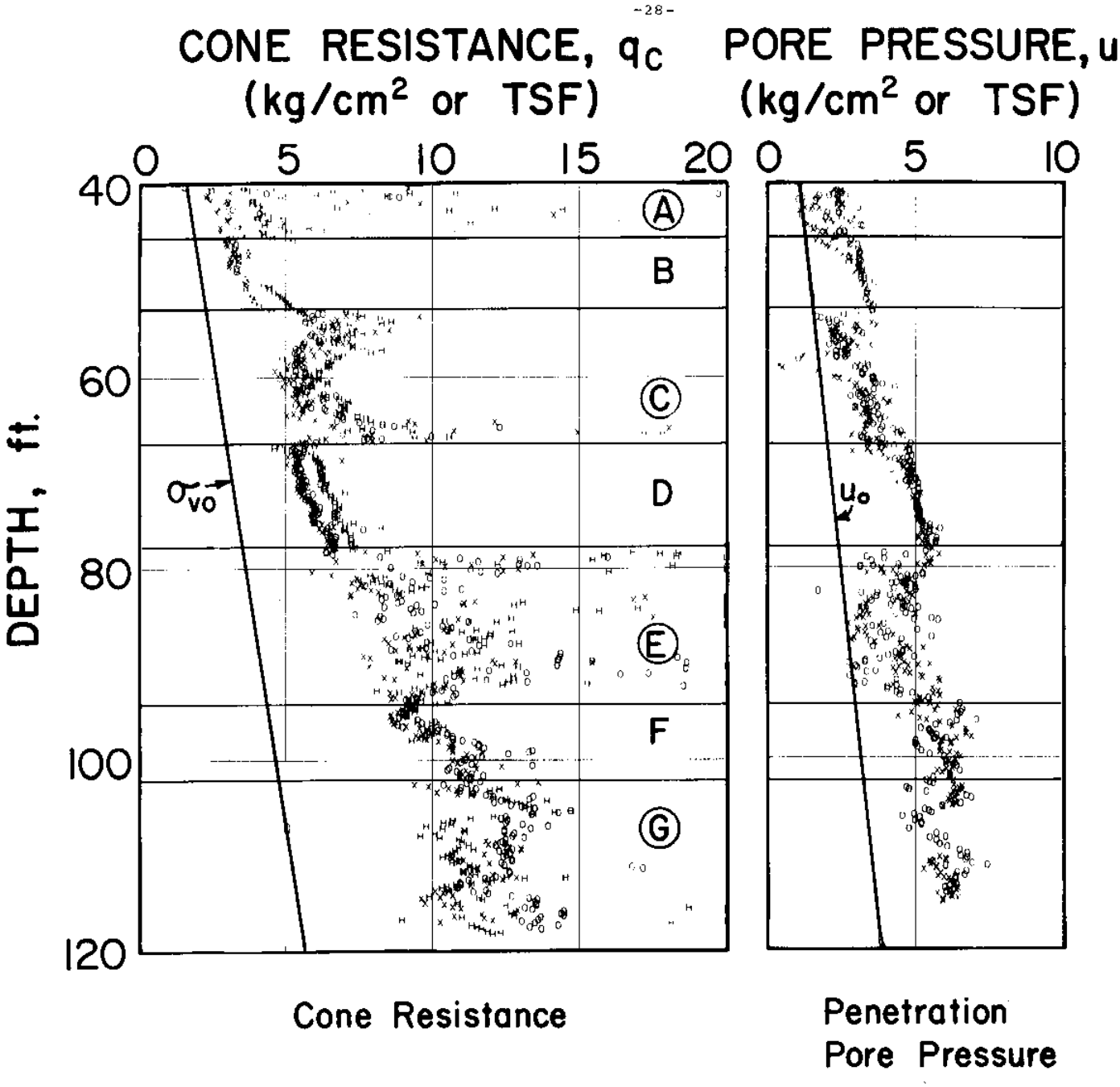

Figure 2.7 Cone penetration data in Atchafalaya clay, Louisiana.

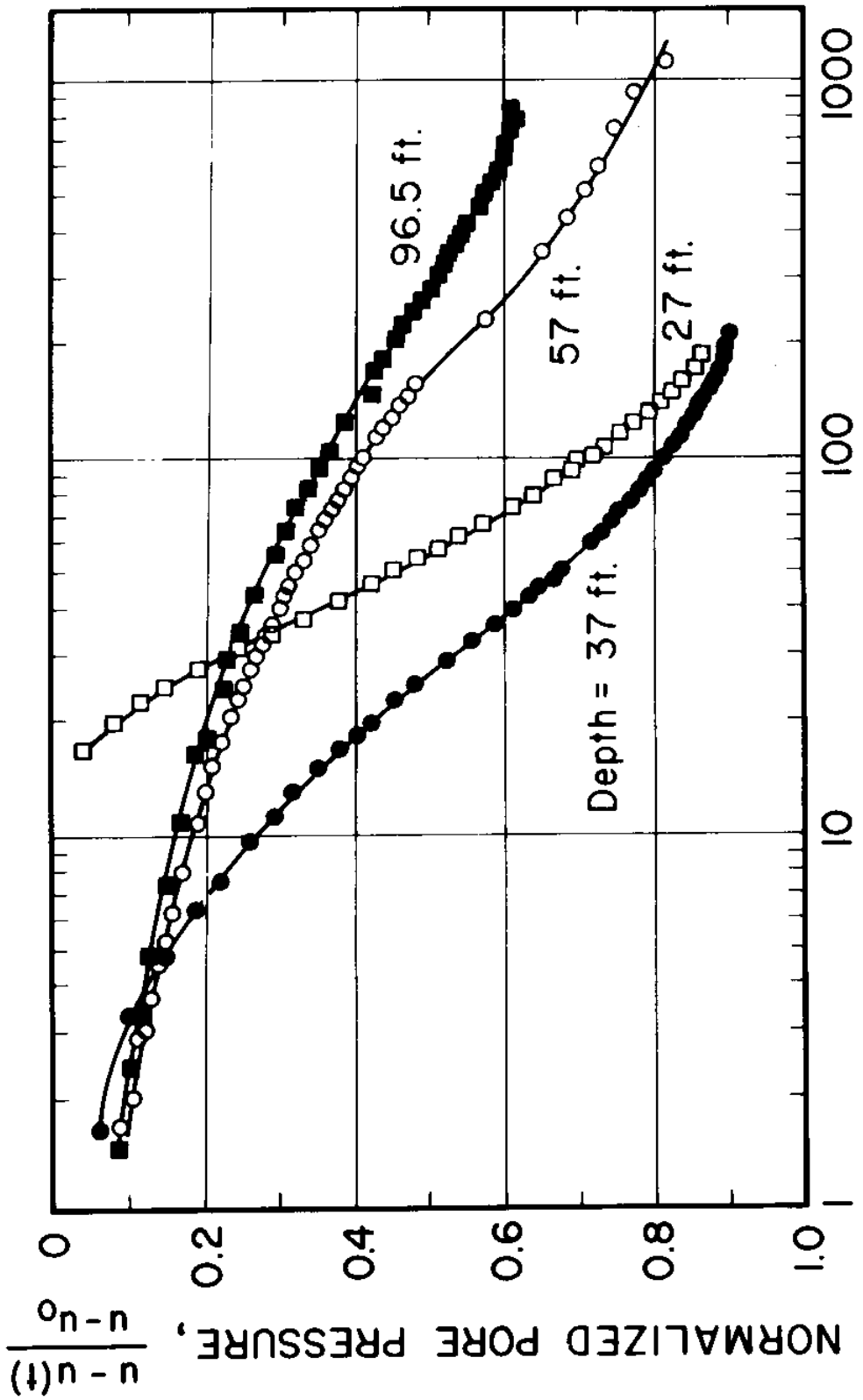

Figure 2.8 Pore pressure dissipation at the tip of an 18° conical probe.

CHAPTER 3

INTERPRETATION OF CONE PENETRATION RESULTS IN CLAYS

Existing equipment enable measurements of the cone resistance, q_c, sleeve friction behind the cone, f_s, and the penetration pore pressures, u to be obtained. Interpretation of these measurements is probably the most important step in cone penetration testing.

Continuous deep penetration of a cone in a homogeneous soil mass represents a steady state problem, i.e., to an observer moving with the cone, the deformation pattern, the strains and stress fields in the soil do not change with time. The steady state condition, the complicated behavior of soils, the large strains and large stress gradients that develop in the soil during cone penetration make the problem extremely complicated. Hence, existing interpretation methods of cone penetration results are either based on empirical correlation or on approximate theoretical solutions that rely on simplifying assumptions regarding: soil behavior; and/or the mode of penetration (e.g, neglecting steady state conditions); and/or the geometry of penetration (e.g., considering one-dimensional cavity expansion instead of the two-dimensional axisymmetric cone penetration).

Geotechnical engineers classify soils into coarse-grained soils consisting of gravels and sands; and fine-grained soils consisting of silts and clays. This classification is needed because of the very different drainage behavior of coarse vs.

fine-grained soils. Coarse-grained soils have a high-permeability ($k > 10^{-4}$cm/sec, say), quickly dissipate excess pore water pressures and hence are subjected to "drained" conditions in most applications. On the other hand, fine-grained soils can have very low permeabilities, retain excess pore pressures for significant periods of time and are sheared under "undrained" conditions.

Cone penetration in saturated clays (and saturated silts) having low enough permeabilities is characterized by its "undrained" mode of deformation, i.e., no significant water flow takes place during penetration. Under undrained shearing, saturated clays are practically incompressible (i.e., do not change in volume).

3.1 THE COMPLICATED UNDRAINED BEHAVIOR OF SATURATED SOILS

During undrained shearing, natural clays exhibit a highly complicated anisotropic, rate-dependent nonlinear and irreversible behavior. Anisotropy can be due to the structural arrangement of clay particles and/or the anisotropic stresses during consolidation. Figure 3.1 illustrates the importance of anisotropy on the stress-strain behavior of clays. Figure 3.1a shows results of K_o-consolidated undrained plane strain compression (PSC), plane strain extension (PSE), and direct simple shear (DSS) tests on normally consolidated (OCR = 1)*

* OCR = overconsolidation ratio
$= \bar{\sigma}_{vm}/\bar{\sigma}_{vc}$
$\bar{\sigma}_{vm}$ = maximum vertical effective stress
$\bar{\sigma}_{vc}$ = vertical effective consolidation stress prior to undrained shearing

Boston Blue Clay, BBC, which is a lean clay with medium sensitivity. The difference in soil behavior between the three types of tests is clear, especially the soil stiffness. The peak shear stress, often used as a measure of the shear strength, s_u, of the soil, is not the same in the three tests and does not take place at the same straining level. Furthermore, $s_u(PSC) > s_u(DSS) > s_u(PSE)$. Figure 3.1b shows the same results for BBC, but for an OCR = 4. Noting the difference in the vertical scale between the two figures, overconsolidation tends to:

1. increase the shear strength of the clay;
2. decrease the degree of anisotropy as expressed by, say the ratio $s_u(PSE)/s_u(PSC)$.
3. decrease the strain softening tendency of PSC tests.

In view of the results in Fig. 3.1 and the other factors affecting the undrained behavior of clays (e.g., rate effects, shear induced pore pressures, initial in situ conditions, ... etc.), it is highly unlikely that cone penetration data (e.g., q_c, u, and f_s) can provide a complete or even detailed description of clay behavior. A more reasonable objective of interpreting cone penetration results is to derive some meaningful engineering properties to be used in specific design problems.

3.2 EXISTING SIMPLE SOLUTIONS

Table 3.1 summarizes the predicted cone penetration resistance, q_c, in clays according to the different theories discussed below.

(1) The plane-strain bearing capacity solution approach.

This approach treats cone penetration as an incipient failure problem and is primarily based on Prandtl's fundamental solution for a strip footing on the surface of a rigid-plastic half-space, Fig. 3.2, (Terzaghi, 1943; Meyerhof, 1951; etc.). Modifications of Prandtl's solution are made by introducing a shape factor to account for the difference in geometry between the plane strain strip footing and the axisymmetric cone, and a factor to account for embedment below the surface. The point resistance q_c of a cone (or pile) is then written as:

$$q_c = N_c s_u + \sigma_{vo} \; ; \qquad (3.1)$$

$$N_c = \text{(shape factor) x (depth factor) x (5.14)},$$

where N_c = the cone resistance factor;

s_u = undrained shear strength of clay, and

σ_{vo} = initial vertical total stress in the soil.

The shape factor is generally assumed to be 1.2 to 1.3 (Terzaghi, 1943; Skempton, 1951), whereas the depth factor is assumed to be 1.5 to 1.6 for deep foundations (Skempton, 1951; Brinch Hansen, 1961 and 1970). Because Prandtl's solution applies to incipient failures, theories based on this approach cannot predict deformations or strains associated with steady cone penetration. In fact, these theories cannot distinguish between bearing capacity and steady cone penetration.

To account for the effect of cone angle, Mitchell and Dorgunoglu (1973) use Meyerhof's solution for incipient (rough) wedge penetration at the surface instead of Prandtl's solution. Thus for a cone with an apex angle 2δ , q_c is given by:

$$q_c = N_c s_u + \sigma_{vo} \tag{3.2}$$

N_c = (shape factor) x (depth factor)

x $(2.57 + 2\delta + \cot \delta)$, where δ is in radians and is equal to or less than $\pi/4$.

Meyerhof (1961) presents another approximate solution to the point resistance of a cone at depth. He assumes that the circumferential stress is the minor principal stress and that the slip line field on a meridian plane in the axisymmetric cone problem is identical to that for the plane-strain wedge penetration. With these assumptions, he obtains the bearing capacity factor numerically, and finds that the bearing capacity of a cone is slightly larger than that of a wedge and is given by:

$$q_c = N_c s_u + \sigma_{vo} \tag{3.3}$$

$N_c \simeq$ (1.09 to 1.15) x $(6.28 + 2\delta + \cot \delta)$

(the shape factor is introduced herein to provide a uniform presentation of different theories).

(2) The cavity expansion approach. This approach is based on the expansion of cylindrical or spherical cavities in an infinite medium, starting from zero radius. Because of the

simplicity of these one-dimensional problems, solutions based on more realistic and complex soil properties (e.g., strain-hardening and strain-softening) can be obtained (Bishop et al. 1945; Chadwick et al., 1963; Ladanyi, 1967 and 1972; Baguelin et al., 1972; Palmer, 1972; Prevost and Hoeg, 1975a and 1975b; etc). For an incompressible elastic-perfectly plastic soil with a shear modulus G, the solution has a very simple form:

$$P_L = P_o + s_u\ (1 + \ell n\ G/s_u) \text{ for a cylindrical cavity;}$$
$$P_S = p_o + 1.33 s_u\ (1 + \ell n\ G/s_u) \text{ for a spherical cavity.} \qquad (3.4)$$

For a cylindrical cavity, P_o is the total horizontal stress and for a spherical cavity, p_o is the isotropic initial stress in the soil (Bishop et al., 1945).

Bishop et al. (1945) recognize that the difference between P_L and P_S is not large and propose that during deep penetration of a smooth cone, q_c lies between P_L and P_S. They also indicate that q_c approaches P_L for sharp cones and approaches P_S for blunt cones, i.e., q_c for smooth cones decreases as the cone angle, 2δ, decreases. Measurements in metals using 40° to 120° lubricated cones seem to support this approximation. However, deformation measurements due to blunt cone penetration discussed subsequently do not support the axially symmetric patterns predicted by spherical cavity expansion.

Gibson (1950) extends the above theory to bearing capacity in clays by making the additional assumption that the shear stress on the cone surface equals the undrained shear strength

of the clay, s_u. Thus for a cone with an apex angle 2δ, he proposed that q_c is given by:

$$q_u = N_c s_u + \sigma_{vo} \quad ;$$
$$N_c = 1.33\ (1 + \ell n\ G/s_u) + \cot\ \delta \quad ; \tag{3.5}$$

where the term cot δ is the friction contribution, and σ_{vo} indicates the influence of the initial stresses (assumed isotropic) in the soil.

Vesic (1975 and 1977) proposes the stress field around the cone tip illustrated by Fig. 3.2. The pressure on a cylindrical surface beneath the cone tip is assumed to equal P_s, and the stresses increase towards the cone face in the same manner as in a radial-fan shear zone of the slip-line theory for a rigid plastic material in plane strain deformation. Vesic also suggests that p_o in Eq. 3.4 represents the in situ octahedral normal stress $\sigma_{oct} = 1/3(\sigma_{vo} + 2\sigma_{ho})$ instead of σ_{vo}. Thus q_c for a blunt cone with $\delta = 90°$ is given by:

$$q_c = N_c s_u + \sigma_{oct} \quad ;$$
$$N_c = 1.33\ (1 + \ell n\ G/s_u) + 2.57\ , \tag{3.6}$$

where the factor 2.57 represents the stress increment in the radial shear fan under the cone tip.

The modifications made by Gibson and Vesic to the cavity expansion solutions derived by Bishop et al. have no solid theoretical basis, but rely mostly on engineering judgement. Therefore, their accuracy and validity can only be judged on

the basis of experimental verification.

Working with Vesic, Al Awkati (1975) related q_c to P_L using an empirical factor determined from experiments. For the undrained shearing of clays, he proposed that:

$$q_c = N_c s_u + \sigma_{oct} \quad ;$$
$$N_c = \lambda(1 + \ell n\ G/s_u) \quad . \tag{3.7}$$

Experiments in sands show that λ is approximately 1.9 for a 60° cone, and 1.85 for $2\delta \geq 83°$. Experiments in clays are still needed. This method is purely empirical and cannot determine deformations and strains.

(3) Steady penetration approach. To account for the continuous nature of cone penetration, Baligh (1975) based his approach on the slip-line solution for steady penetration of a rigid wedge in a rigid perfectly plastic material developed by Baligh (1972) and Baligh and Scott (1976). The axisymmetric counterpart of this problem is that of a cone with no rigid boundary behind it to constrain soil deformation. He proposes that the work, q_c, required to push a conventional cone a unit distance, Fig. 3.3a, is the sum of the work required to push the cone in Fig. 3.3b and the work required to keep the cavity open, Fig. 3.3c. The first component is estimated as 1.2 times the penetration resistance of a wedge (i.e., using a shape factor = 1.2), while the second component is the expansion pressure for a cylindrical cavity, P_L, (Eq. 3.4). According to this theory, q_c is given by:

$$q_c = N_c s_u + \sigma_{ho} \quad ;$$

$$N_c = 1.2(5.71 + 3.33\delta + \cot \delta) + (1 + \ell n\, G/s_u). \tag{3.8}$$

Subsequently, Baligh et al. (1978) used the q_c in Eq. 3.8 as an upper bound for cone resistance. They also proposed a lower bound on q_c for conventional (unenlarged) cones and provided solutions for enlarged cones.

Vivatrat (1978) extended Baligh's results by deriving the steady wedge penetration resistance in anisotropic clays obeying the elliptical model proposed by Davis and Christian (1971). Since the undrained shear strength of an anisotropic clay is not unique, the wedge resistance factor N_w depends on the shape of the yield contour of the soil described by three parameters: $s_u(V)$, K_s and b/a (say).

$$K_s = \frac{s_u(H)}{s_u(V)}$$

$$a = 1/2\ [s_u(V) + s_u(H)] \tag{3.9}$$

$$b = s_u(45°)/\sqrt{s_u(V)\ s_uH)}$$

where $s_u(V)$, $s_u(H)$ and $s_u45°)$ are the undrained shear strengths corresponding to failure states when the major principal stress is vertical, horizontal and at 45°, respectively. For plane strain testing conditions:

$s_u(V) = s_u(PSC)$ in plane strain compression

$s_u(H) = s_u(PSE)$ in plane strain extension

$s_u(45°) \simeq s_u(DSS)$ in direct simple shear.

Results of Vivatrat's theory are shown in Fig. 3.4.

In practice, the inverse problem is usually of interest, i.e., given the wedge (or cone) resistance, q_w, what can we infer regarding the soil strength? Vivatrat (1978) shows that, within an error of ± 15°, an average strength of the clay, $s_u(AVE)$, can be estimated by the isotropic theory (Baligh, 1975) where:

$$s_u(AVE) = \alpha[s_u(PSC) + s_u(PSE)]$$

or $$s_u(AVE) = \alpha(1 + K_s)\ s_u(PSC)\ . \qquad (3.10)$$

The parameter α varies between 0.45 and 0.49 for most clays ($0.5 \leq K_s \leq 1.0$, $0.65 \leq b/a \leq 1.0$) and, for all practical purposes, can be approximated as 0.47.

3.3 STRAIN-PATH SOLUTIONS

In deep penetration problems, experimental observations (Rourk, 1961; Vesic, 1963; Robinsky and Morrison, 1964; Szechy, 1968; and others) indicate that soil deformations caused by penetration of a rigid indenter are similar in different soils even though the penetration resistance can be drastically different (i.e., soil stresses are very different). This implies that deep steady cone penetration problems are basically strain-controlled and that the associated deformations are not very sensitive to soil behavior. Baligh (1975) outlined an approximate method that he later called the "strain path method" (Baligh et al., 1978) for solving these problems.

In this approach, the strain path of selected elements is estimated from a deformation pattern (velocity field) chosen on the basis of kinematic requirements. Laboratory tests are then conducted or, alternatively, appropriate constitutive laws used, to determine the deviatoric stresses in these elements when subjected to the estimated strain paths. The octahedral (isotropic) stresses are then estimated by integrating the equilibrium equations.

Figure 3.5 compares the strain path method with the more familiar stress path method (Lambe, 1967) to identify their strong similarities. As indicated in Fig. 3.5, the strain path method is approximate because the estimated stresses will not, in general, satisfy the equilibrium requirements, unless the estimated strain field is identical to the actual one.

Levadoux and Baligh (1980) applied the strain path method to cone penetration in resedimented normally consolidated Boston Blue Clay by following the steps presented in Fig. 3.6. A complete description of their solution methods, assumptions, and results is beyond the scope of this report. However, the different types of results obtained by Levadoux and Baligh are illustrated by Figs. 3.7 through 3.17 where we note:

1) Assuming that the soil provides no shearing resistance during cone penetration, the velocities, deformations and strain paths of various soil elements are obtained by superimposing the effect of a suitable distribution of sources and sinks. Figure 3.7 shows the distortion of a square grid during penetration of a 60° cone. Deformations are clear to

the naked eye and hence are expected to cause large (non-infinitesimal) strains. Figure 3.8 shows the strain path of soil elements initially located at a radial distance r_o = 0.2, 0.5 and 1 times the cone shaft, R. Clearly, strains are large and complicated and the soil is subjected to a strain reversal behind the cone base. Figure 3.9 shows contours of the deviatoric strain, γ_{oct}, in the soil due to penetration of 18° and 60° cones. γ_{oct} is a good measure of the shear strain in the soil.*

2) Figure 3.10 shows the contour of the octahedral strain rates in the soil, $\dot{\gamma}_{oct}$, during "standard" penetration testing with a $10cm^2$ cross sectional area cone pushed at a rate of 2 cm/sec. Noting that laboratory tests are typically conducted at vertical strain rate $\dot{\varepsilon}_v$ = 0.5%/hr, (corresponding to $\dot{\gamma}_{oct}$ = 0.35%/hr), Fig. 3.10 indicates that cone penetration involves much higher levels of straining rates. For example, in the dark zone in Fig. 3.10, the soil is sheared at a rate in excess of 10^4 times faster than in the laboratory tests. Because of the rate-dependent behavior of clays, this result is important in evaluating and interpreting cone penetration results.

---

* $\gamma_{oct} = \frac{1}{3}[(\varepsilon_{rr}-\varepsilon_{zz})^2 + (\varepsilon_{zz}-\varepsilon_{\theta\theta})^2 + (\varepsilon_{\theta\theta}-\varepsilon_{rr})^2 + 6\varepsilon^2_{rz}]^{1/2}$

3) Using a sophisticated total stress model based on incremental plasticity theory, the predicted deviatoric stress paths at a soil element initially located at r_o = 25R from the axis of a 60° cone is illustrated in Fig. 3.11. The soil is clearly subjected to a very complicated non-monotonic stress path. This is further shown in Fig. 3.12 with the results of a soil element closer to cone axis, r_o = R. Figure 3.13 shows contours of the octahedral stress, τ^*_{oct}, representing a good measure of the level of shearing in the soil and the extent of the failure zone where the soil has reached its peak (or maximum strength.

4) Using a new model for the shear-induced pore pressures and by satisfying the equilibrium equations, the total stresses, effective stresses, and excess pore pressures, Δu, due to cone penetration were computed. Figure 3.14 shows the predicted contour lines of $\Delta u/\bar{\sigma}_{vo}$ during penetration by 18° and 60° cones in resedimented normally consolidated BBC.

5) Figure 3.15 evaluates the predicted distribution of normalized** excess pore pressures, $\Delta u/\Delta u_{(sh)}$, by comparing predictions vs. measurements obtained at different locations on 18° and 60° cones, and the shaft behind them, in a deposit

---

* $\tau_{oct} = \frac{1}{3}[(\sigma_{rr}-\sigma_{\theta\theta})^2 + (\sigma_{\theta\theta}-\sigma_{zz})^2 + (\sigma_{xx}-\sigma_{rr})^2 + 6\sigma_{rz}^2]^{1/2}$

** The normalizing parameter is the pore pressure, $\Delta u_{(sh)}$, on the shaft far behind the cone base.

of Boston Blue Clay (BBC) at Saugus, Mass. Clearly, predictions* are close to measurements not only in the soft deposit with an overconsolidation ratio, OCR = 1.3, but in the clay having an OCR = 2 and 3. However, when predicted values of Δu corresponding to properties of resedimented normally consolidated BBC were compared to measurements conducted in the soft BBC deposit (OCR = 1.3), a significant overestimate of Δu, by a factor of two, was found. This is probably due to the difference between the soil parameters describing the behavior of the resedimented NC clay vs. the in situ slightly OC clay.

6) By integrating the total normal stresses on the cone face and by assuming that: 1) the shear strength, s_u, of the normally consolidated BBC is proportional to $\bar{\sigma}_{vo}$ ($s_u = \alpha\bar{\sigma}_{vo}$); and: 2) s_u for overconsolidated BBC is proportional to $(OCR)^{0.8}$, Levadoux and Baligh computed the cone resistance, q_c, for smooth and rough cones. Smooth cones have no shear stress, τ, on the cone face and rough cones have an assumed value of $\tau = 0.15\ \bar{\sigma}_{vo}$ for normally consolidated BBC. Figure 3.16 compares predicted q_c values with measurements conducted by Baligh et al. (1978) using three cone angles (18°, 30° and 60°). Predictions based on rough-cone solutions are reasonably close to measurements, especially when the OCR of the clay is low. Figure 3.17 illustrates this comparision for 18° and 60° cones.

---

* Recall that predictions are made for normally consolidated resedimented BBC.

In summary, strain path solutions provide useful predictions to: 1) Better understand the mechanism of cone penetration and hence better evaluate cone penetration results; and, 2) Estimate cone resistance, q_c, and penetration pore pressures, u, given a detailed description of the in situ clay characteristics and properties. However, the strain path method cannot, at this time, be used to provide a direct interpretation method to estimate an undrained shear strengh (say) from q_c and/or u measurements.

3.4 EMPIRICAL CORRELATIONS

Due to the complicated behavior of clays and the difficulties associated with the cone penetration mechanism, rigorous interpretation methods for cone penetration results (q_c and u) in clays are not available.* On the other hand, empirical correlations between q_c and/or u vs. specific properties of clays (e.g. the undrained shear strength, s_u) and/or foundation performance are possible to establish.

3.4.1 Correlations between the FUGRO Cone Resistance and the Field Vane Strength.

The FUGRO cone has a 60° angle, a base diameter equals to that of the shaft, and is pushed at a rate of 2cm/sec. Since this cone geometry and pushing rate appear to gain a wider acceptance by the geotechnical profession

* Except, possibly, for enlarged cones when pore pressure measurements behind the tip are available, see Baligh et al., 1978.

and since these cones were used in the offshore testing program discussed subsequently, empirical correlations discussed below are limited to the FUGRO cones.

The field vane strength of clays, $s_u(FV)$, can be considered a reliable (repeatable) index property in soft to stiff clays, which has been carefully calibrated by evaluated experience on foundation failures (Bjerrum, 1972 and 1973; Ladd et al., 1977). Therefore, $s_u(FV)$ provides a good framework for the practical use of q_c in design until q_c is directly correlated to foundation performance.

Following the traditional bearing capacity equation in soil mechanics, an empirical cone factor $N_c(FV)$ can be defined as:

$$q_c = N_c(FV) \cdot s_u(FV) + \sigma_{vo} \quad , \tag{3.11}$$

Figures 3.18 through 3.20 show the mean and the $\pm 2\sigma$ band of $N_c(FV)$ (σ = standard deviation) computed from Eq. 3.11 for tests conducted by MIT in three clay deposits: Boston Blue Clay, Atchafalaya Basin Clay, and Connecticut Valley Varved Clay. The geology and soil conditions at these sites are described by Baligh et al. (1978). In computing the factor $N_c(FV)$, q_c data is obtained from two to three FUGRO cone tests performed within a close proximity (40-ft radius). On the other hand, $s_u(FV)$ are the average of existing field vane measurements conducted within a 200-ft radius of the cone tests.* The

* The field vane tests in the Boston Blue Clay and Connecticut Valley Varved Clay were performed by MIT, using the ASTM Standards with the Geonor equipment; in the Atchafalaya Basin Clay, they were performed by the U.S. Corps of Engineers.

computed $N_c(FV)$ data are filtered to reduce the influence of clear local soil inhomogeneities (e.g. sand lenses). The variability of $N_c(FV)$ shown in Fig. 3.18 thus reflects the variability of the cone tests, but not the scatter of the field vane data. The results in these clay deposits and some results reported by others are discussed below.

1) Boston Blue Clay. Figure 3.18 shows that the average value of $N_c(FV)$ decreases from 12 (or higher) in the stiff crust* to about 7.5 at a depth of 35 ft. Below this depth, the average $N_c(FV)$ increases almost linearly to 14 at a depth of 120 ft. Furthermore, the point variability of $N_c(FV)$, i.e., its standard deviation σ, tends to decrease slightly with depth. The $\pm 2\delta$ band, which includes approximately 95% of the (filtered) data points, corresponds to an uncertainty of $N_c(FV)$ of $\pm$ 2 in the top 40 ft (heavily overconsolidated) and $\pm$ 1.5 in the bottom 60 ft (slightly overconsolidated). Finally, we notice in Fig. 3.18 that below a depth of 60 ft where OCR $\leq$ 2, the average value of $N_c(FV)$ is approximately given by 12 $\pm$ 2.

2) EABPL Clay. The soil profile at this site is very variable (see q_c in Fig. 2.7) and the estimated profile of the average $s_u(FV)$ involves significant local uncertainty. The variability of q_c is illustrated by the large scatter in $N_c(FV)$ shown in Fig. 3.19; especially in the 3 layers: above a depth of 44 ft (where the soil is highly organic), between 54 to 66 ft

---

* See Fig. 3.17 for a profile of the overconsolidation ratio at the site and Fig. 2.6 for a profile of q_c.

and between 78 to 92 ft (because of numerous silt lenses; USCE, 1968). In the remaining layers, the point variability of $N_c(FV)$ is small, i.e., $2\sigma \leq \pm 2.5$. Finally, the average value of $N_c(FV)$ throughout this deposit (with OCR $\leq$ 1.5) is mostly within the range 9 ± 4.

3) Connecticut Valley Varved Clay. In this deposit, $N_c(FV)$ decreases from more than 15 in the crust to a very uniform value of 10 to 12 up to a depth of 40 ft (see Fig. 3.20). A dip in $N_c(FV)$ near depth = 45 ft is probably caused by soil variability between the locations where cone and field vane tests were conducted. (The cone tests detect slightly weaker soil at depths of about 46 ft, whereas the field vane test, conducted 200 ft away, detects it at about 52 ft depth.) The point variability of $N_c(FV)$ is relatively small, i.e., $2\sigma = \pm$ (1 to 1.5). The average values of $N_c(FV)$ is within the range of 11 ± 2 (excluding the region between 42 and 52 ft). Thus the variation of $N_c(FV)$ with depth in this case is of the same order as its point variability.

4) Comparison of $N_c(FV)$ in different clay deposits.

Figure 3.21 shows the average field vane strength, $s_u(FV)$, at the three sites tested by MIT (curves B, C, L), and also at six Scandinavian sites (curves 1 to 6) where cone resistance data were obtained by NGI-FUGRO (Lunne et al., 1976). Table 3.2 provides soil information on the Scandinavian sites. More details are given by Lunne et al. (1976).

Figure 3.22 presents the average $N_c(FV)$ profiles obtained from these nine sites. We note that:

1. Excluding site No. 2, where s_u(FV) below a depth of 15m is unusually low (probably because of the high sensitivity of the clay, Table 3.2 and Fig. 3.21), the values of N_c(FV) are between 5 and 21 for the remaining eight sites.
2. N_c(FV) profiles obtained by MIT are either constant with depth or tend to increase with depth, whereas N_c(FV) profiles obtained by NGI-FUGRO tend to decrease with depth.
3. Comparing the average value of N_c(FV) in each deposit, we note that the values obtained by MIT are generally lower than those obtained by NGI-FUGRO.

The different trends and values in N_c(FV) shown in Fig. 3.22 can be attributed to one or more of the following reasons:

1. Errors or distortions in s_u(FV), q_c, or both.
2. The inability of Eq. 3.11 to account for the dependence of q_c on depth.
3. Differences in the clay properties among these sites, e.g., plasticity index and/or sensitivity as well as the stress history and/or strength. For example, curves 1 and 4 showing N_c(FV) decreasing with depth correspond to deposits where sensitivity decreases with depth. Curve L with the lowest value of N_c(FV) corresponds to the highest value of plasticity index. Curve 3 below 12m with very high value of N_c(FV) corresponds to a very sensitive clay.

Lunne et al. (1976) do not consider the dependence of $N_c(FV)$ on depth, but indicate a relationship between $N_c(FV)$ and PI for "medium" to "very soft" clays. Their data are shown in Table 3.2 and are replotted in Fig. 3.23a with the uncertainty bands indicated by Lunne et al. (1976). Also shown for comparison in Fig. 3.23a are the results from the MIT test sites, excluding the "stiff" or heavily overconsolidated clays and the more variable regions in the profiles, Table 3.3 and Figs. 3.18 through 3.20. The data in Fig. 3.23a indicate a decreasing trend in $N_c(FV)$ with increasing PI. At any value of PI, the scatter in $N_c(FV)$ is approximately ± 5.

5) Application of Bjerrum's Correction Factor. Case studies of embankment and footing failure indicate that $s_u(FV)$ is not always the appropriate strength to use in bearing capacity or stability analyses.* A better estimate of the field strength is obtained if $s_u(FV)$ is corrected by the empirical factor, μ, based on actual failures (Bjerrum, 1972 and 1973, Ladd et al., 1977). Lunne et al. (1976) use Bjerrum's empirical correction factor, μ, to compute another empirical cone factor, $N_c'(FV)$ defined by:

$$N_c'(FV) = \frac{q_c - \sigma_{vo}}{\mu\ s_u(FV)} \qquad (3.12)$$

Therefore, the factor N_c' provides an empirical means of estimating the field strength (to be used in the design of embankments and in problems involving bearing capacity of clays)*

* Baligh et al. (1978) discuss the validity of using the same strength for these two types of problems.

from q_c measurements.

Figure 3.24 shows profiles of the average values of $N_c'(FV)$ for the deposits described in Fig. 3.22 (data tabulated in Tables 3.2 and 3.3). Comparing Fig. 3.22 and Fig. 3.24, we note that the correction factor slightly reduces the scatter in the empirical cone factor at any given depth. However, each $N_c'(FV)$ curve shows almost as much dependence on depth as $N_c(FV)$. Furthermore, we note in Fig. 3.24 that:

1. Values of N_c' obtained from all nine sites are mostly within a band described by the expression:

$$N_c' = 14 \pm \alpha \tag{3.13}$$

where $\alpha = 8 - 0.15z$

z = depth in meters (1m = 3.28 ft) $\leq$ 40m

2. The only exceptions to the above bands are some results obtained by NGI-FUGRO at site 3 (Børresen, where PI is very low, the sensitivity very high and $s_u(FV)$ is suspiciously low (Fig. 3.21); and, the EABPL site (tested by MIT, Table 3.3) where the soil is too variable to give reliable values of N_c' (see, for example, Fig. 3.19).

3. Low value of N_c' (near the $N_c' = 14 - \alpha$ band) are obtained by MIT (at the three sites denoted by B, L and C) whereas high values of N_c' (near the $N' = 14 + \alpha$ band) were determined at the Scandinavian sites. Noting that the clays tested by MIT are generally

stiffer than the Scandinavian sites, (see Fig. 3.21) this indicates that N'_c is probably related to OCR.

Figure 3.23b shows a plot of $N'_c(FV)$ vs. PI for "medium" to "very soft" clays at the nine sites under consideration. Comparing this figure to Fig. 3.23a, we note that $N'_c(FV)$ does not vary with the plasticity index, PI, as much as $N_c(FV)$. The range of $N'_c(FV)$ for these "medium" to "very soft" clays is 8 to 20 for PI greater than 10%. At any PI, the uncertainty in $N'_c(FV)$ is the same as in $N_c(FV)$, and is about ± 5. For a mean value of $N'_c(FV)$ of 14 to 15, this uncertainty range is about ± 33%, which is larger than the scatter of the data associated with Bjerrum's correction factor for the field vane test (± 25%). However, the greater uncertainty involved in interpreting cone resistance compared to field vane data based on this purely empirical approach should be expected since $s_u(FV)$ (or corrections thereof) is assumed to represent the field strength. Direct correlations between q_c and actual performance of foundations should provide more reliable empirical interpretation methods.

6) Other Correlations

Reliable general correlations in stiff to hard clays are difficult to establish because of the difficulties associated with describing the undrained shear strength, s_u, of these materials. Composition, fabric, sample disturbance, size effects and shearing rates are among the factors that might affect s_u.

Figure 3.25 shows $N_c(FV)$ correlations established by the Norwegian Goetechnical Institute (NGI)(1975) in heavily overconsolidated clays. Compared to results in Fig. 3.23, overconsolidation tends to reduce $N_c(FV)$. Marsland and Powell, (1979) present cone factors N_c based on Eq. 3.11 where the undrained shear strength is obtained from large plate load tests (86.5cm in diameter) and base failures [instead of $s_u(FV)$]. Reported N_c values vary between 11 and 30 approximately. For safety, Marsland and Powell suggest that design values of N_c should be selected on the high side and recommend N_c values that increase with the undrained shear strength of the soil. This contradicts the trend of the NGI results in Figs. 3.23 and 3.25.

Numerous other correlations between the cone resistance q_c, and the undrained shear strength, s_u, of clays are available in the literature. For more data on these correlations and other aspects of cone penetration technology, the reader is referred to Sanglerat (1972), the proceedings of the European Symposium of Penetration testing, ESOPT*, Stockholm (1974), Schmertmann (1975, and 1978b), Mitchell and Gardner (1975) and Semple and Johnston, (1979).

* See, in particular, articles by Niccolai et al. and Appendino.

3.4.2 Penetration Pore Pressures. Reliable measurements of pore pressures during cone penetration are scarce in the geotechnical literature because piezometer probes with sufficiently rapid response time were recently developed (1975). The data presented below were obtained by MIT in three onshore clay deposits.

1) Boston Blue Clay. Measurements conducted at the Saugus, Massachusetts test site are shown in Figs. 3.26 through 3.32 as reported by Baligh et al. (1978, 1980).

Figures 3.26 and 3.27 show the measured pore pressures, u, during the steady penetration of 18° unenlarged and enlarged cones, respectively. Different curves represent the results obtained in adjacent holes. For the unenlarged cone, Fig. 3.26 indicates that, above a depth of 50 ft, the u profiles are not consistent, probably because of significant soil variability. Below 40 ft, all u profiles are approximately parallel and show the same pattern with depth. The largest pore pressure, u, is measured at mid-height of the cone (curve "2") and decreases behind the tip. Torstensson (1975) observes similar trends in pore pressure measured at the tip and behind a 60° cone during steady penetration in a normally consolidated clay, using a different probe design.

Pore pressures measured at the tip of the cone (curve "1") are about 1kg/cm^2 lower than at the middle of the cone (curve "2"). On the cylindrical shaft behind the conical tip, u decreases for a distance of 4d to 5d (d is the shaft diamater = 3.8cm for the pore pressure probes), and then appears to

remain constant, at least to a distance of 11d behind the tip.

Pore pressure variation along the cone and shaft behind it can result from one of two reasons:

1. A change in the total stress along the cone and shaft;
2. Pore pressure dissipation, i.e., soil consolidation.

In order to assess the effect of consolidation on the pore pressure difference between points 3 and 6 on the shaft behind the cone, we first estimate the time required for a soil particle to travel the distance 11d between the two points. For a penetration velocity of 1 to 2cm/sec used in the tests, this time is about 20 to 40sec. During such a time period, records of pore pressure decay after penetration is stopped (for a u measurement behind the tip) indicate that little consolidation takes place. This, in addition to the very close values of u at points 5 and 6, suggest that the measured pore pressures in Fig. 3.26 reflect the variation in the total stresses along the cone and shaft. The magnitude and variation of these total stresses, in turn, affect cone resistance.

Figure 3.27 shows the steady state pore pressures u along an 18° enlarged cone (D/d = 1.9). As in the case of an unenlarged cone, we note that u at the cone tip (curve "1") is greater than u behind the cone (curves "2" and "3"). The pore pressure at the tip is essentially the same as u (tip) for an unenlarged cone, Fig. 3.26. Furthermore, u behind the enlarged cone is uniform along the shaft at least up to a distance 11d. This supports the theoretical prediction of a cavity behind enlarged cones. Comparing this cavity pressure

to the pore pressure far behind an 18° unenlarged cone (curves "5" and "6" in Fig. 3.26), we note that they are essentially identical below a 70-ft depth, but at shallower depths u behind the enlarged cone is about 0.5 to 1kg/cm^2 smaller than u far behind the unenlarged cone.

Figure 3.28 and 3.29 show the steady penetration pore pressures around unenlarged and enlarged 60° cones. As in the case of 18° cones, Fig. 3.28 indicates that u at the tip of an unenlarged cone is higher than u on the shaft behind that tip. Figure 3.29 shows that u is uniform behind an enlarged cone. u at a distance of 3.2d behind the base of the unenlarged 60° cone is consistently about 1kg/cm^2 larger than u behind the enlarged 60° cone, and is essentially identical to u at the same distance behind an 18° unenlarged cone (curve "4" in Fig. 3.26). Since u is not measured very far behind the 60° unenlarged cone, no conclusion can be drawn regarding the effect of cone angle on this pore pressure. For the enlarged cones, however, u behind the 60° cone is consistently about 0.5 to 1.0kg/cm^2 larger than u behind the 18° cone.

The pore pressures behind cones are of practical interest in the understanding and prediction of shaft behavior during and after pile installation. From the data presented below, we note that these pore pressures are generally large ($> \sigma_{vo}$).

Figure 3.30 shows q_c, u (tip) and u (far behind) for an 18° unenlarged cone (2δ = 18°, D/d = 1). Clearly q_c exceeds u throughout the profile. Above a depth of 60 ft

(OCR > 2), both u (tip) and u (far behind) are small compared to q_c. Below a 60 ft depth (OCR = 1.2 to 2), u (tip) is about 70% of q_c, whereas u (far behind) is about 55% of q_c.

Figure 3.31 shows q_c and u (tip) for a 60° unenlarged ($2\delta = 60°$, D/d = 1) cone which exhibits trends similar to the 18° cone in Fig. 3.39. However, below a depth of 60 ft, u (tip) exceeds q_c by about 10%. This is contrary to theoretical predictions and is believed to reflect inaccuracies in q_c measurements.*

Figure 3.32 shows the smoothed profiles of the u/q_c ratio obtained from filtered u and q_c data where anomalies due to small scale inhomogeneities in the soil (e.g., sand or silt lenses) have been eliminated. The two u/q_c profiles in Fig. 3.32 increase with depth to about 70 ft and thereafter remain constant. The curve corresponding to a 60° cone where u is measured at the tip, shows the highest value of u/q_c. This curve is particularly significant for the offshore measurements and correlations in Chapter 4. Values of $u/q_c > 1$ attained by this curve below a depth of 60 ft are believed to be caused by inaccuracies in q_c measurements as discussed earlier.

2) Atchafalaya Basin Clay. Figure 3.33 shows the cone resistance, q_c, the steady state pore pressure at

---

* q_c measurements for unenlarged cones can underestimate the actual cone resistance by as much as 15% due to pore pressures u acting behind the tip (location 3 in Fig. 3.26). This error is, however, reduced when u at this location is small compared to q_c.

the tip of the cone, u (tip), and u far behind an unenlarged 18° cone. Generally, steady penetration pore pressures, u, are smaller in this plastic (high PI) clay deposit than in the lean (low PI) Boston Blue Clay. u (far behind) is less than σ_{vo} except between depths of 40 to 53 ft, 70 to 83 ft, and below 95 ft, where it is approximately equal to σ_{vo}. These locations correspond to regions of normally consolidated clay. u (tip) shows a variation with depth identical to that of u (far behind), and the difference in their magnitudes is almost uniform in the normally consolidated regions, as was observed in the Boston Blue Clay below the desiccated crust. Both pore pressures tend to decrease when q_c increases. This important feature will be discussed subsequently when the ratio u/q_c is treated.

Figure 3.34 shows q_c and u (tip) for a 60° unenlarged cone. In this case, u (tip) exceeds q_c at a depth of about 50 ft, and is almost equal to q_c at a depth of 70 ft. Again, these locations of high pore pressure correspond to normally consolidated regions in the deposit.

Figure 3.34 shows the smoothed u/q_c profiles which clearly show three "soft" strata where u/q_c is "large". It is perhaps worth mentioning that the two curves in Fig. 3.35 showing identical patterns of u/q_c are obtained from four different instruments.

3) Connecticut Valley Varved Clay. Figure 3.36 shows the soil profile at the Amherst, Massachusetts test site. Figure 3.37 shows q_c and u (tip) for an 18° unenlarged cone. In this deposit, u (tip) is relatively close to q_c except in the desiccated crust near the surface and in the sandy material below a depth of 60 ft. Figure 3.38 shows a q_c and u (tip) for a 60° unenlarged cone which shows the same pattern as the 18° cone, except that the difference between u and q_c becomes very small. Figure 3.38 shows that the smoothed u/q_c profiles are relatively constant and equal to 0.8 and 0.9 between depths of 30 to 60 ft, where OCR varies between 1.3 and 2.

Type of Approach	Reference	$q_c = N_c s_u + p_o$ Expression for N_c	N_c for $2\delta = 60°$		p_o
			$G/s_u = 100$	$G/s_u = 400$	
Bearing Capacity	Terzaghi (1943) Meyerhof (1951)	(shape factor)(depth factor) x 5.14	9.25	same	σ_{vo}
	Mitchell and Dorgunoglu (1973)	(shape factor)(depth factor) x (2.57 + 2 δ + cot δ)	9.63	same	σ_{vo}
	Meyerhof (1961)	(1.09 to 1.15) x (6.28 + 2 δ + cot δ)	10.2	same	σ_{vo}
Cavity Expansion	Bishop et al (1945)	$1.33(1 + \ln G/s_u)$	7.47	9.30	unspecified
	Gibson (1950)	$1.33(1 + \ln G/s_u) + \cot \delta$	9.21	11.03	σ_{vo}
	Vesic (1975,1977)	$1.33(1 + \ln G/s_u) + 2.57$	10.04	11.87	σ_{oct}
	Al Awkati (1975)	(correction factor) x $(1 + \ln G/s_u)$	10.65	13.28	σ_{oct}
Steady Penetration	Baligh (1975)	$1.2(5.71 + 3.33\ \delta + \cot \delta) + (1 + \ln G/s_u)$	11.02 + 5.61 =16.63	11.02 + 6.99 =18.01	σ_{ho}

Table 3.1 Summary of existing theories of cone penetration in clays.

SITE	DEPTH m	PLASTICITY INDEX P.I.,%	SENSITIVITY S_t	N_c(FV)	N_c(FV)* corrected
1. Sundland (Drammen Clay)	4-9	23-30	6-14	17-18	17-19
	9-14	7-10	1-2	18-20.5	16.5-18
	16-22	9-12	2-3	15.5-16.5	14-15
2. Dansviks Gate (Drammen)	3-10	20-35	6-9	13.5-17	15-16
	11-20	10-14	2-4	14-18	13-18
	20-35	10	3-4	13-16	12-14.5
3. Børresen Gate (Drammen)	6-12	15-20	13-22	17-20	16-19
	12-15.5	8	5-14	25-26	22.5-23.5
	15.5-30	4-5	40-130	20-26	18-23
4. Onsøy	2-9	25-30	5-10	17-19	18-19
	9-27	36	4-7	12-17	14-18
5. Göteborg	2-10	45-60	11-24	12-15	17-20
	10-20	50-60	15-19	13	
	20-31	40	13-17	12-14	14-16
6. Ska-Edeby	2-4	40	6-9	8-9	10
	4-12	35-50	10-12	10.5-12.5	12.5-14.5

* corrected in each 1 - m section using applicable PI, exclude extreme values

Table 3.2 Tabulation of correlations between cone resistance and the field vane strengths at NGI-FUGRO sites (data from Lunne et al., 1976).

Test Site	Depth (ft)	PI (%)	S_t [1]	$N_c(FV) = \frac{q_c - \sigma_{vo}}{s_u(FV)}$	$N'_c(FV)$ [2] $= \frac{q_c - \sigma_{vo}}{\mu\, s_u(FV)}$
Saugus, MA (Boston Blue Clay)	65 - 125	≃ 24	6	9 - 15	9 - 15
EABPL, LA (Atchafalaya Basin Clay)	50 - 120	60 - 80	1 ?	5.5 - 12.5	9 - 17
Amherst, MA (Connecticut Valley Varved Clay)	15 - 65 (excluding) 42 - 52	≃ 30 (bulk)	4 - 7	9 - 13	10 - 14

(1) from field vane data

(2) computed from the range of $N_c(FV)$

Table 3.3 Tabulation of correlations between cone resistance and the field vane strengths at M.I.T. test sites.

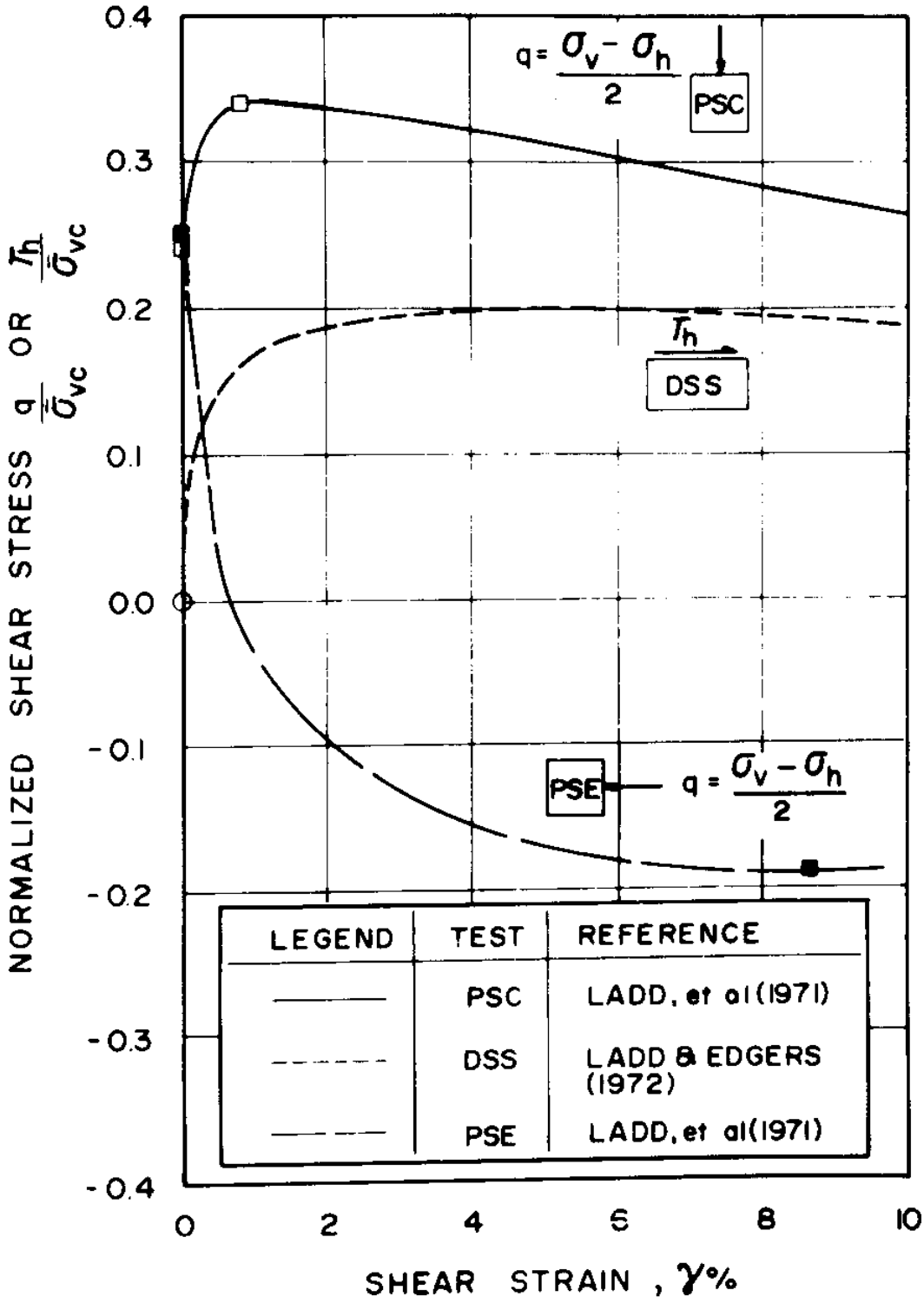

Figure 3.1a Normalized stress-strain relations from $\overline{CK_oU}$ tests on normally consolidated Boston Blue Clay. (from Azzouz and Baligh, 1978)

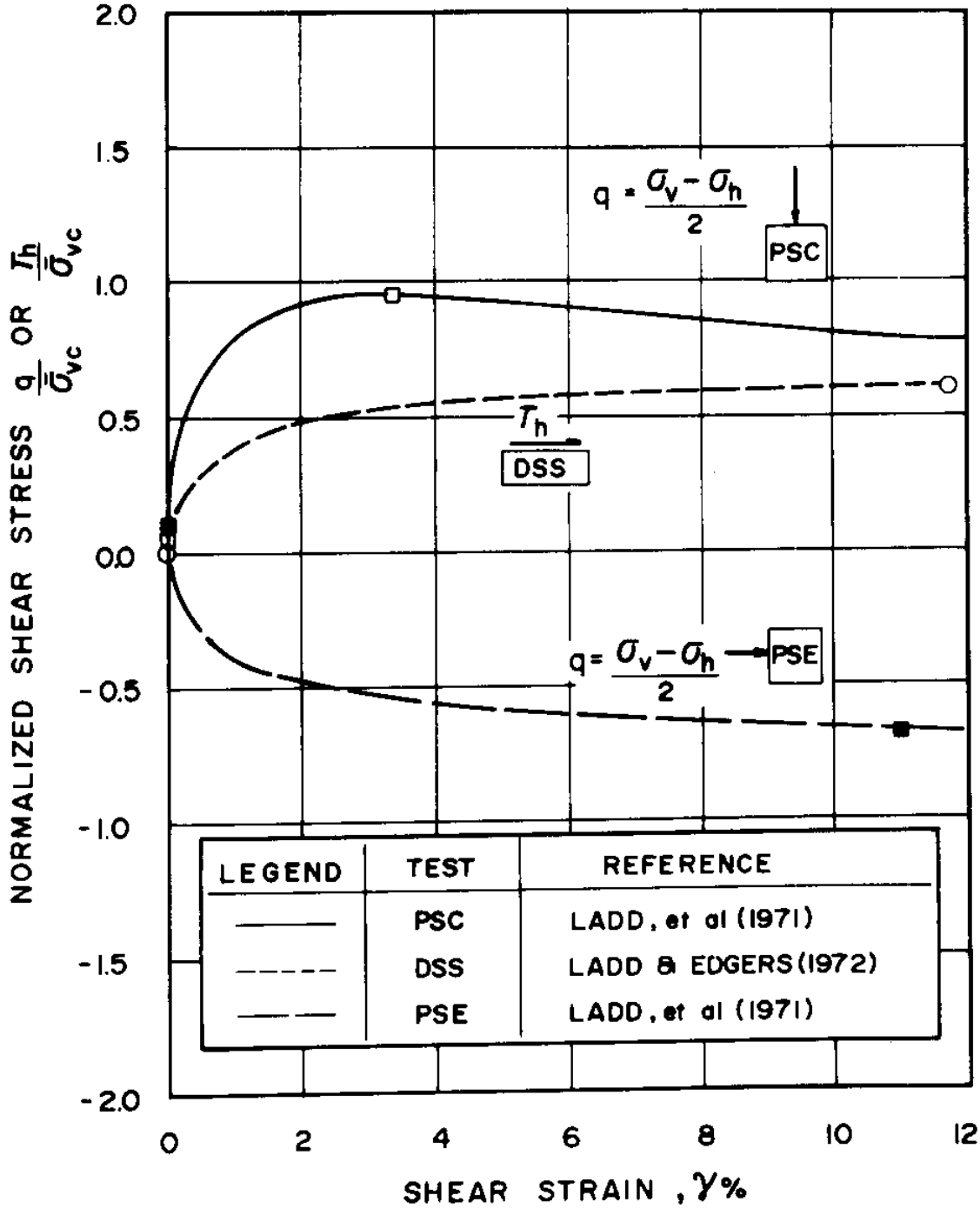

Figure 3.1b Normalized stress-strain relations from $\overline{CK_oU}$ tests on Boston Blue Clay (OCR=4) (from Azzouz and Baligh, 1978).

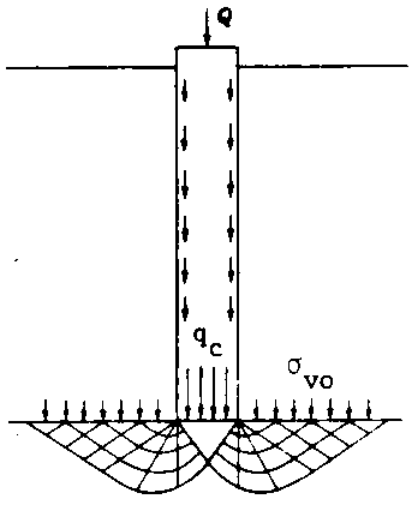

Prandtl (1920)
Reissner (1924)
Caquot (1934)
Buisman (1935)
Terzaghi (1943)

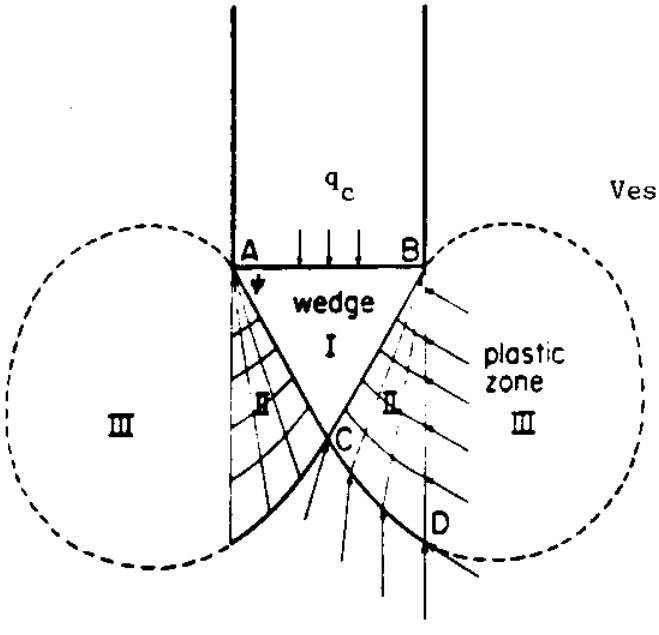

Vesic (1977)

Figure 3.2 Assumed failure patterns for deep penetration. (from Vesic, 1978; 1977)

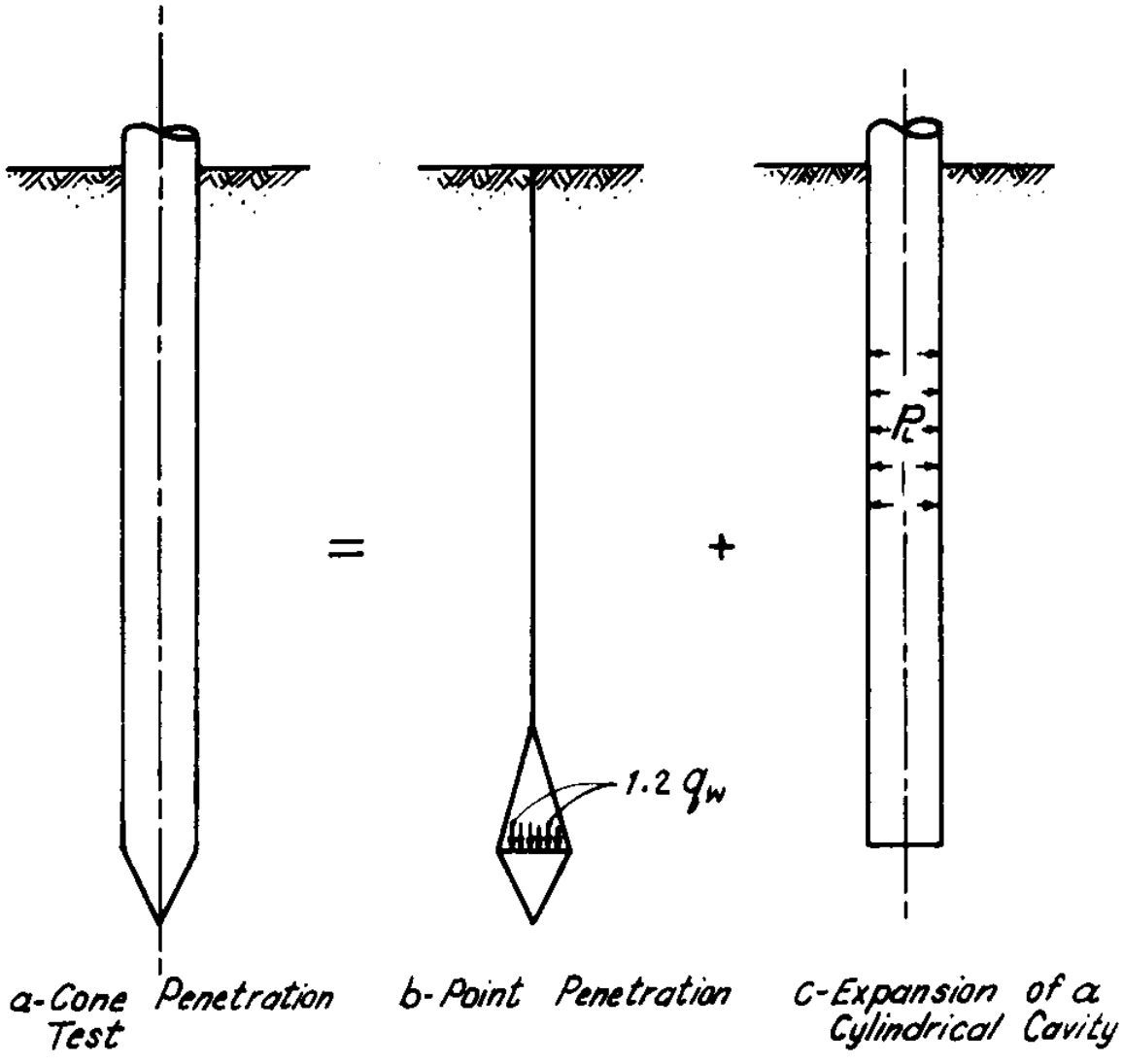

Figure 3.3 Model for cone penetration mechanism according to Baligh (1975).

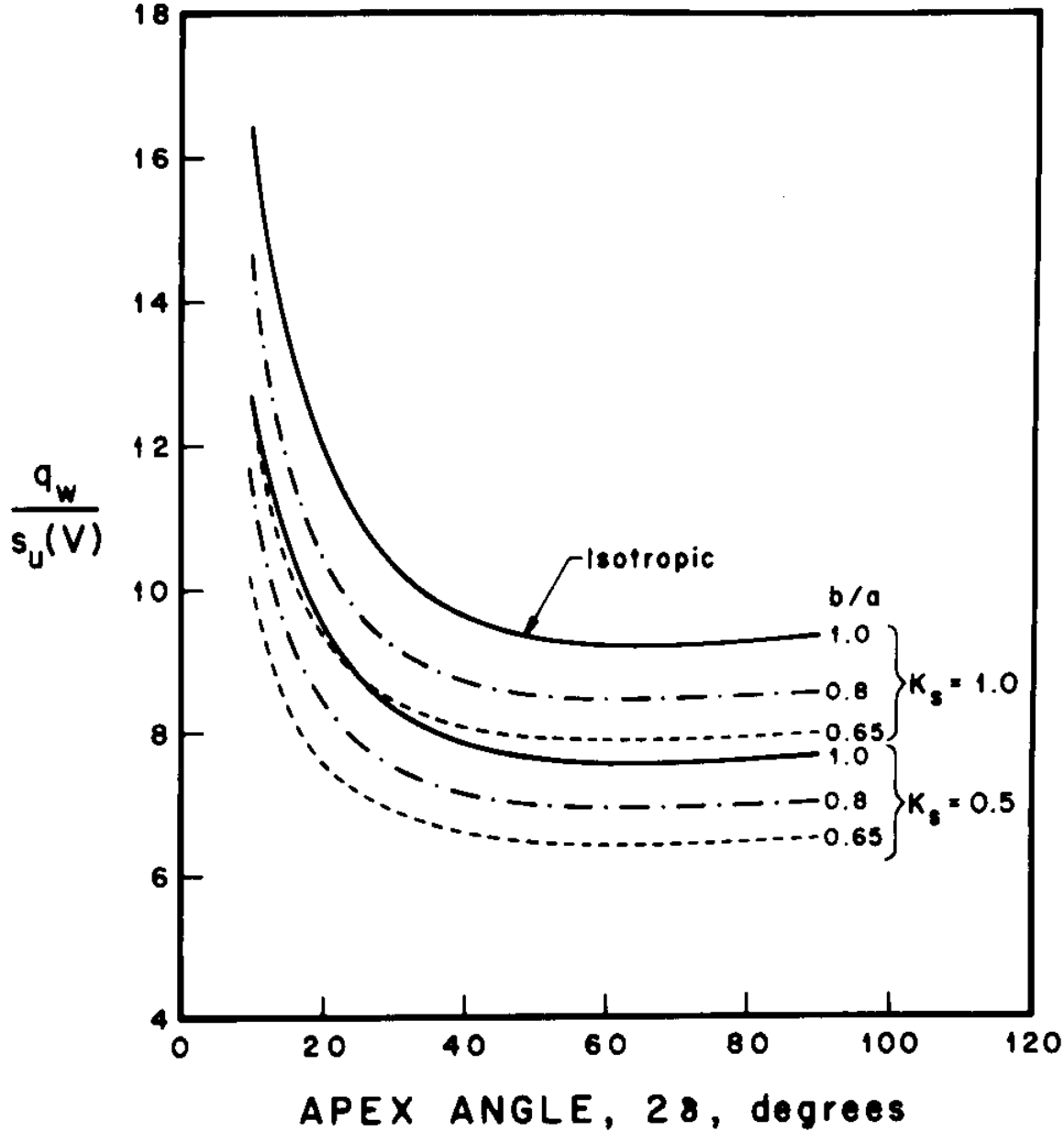

Figure 3.4 Sharp rough wedge resistance factors for steady penetration in anisotropic clays.

Stress Path Method	Strain Path Method
APPLICATIONS	
Surface Problems	Deep Problems
STEPS	
1. Estimate initial stresses 2. Estimate incremental stresses 3. Perform stress path tests on samples (or use adequate soil model) to obtain strains at selected locations. 4. Estimate deformations by integrating strains	1. Estimate initial stresses 2. Estimate incremental strains 3. Perform strain path tests on samples (or use adequate soil model) to obtain deviatoric stresses at selected locations. 4. Estimate octahedral (isotropic) stresses by integrating equilibrium equations.
APPROXIMATION	
In step 2, stresses are approximate thus leading to strains not satisfying compatibility requirements. i.e., deformations in step 4 depend on strain integration path.	In step 2, strains are approximate thus leading to stresses not satisfying all equilibrium conditions. i.e., octahedral stresses in step 4 depend on equilibrium integration path.

Figure 3.5 Comparison of stress path and strain path methods.

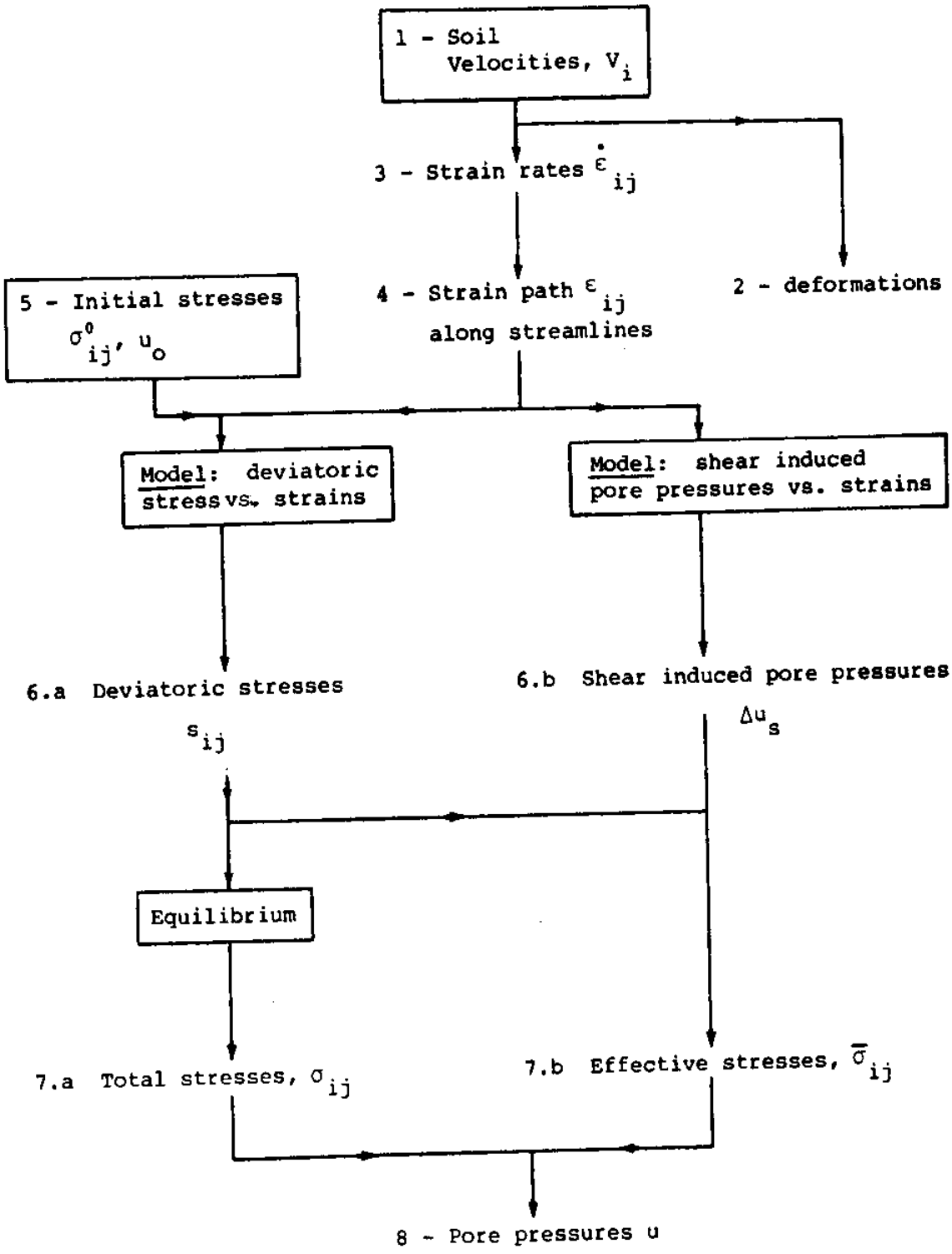

Figure 3.6 Application of the strain path method to deep steady cone penetration: Flow Chart.

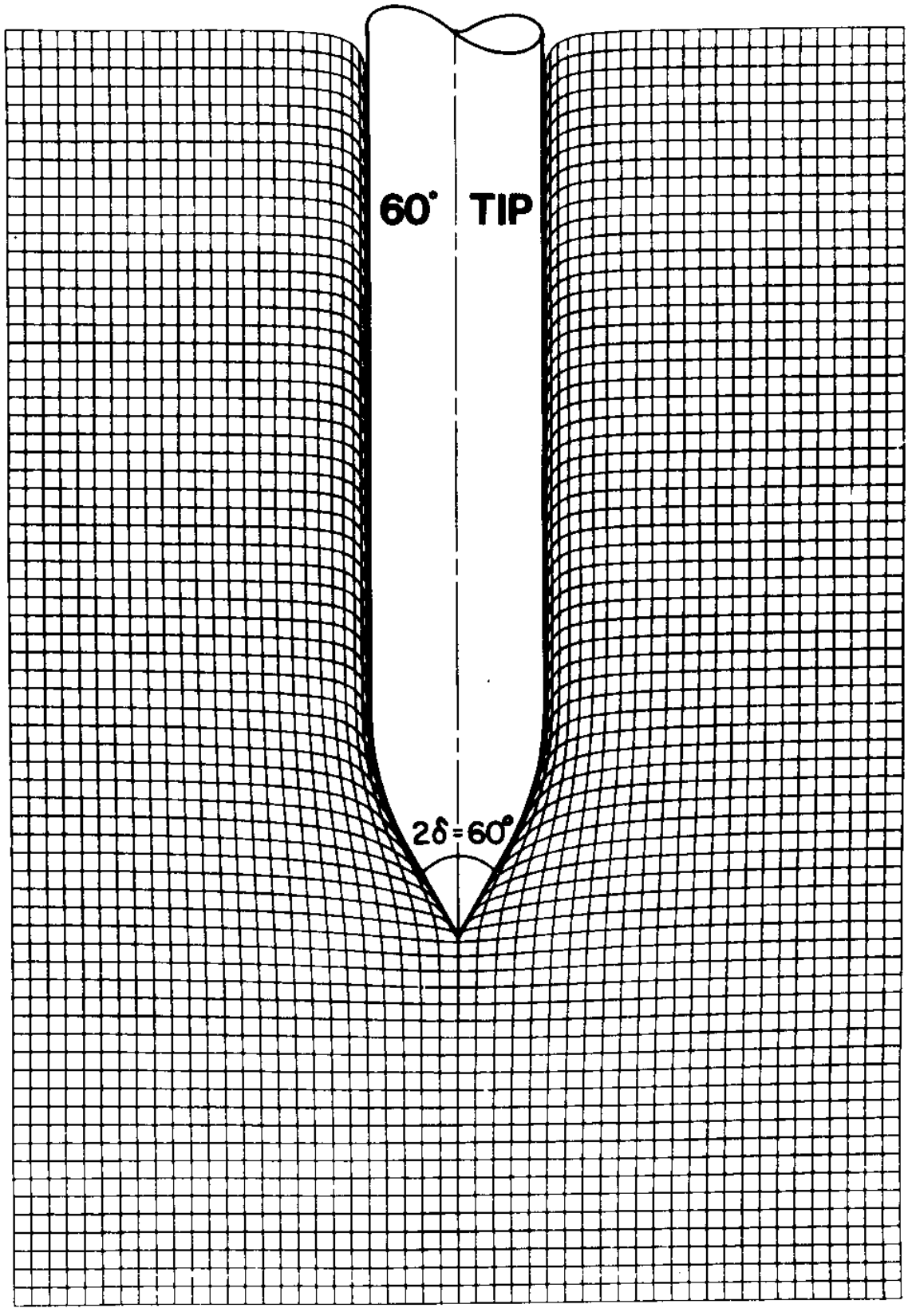

Figure 3.7 Predicted deformation pattern around a 60° cone.

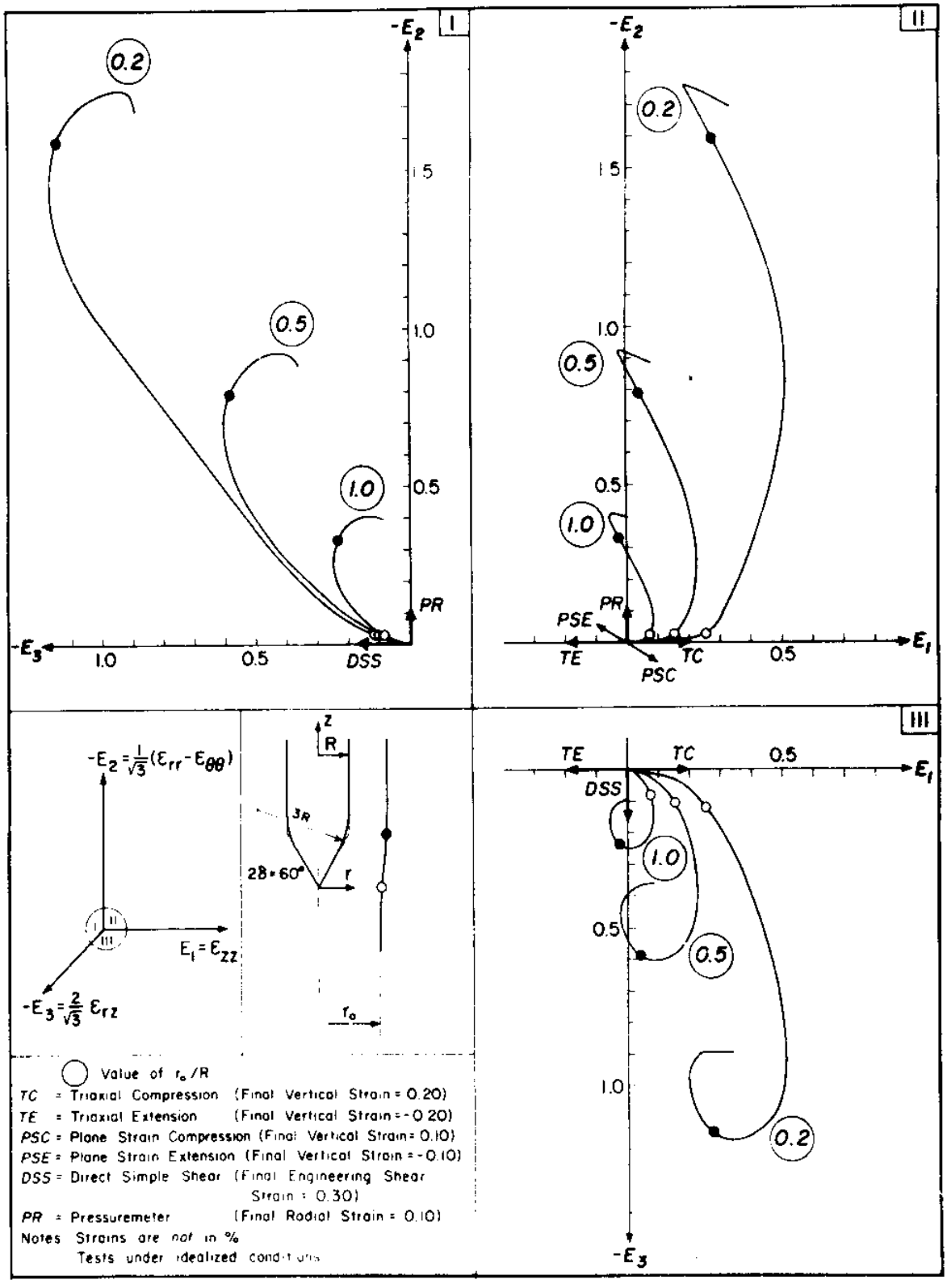

Figure 3.8 Strain paths of selected elements during penetration of a 60° cone.

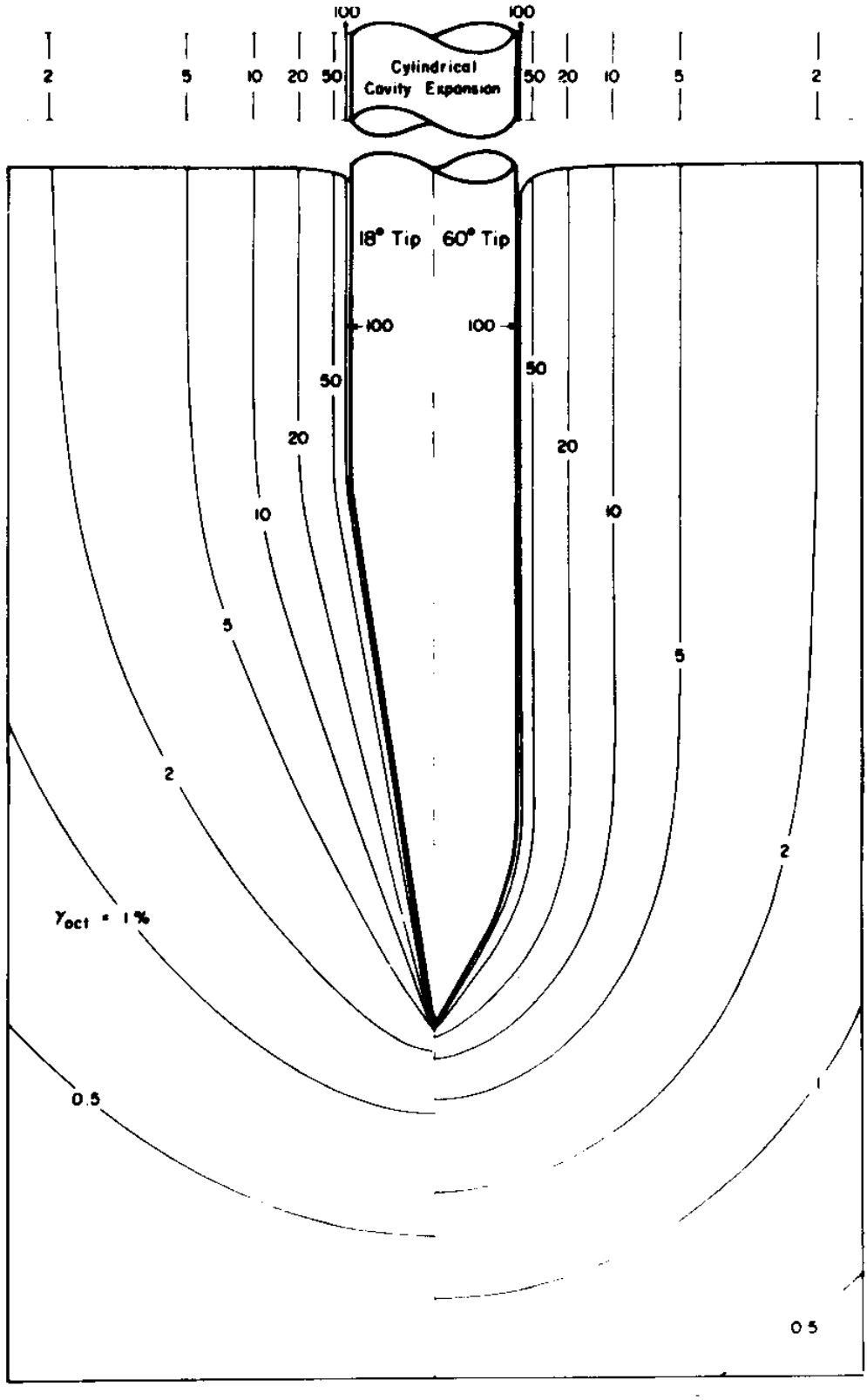

Figure 3.9 Contours of octahedral shear strain, γ_{oct}.

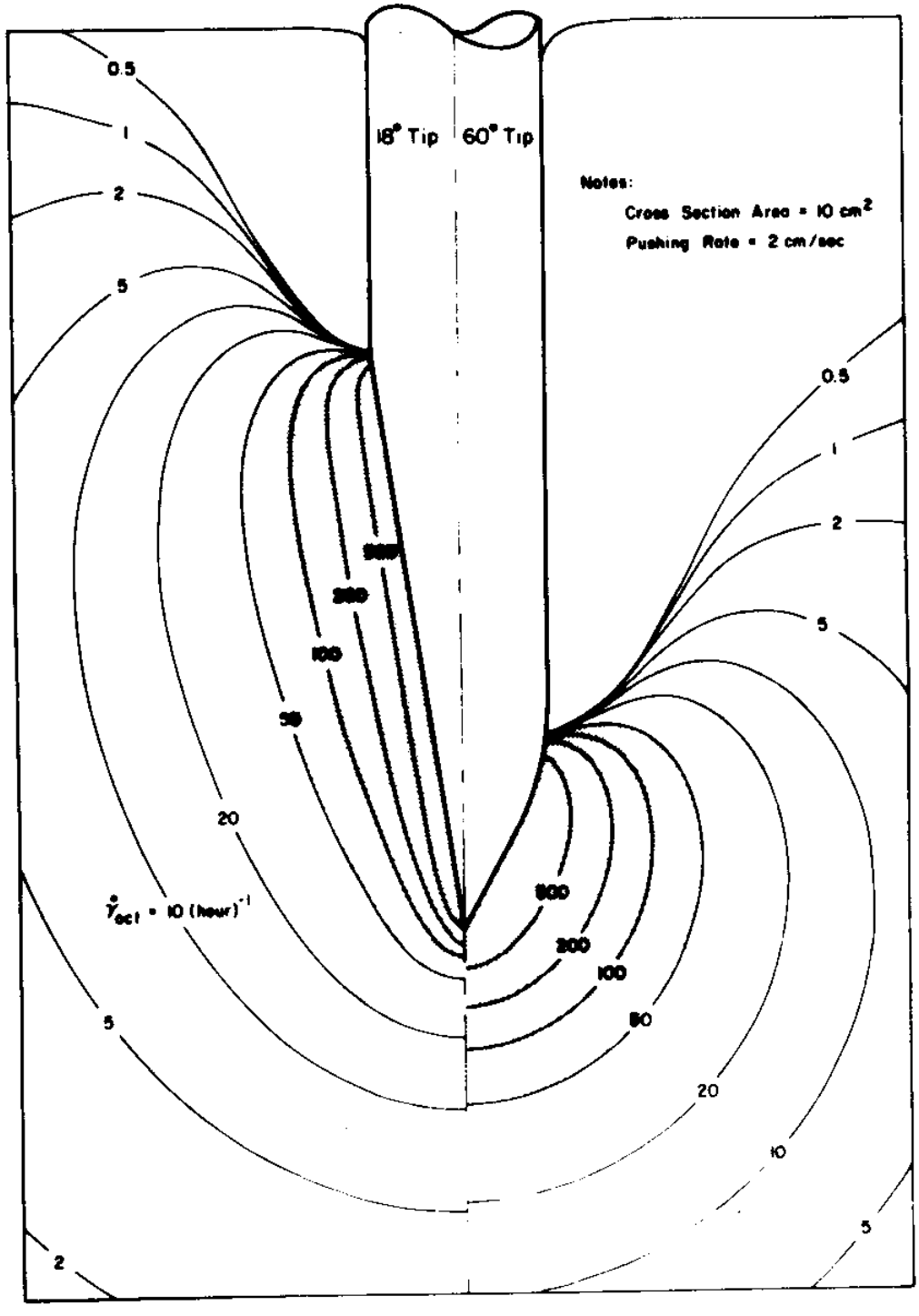

Figure 3.10 Contours of octahedral shear strain rate, $\dot{\gamma}_{oct}$.

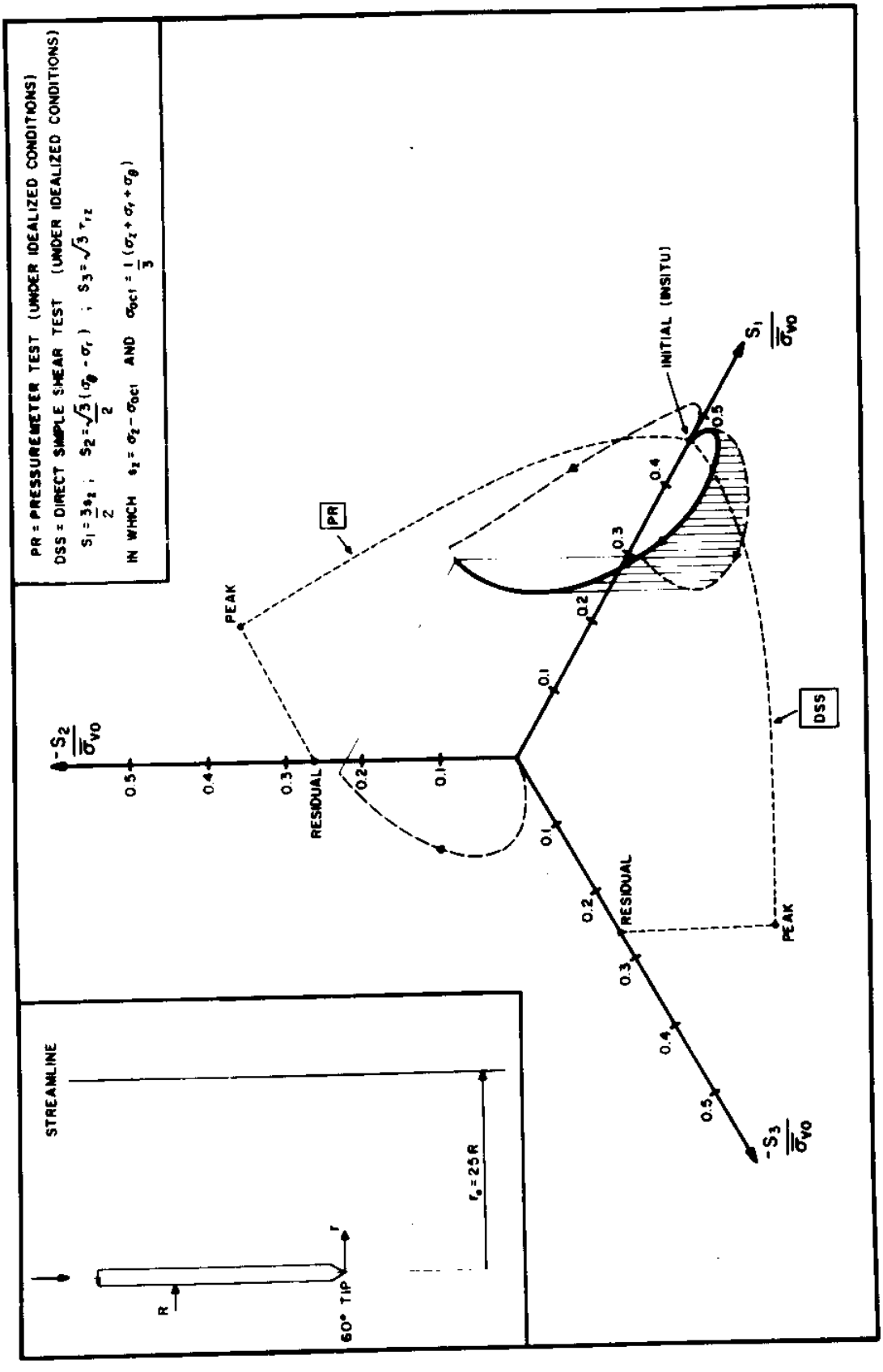

Figure 3.11 Predicted three-dimensional deviatoric stress path during steady penetration of a 60° cone in normally consolidated Boston Blue Clay.

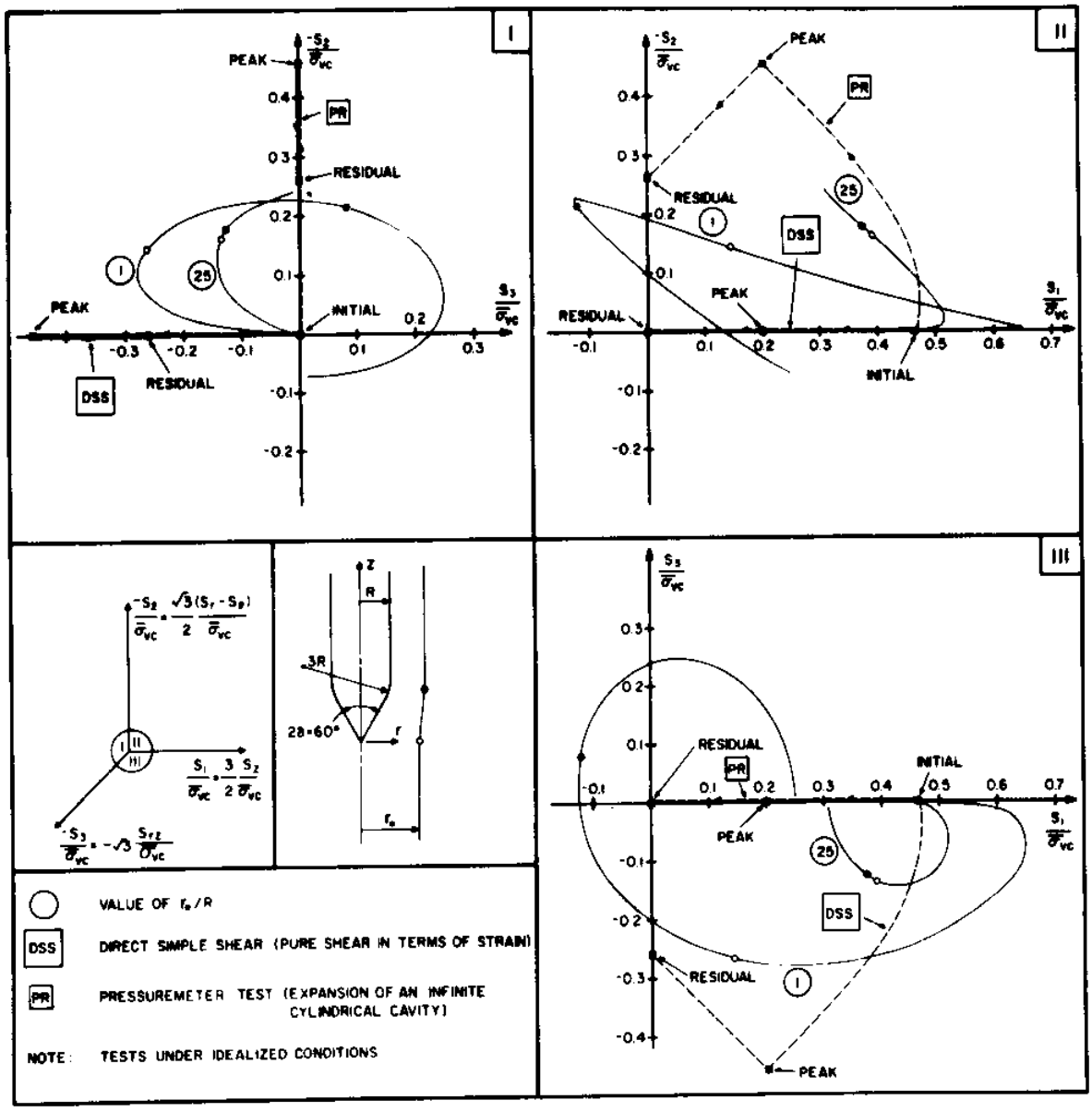

Figure 3.12 Predicted deviatoric stress paths along two streamlines during steady penetration of a 60° cone in normally consolidated Boston Blue Clay.

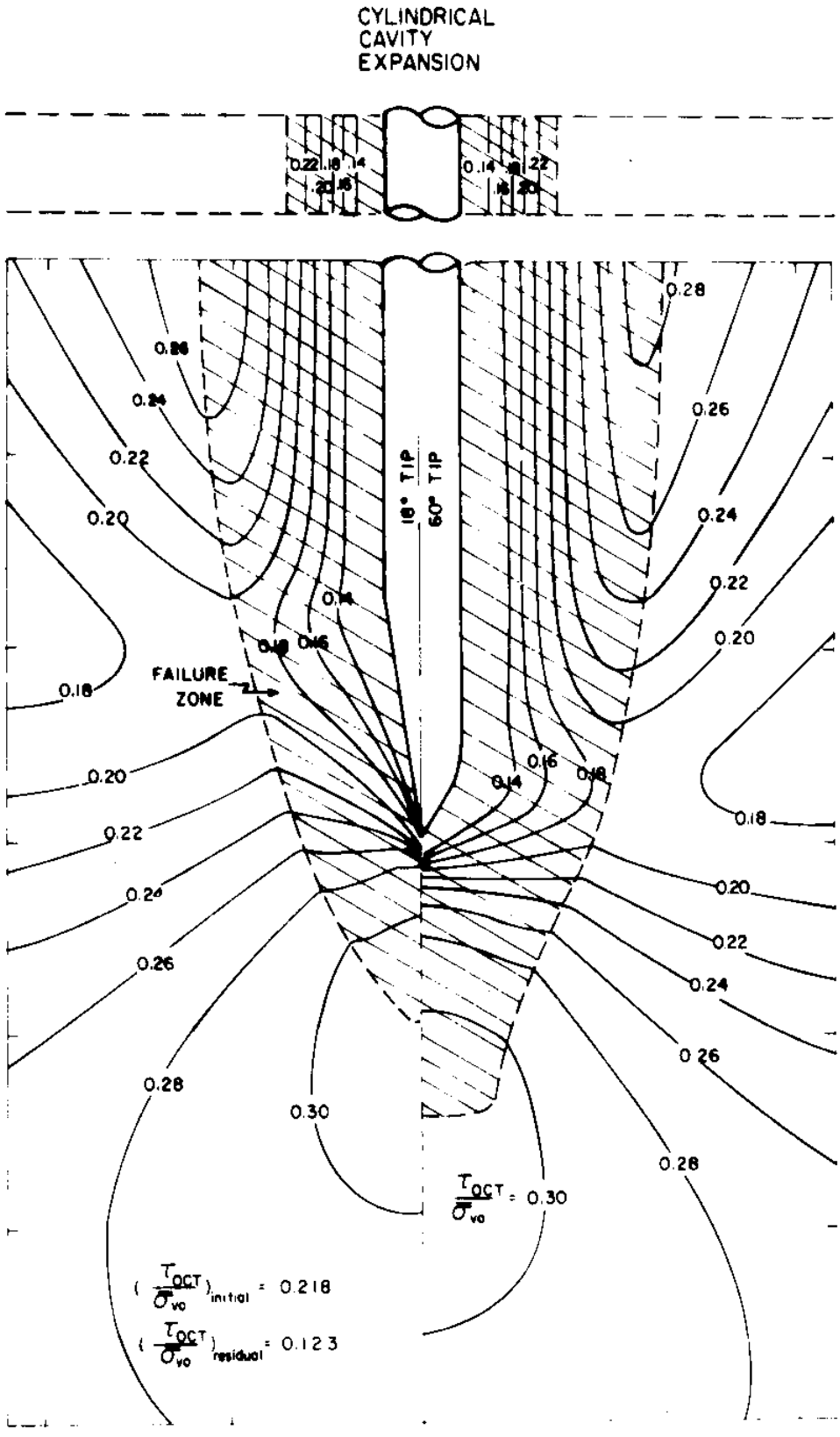

Figure 3.13 Predicted contours of normalized octahedral shear stress, γ_{oct}, and extent of failure during steady cone penetration in normally consolidated Boston Blue Clay (18° and 60° tips).

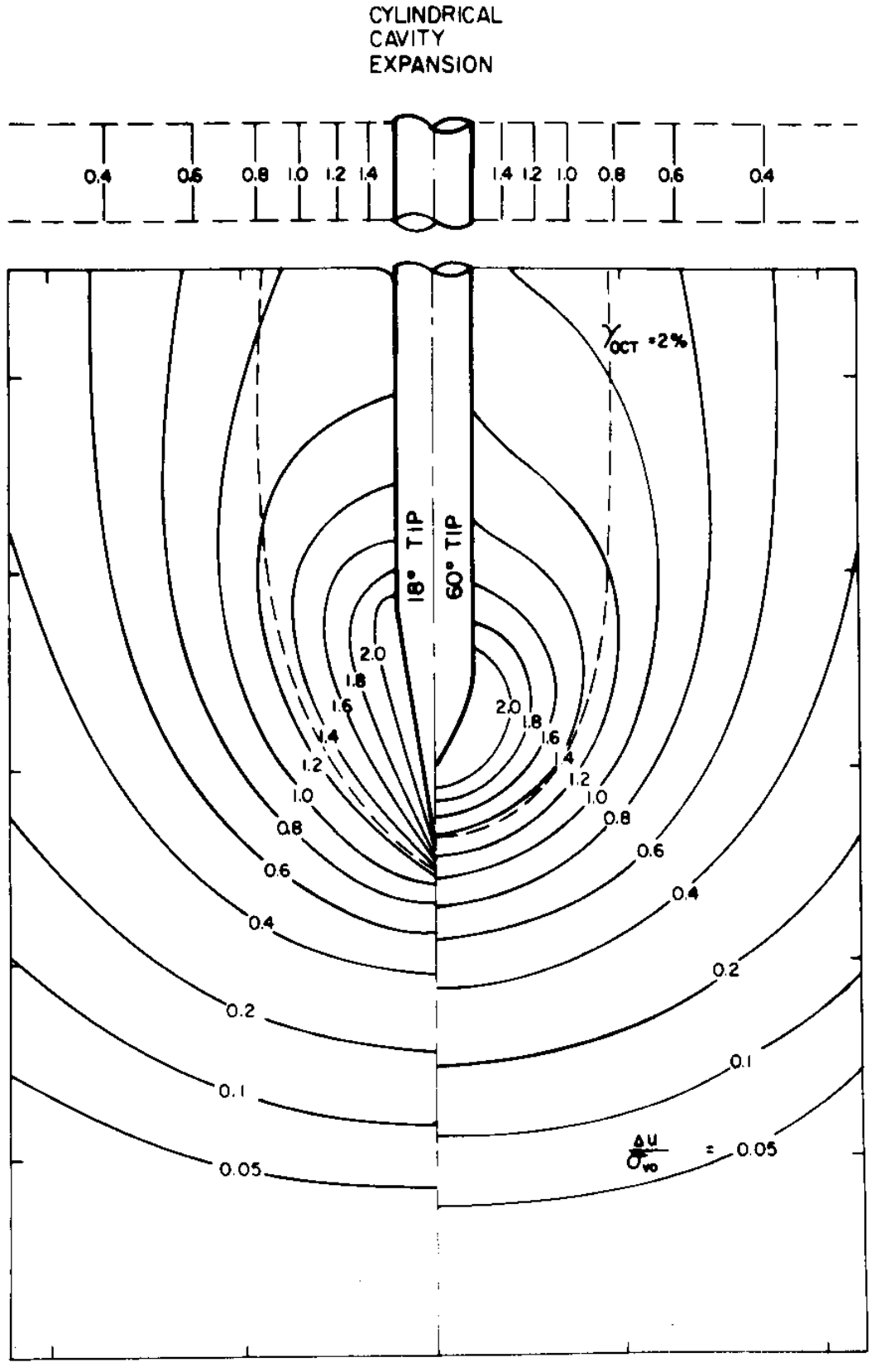

Figure 3.14 Predicted contours of normalized excess pore pressure, Δu, during steady cone penetration in normally consolidated Boston Blue Clay (18° and 60° tips).

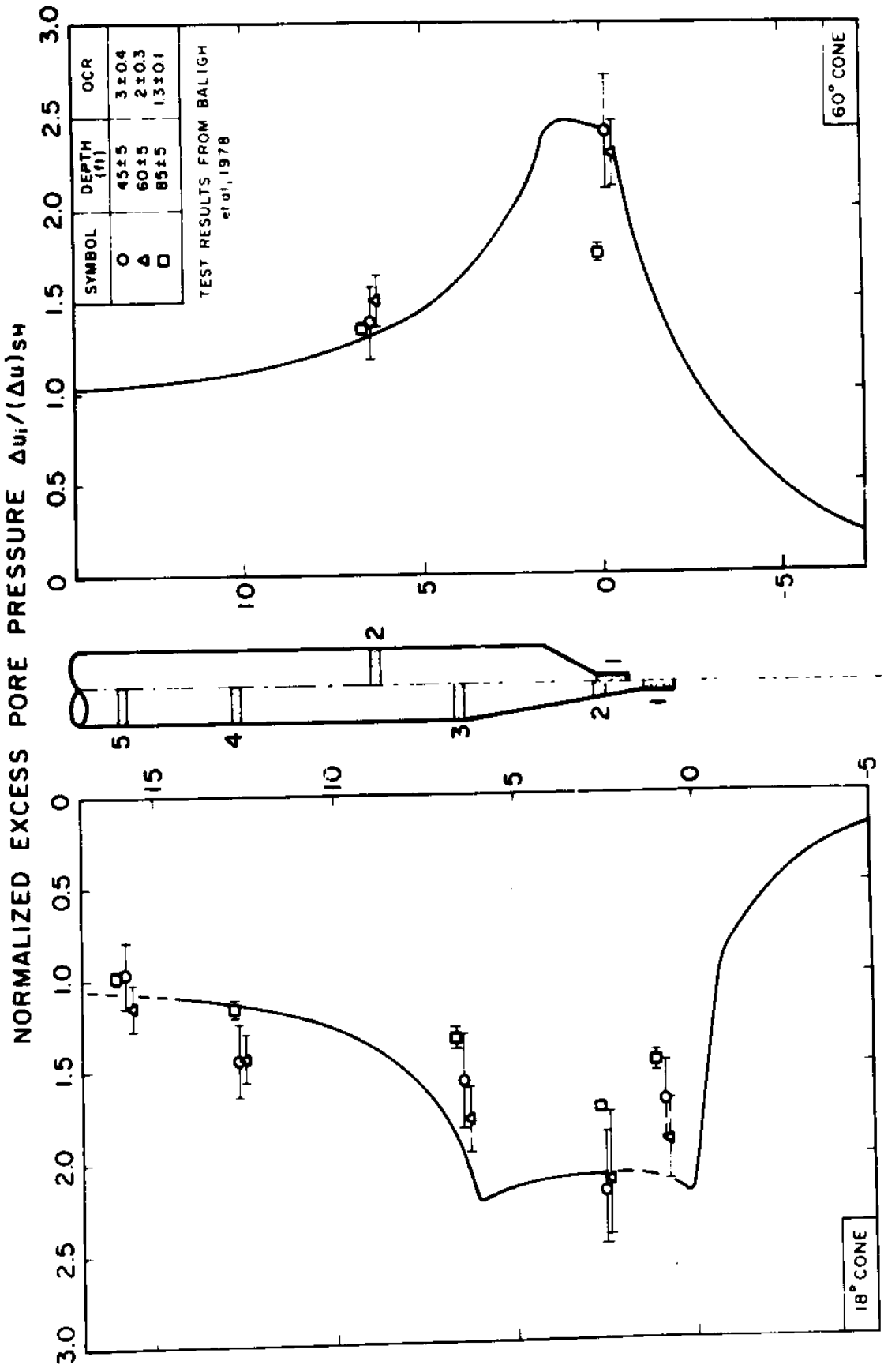

Figure 3.15 Predicted vs. measured longitudinal distributions of normalized excess pore pressures along 18° and 60° cones during steady penetration in Boston Blue Clay.

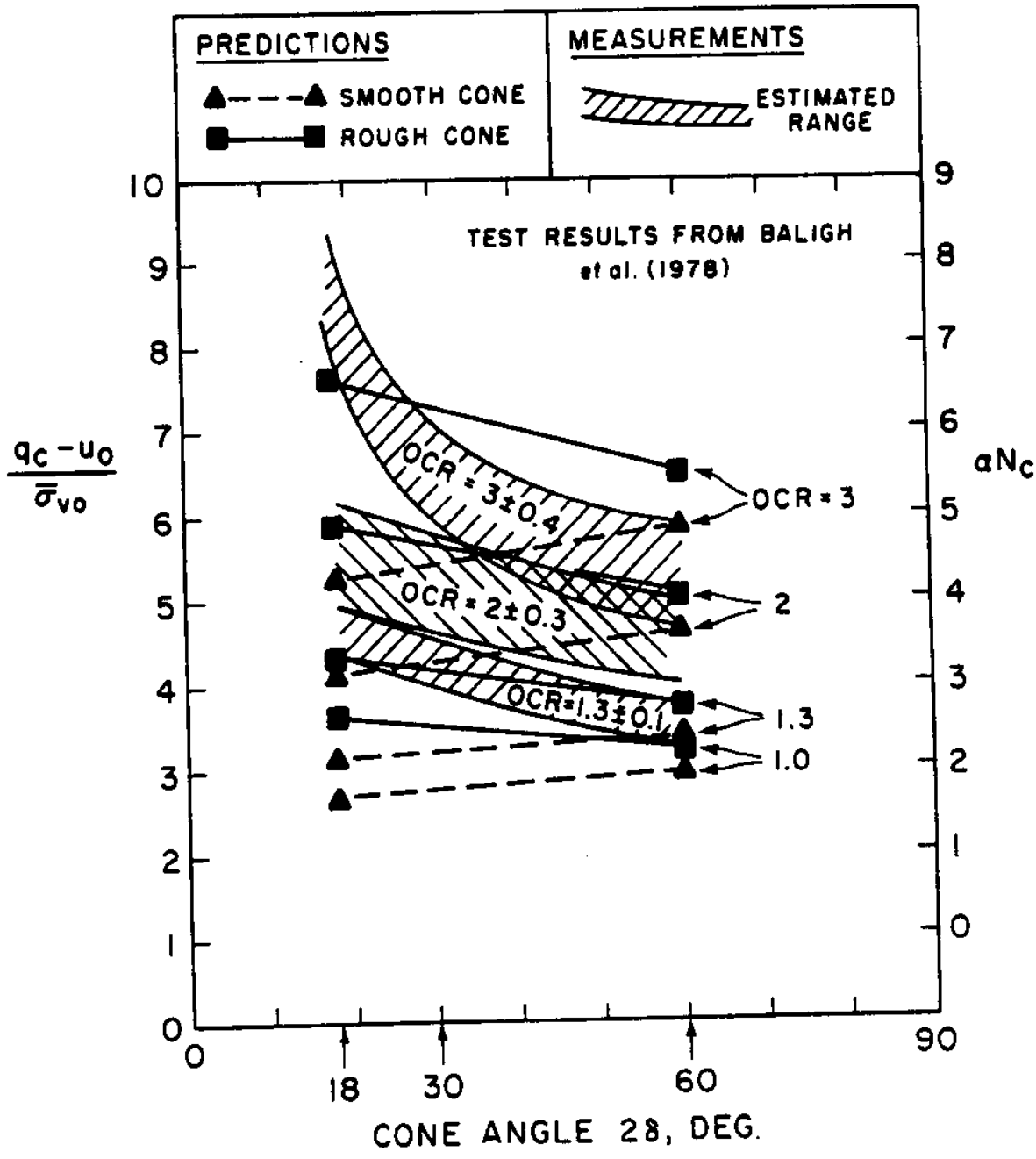

Figure 3.16 Comparison of predicted and measured cone resistances in Boston Blue Clay.

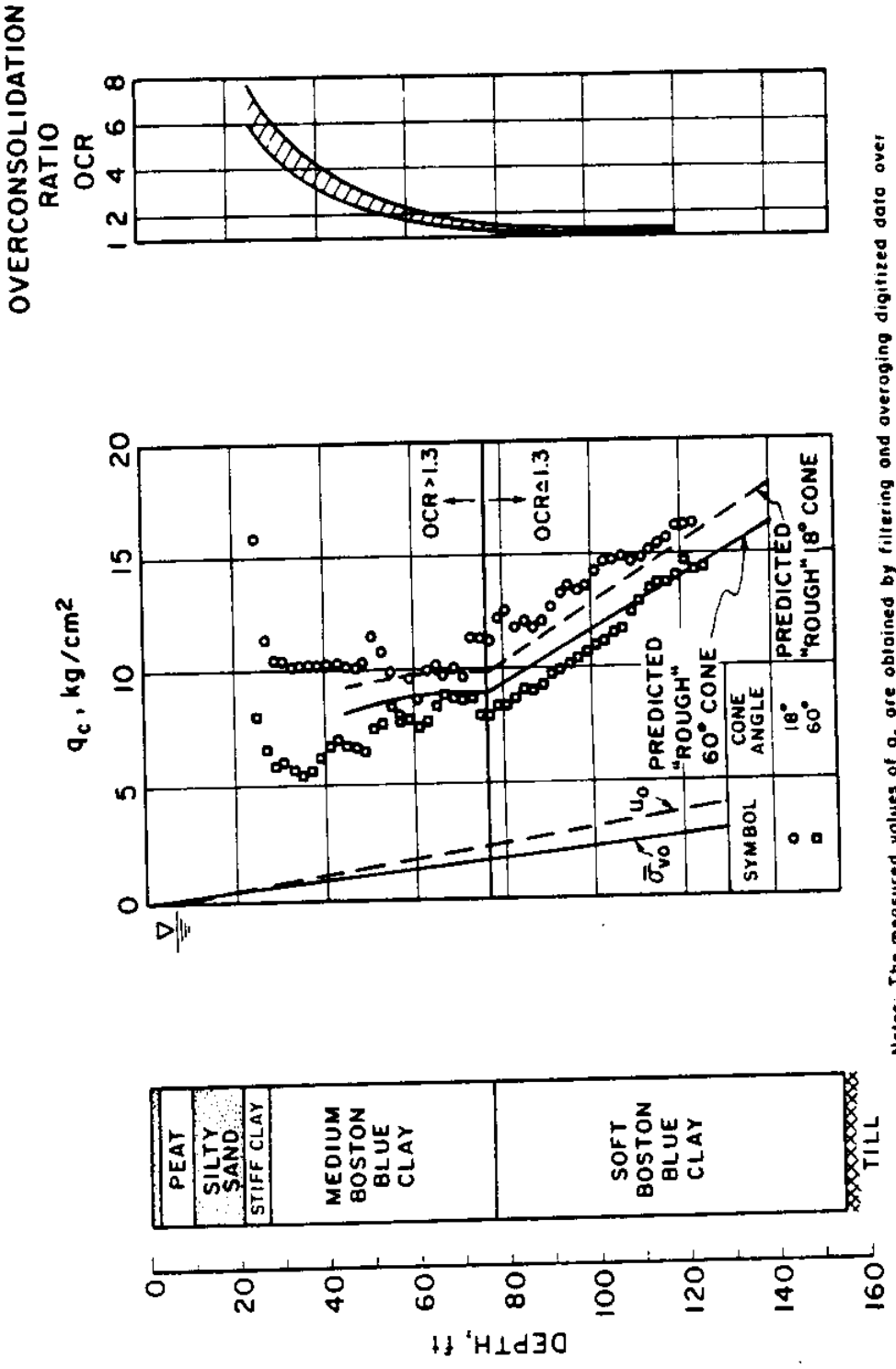

Figure 3.17 Predicted and measured point resistance in Boston Blue Clay (18° and 60° tips) at Station 246, Saugus, Massachusetts.

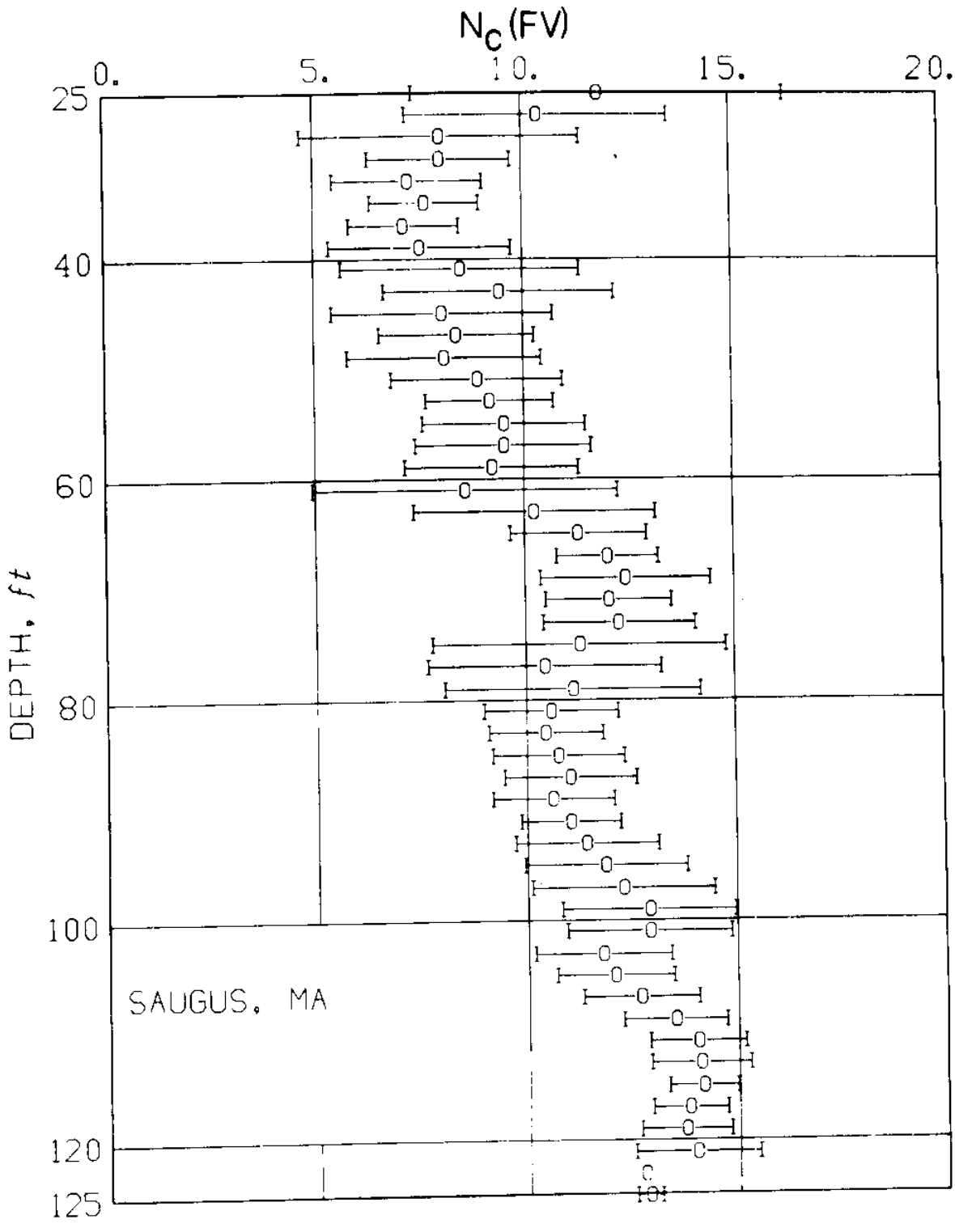

Figure 3.18 Empirical Cone Factor, $N_c(FV) = [q_c - \sigma_{vo}]/s_u(FV)$, at the Saugus, MA, test site.

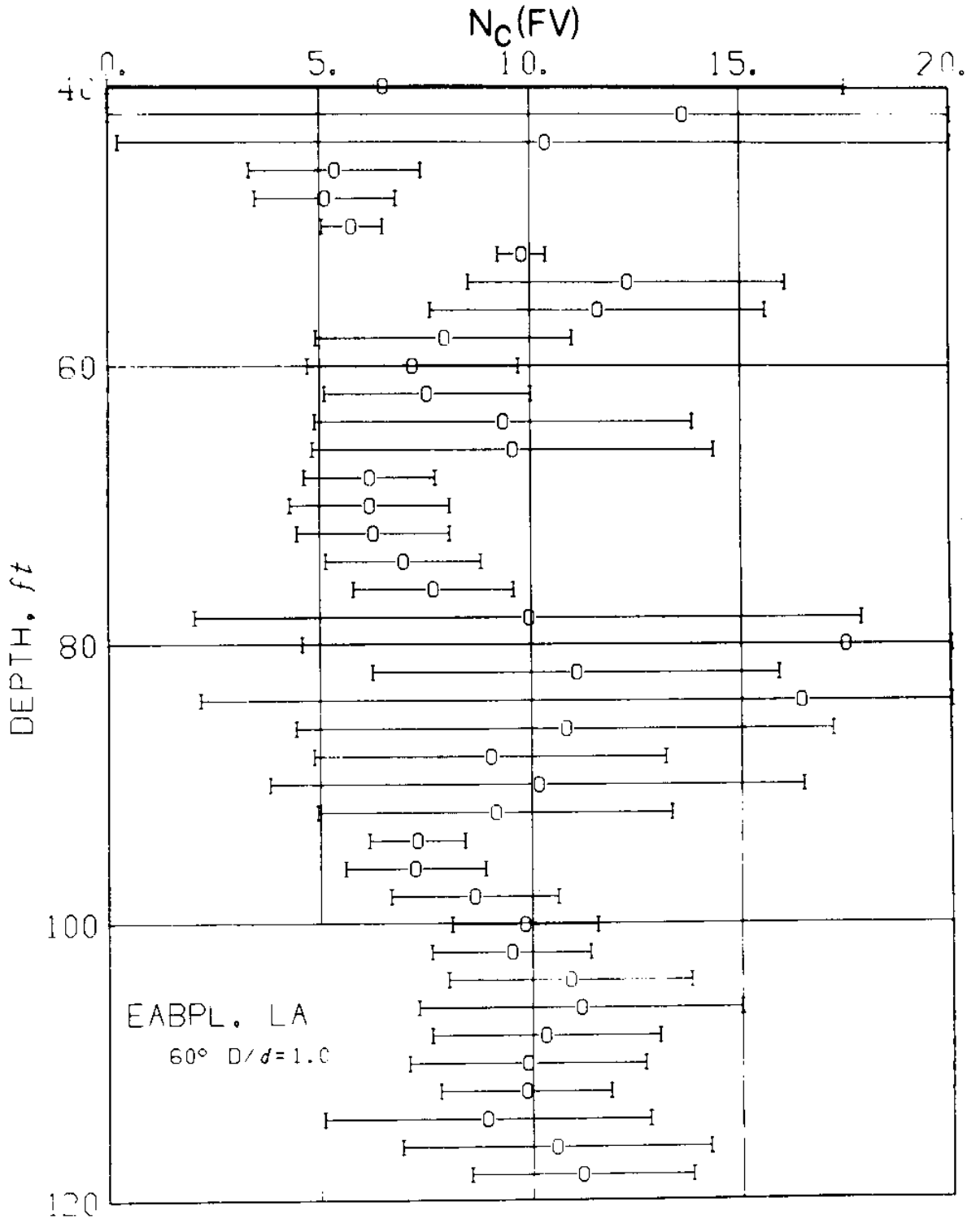

Figure 3.19 Empirical Cone Factor, $N_c(FV) = [q_c - \sigma_{vo}]/s_u(FV)$, at EABPL, LA.

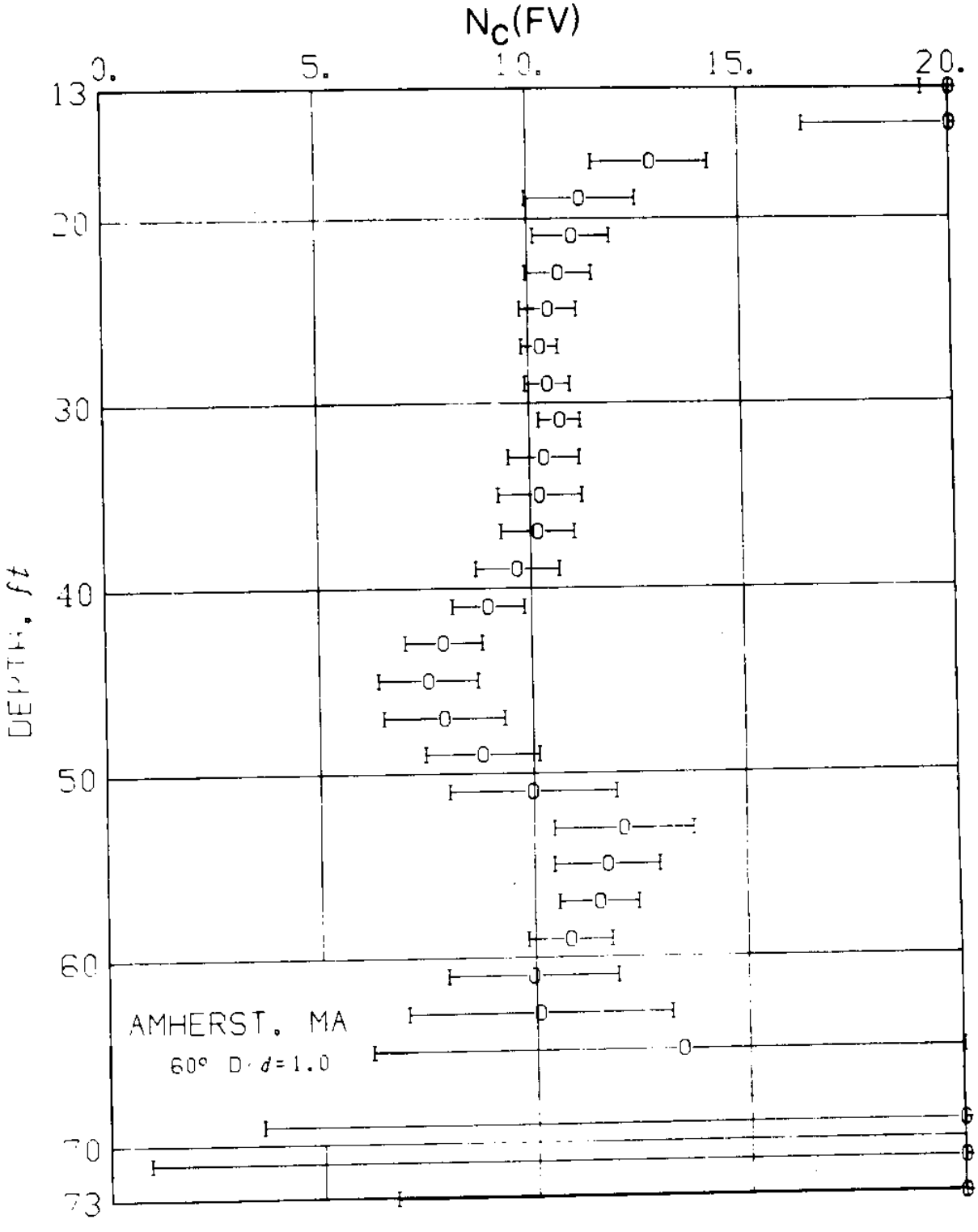

Figure 3.20 Empirical Cone Factor, $N_c(FV) = [q_c - \sigma_{vo}]/s_u(FV)$, at Amherst, MA.

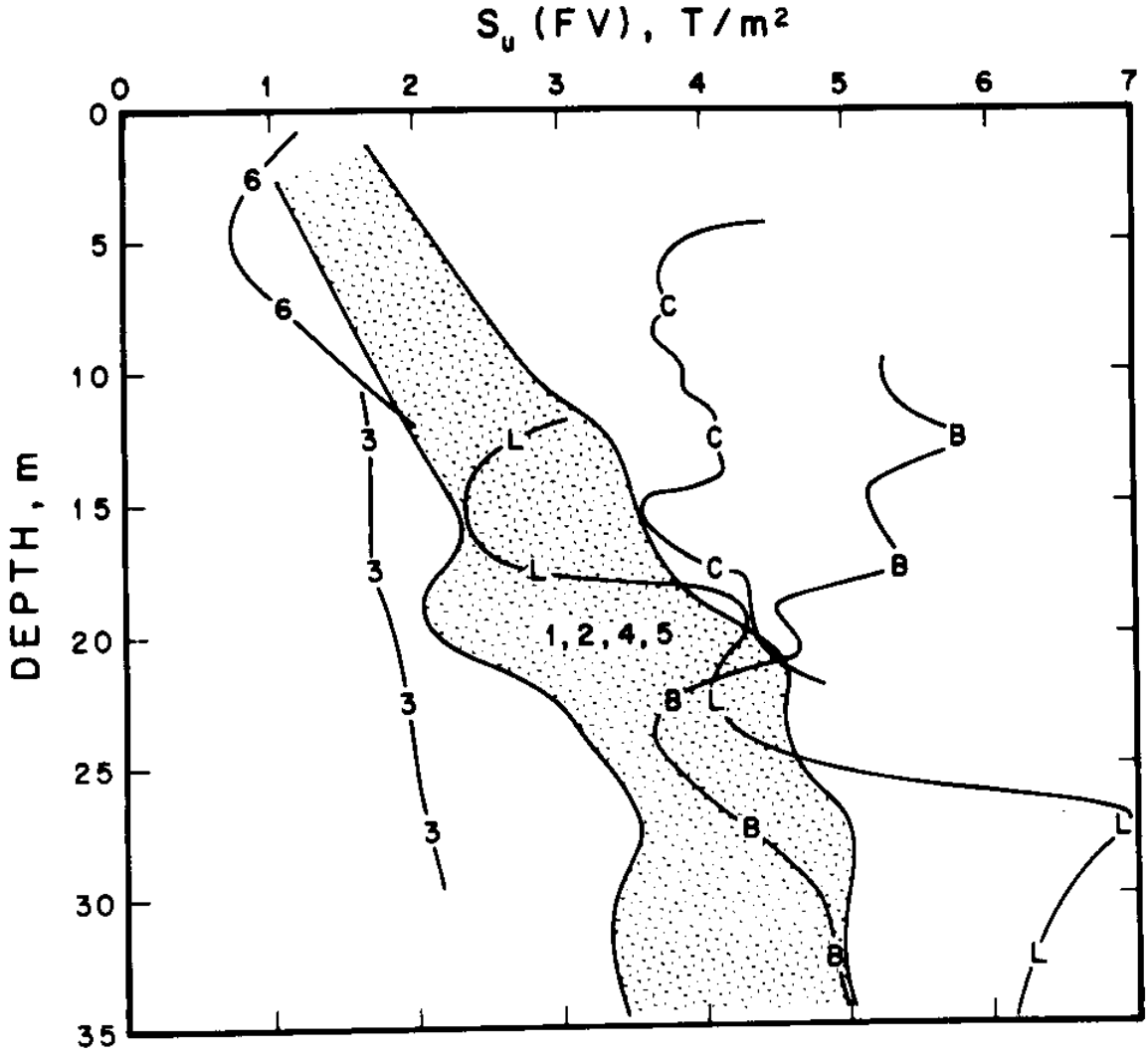

Figure 3.21 Average field vane strength profiles at M.I.T. and NGI-FUGRO test sites (see Tables 3.2 and 3.3 for site identification.

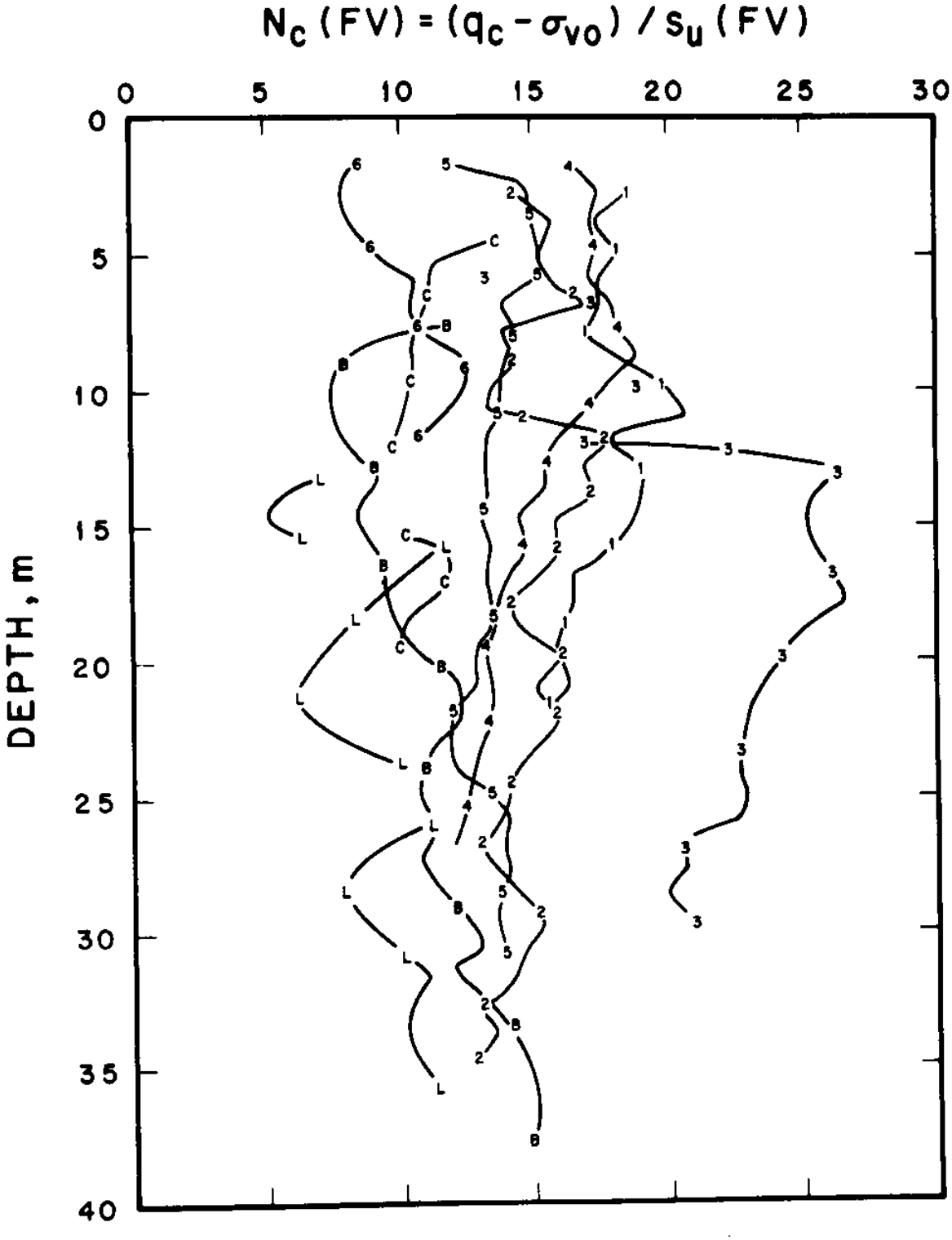

Figure 3.22 Empirical cone factor N_c(FV) vs. depth for nine clay deposits.

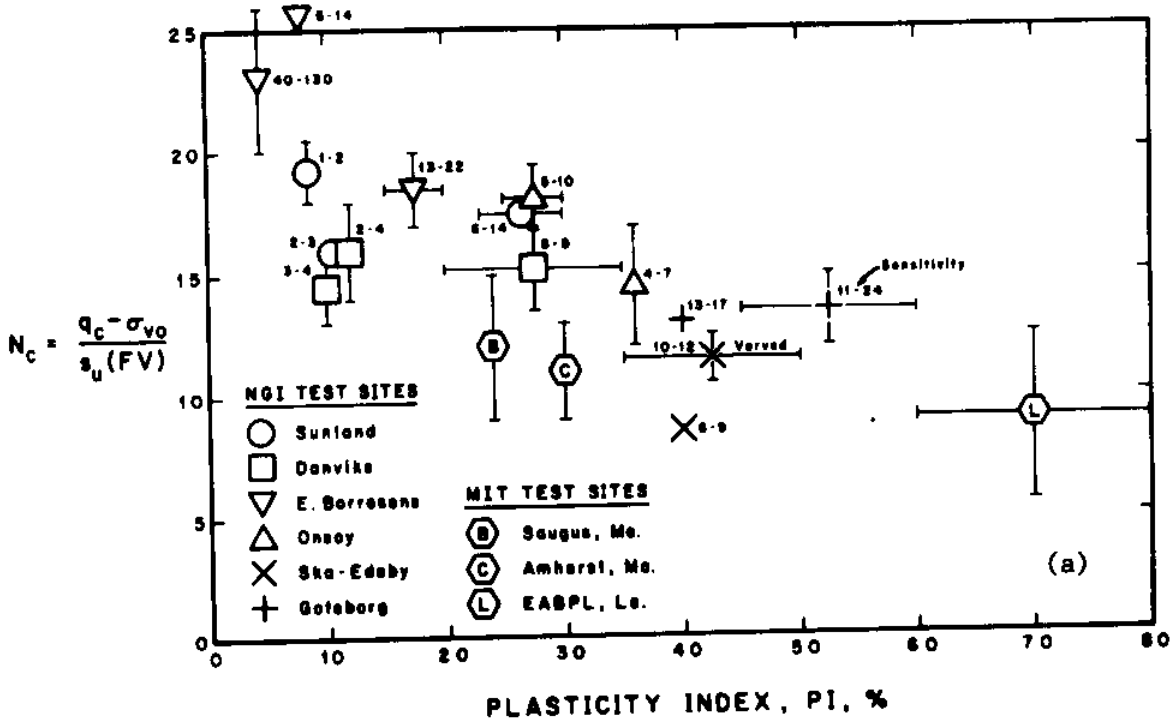

a - cone factor N_c(FV)

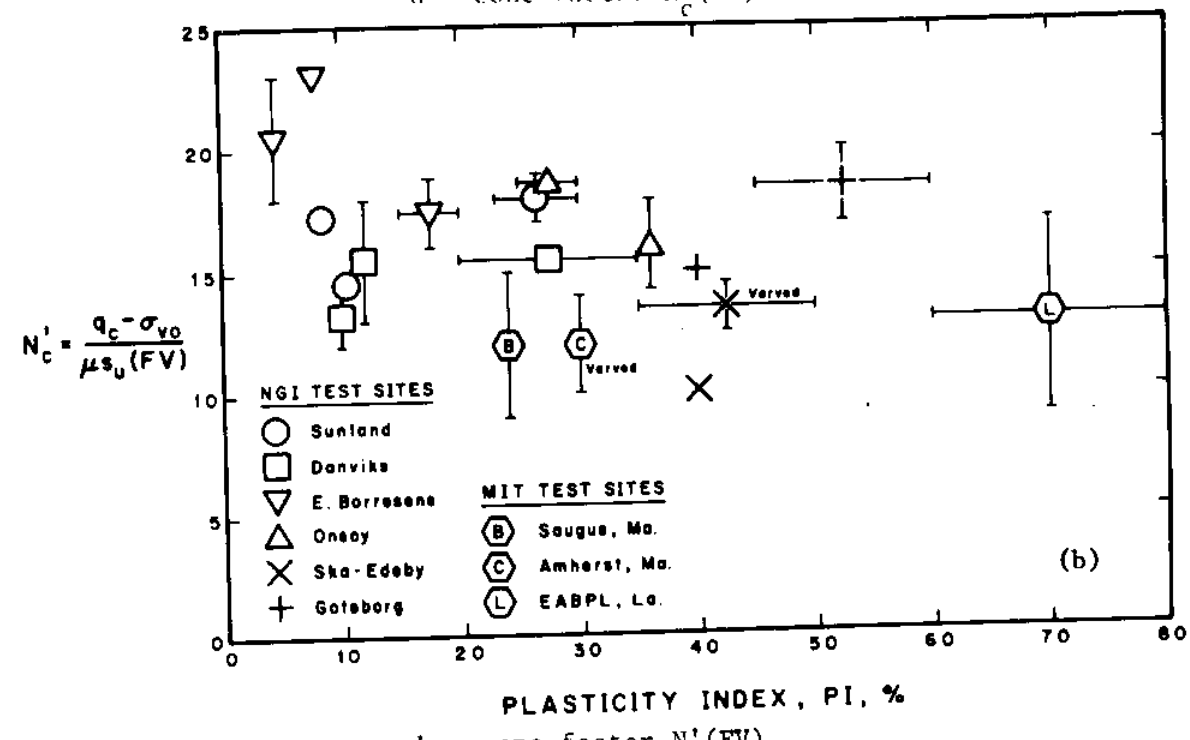

b - cone factor N_c'(FV)

Figure 3.23 Empirical cone factors N_c(FV) and N_c'(FV) for very soft to medium clays.

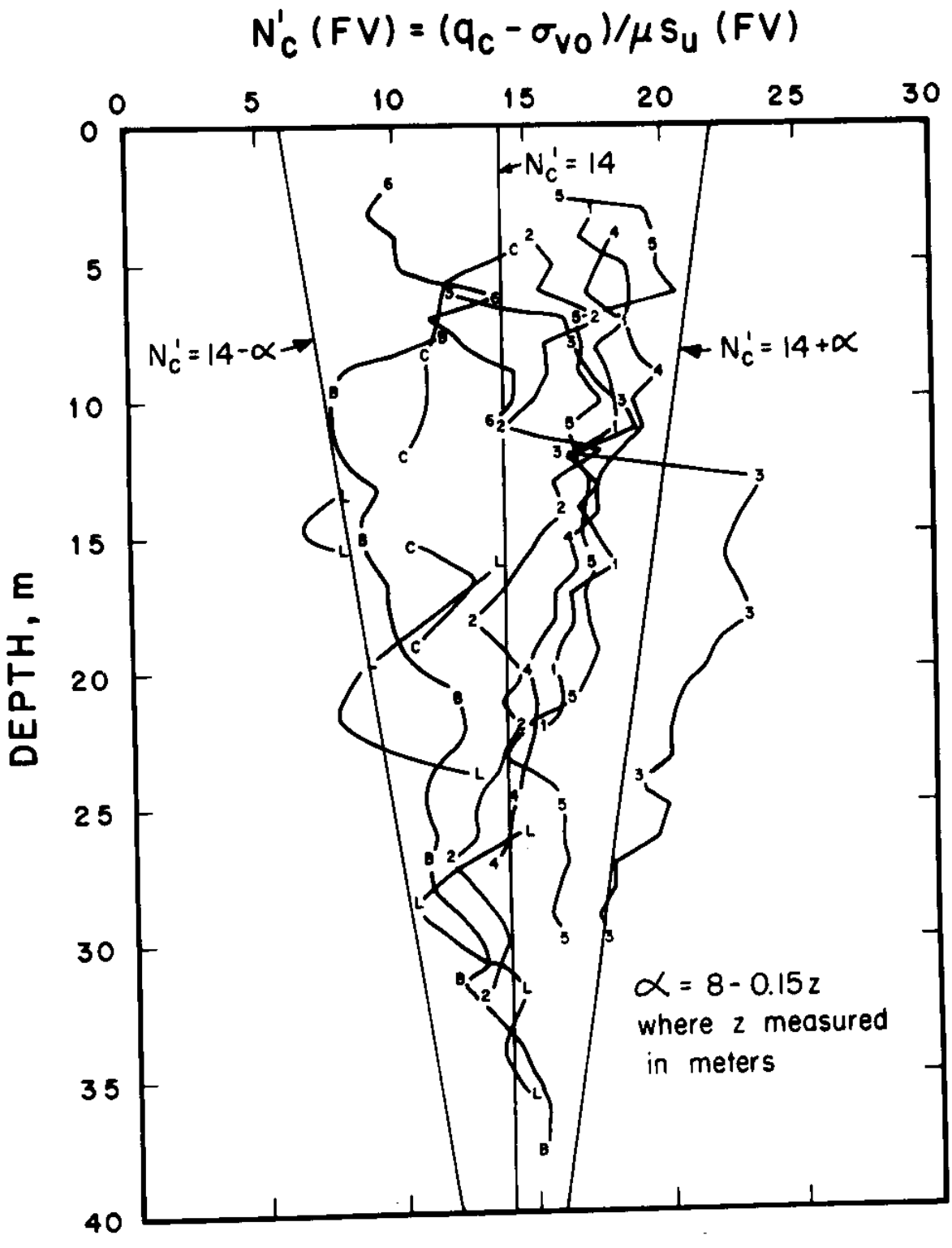

Figure 3.24 Empirical cone factor $N'_c(FV)$ vs. depth for nine clay deposits.

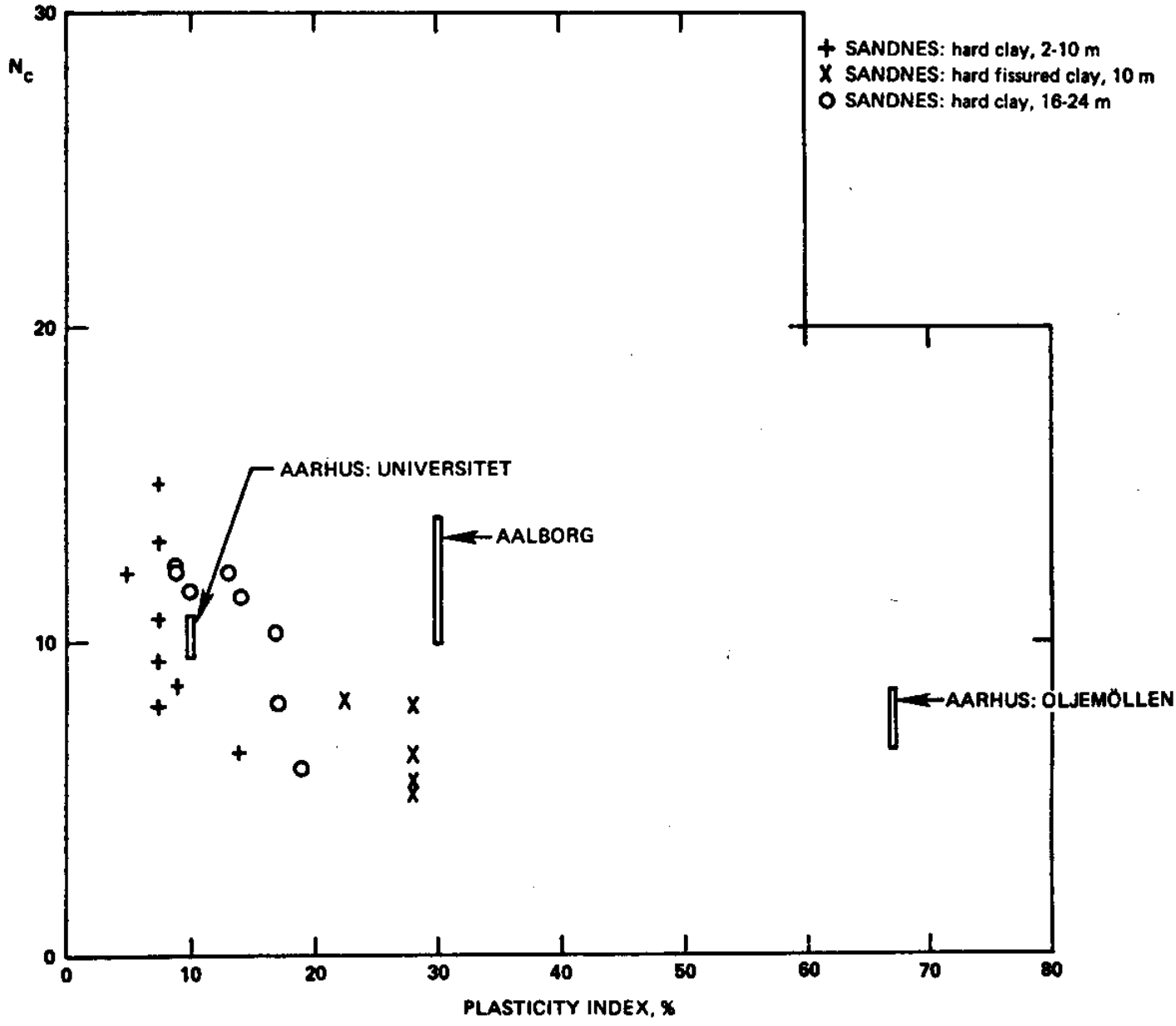

Figure 3.25 Empirical cone factors for stiff clays (NGI, 1975).

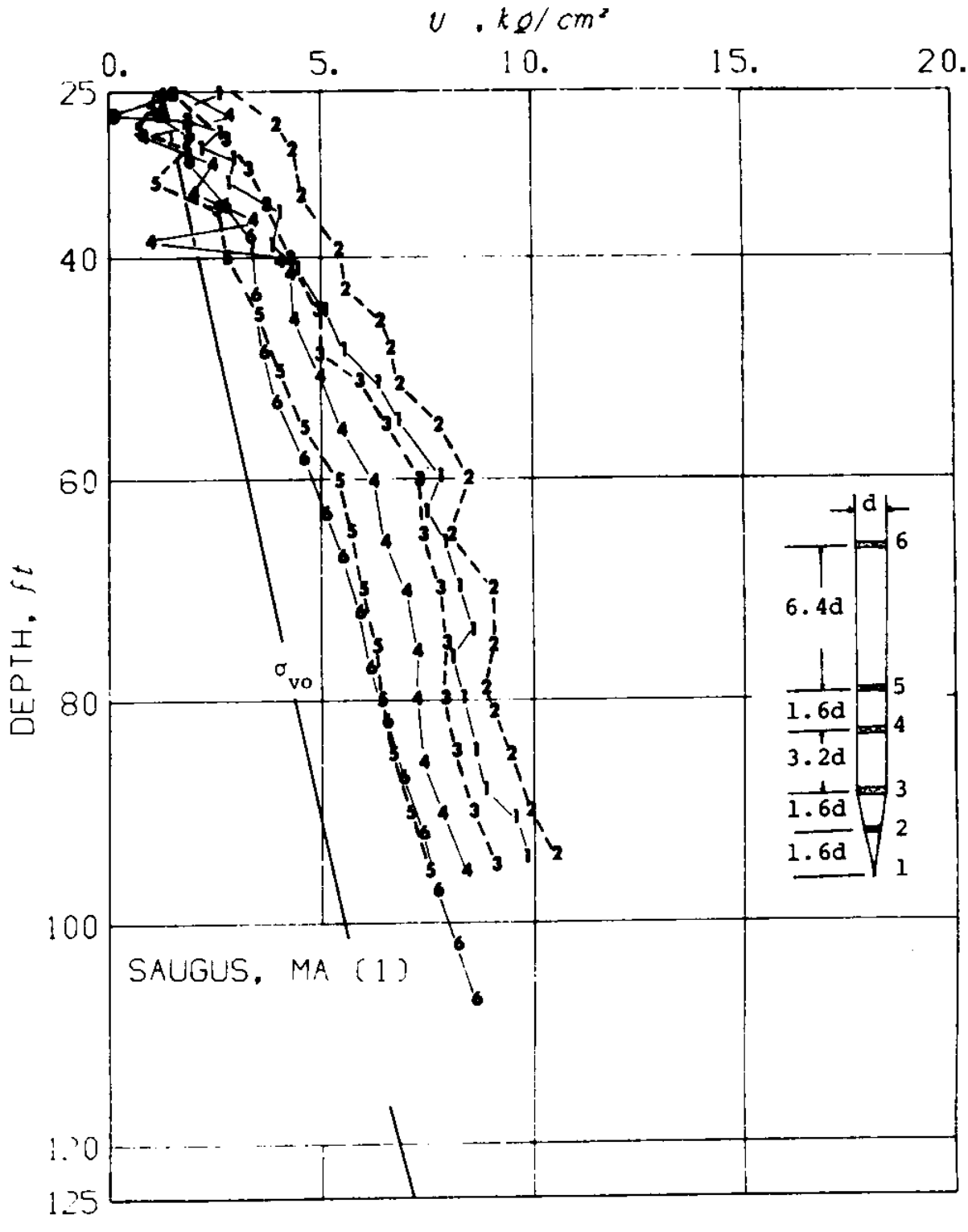

Figure 3.26 Pore pressures measured along an 18° unenlarged cone during steady penetration.

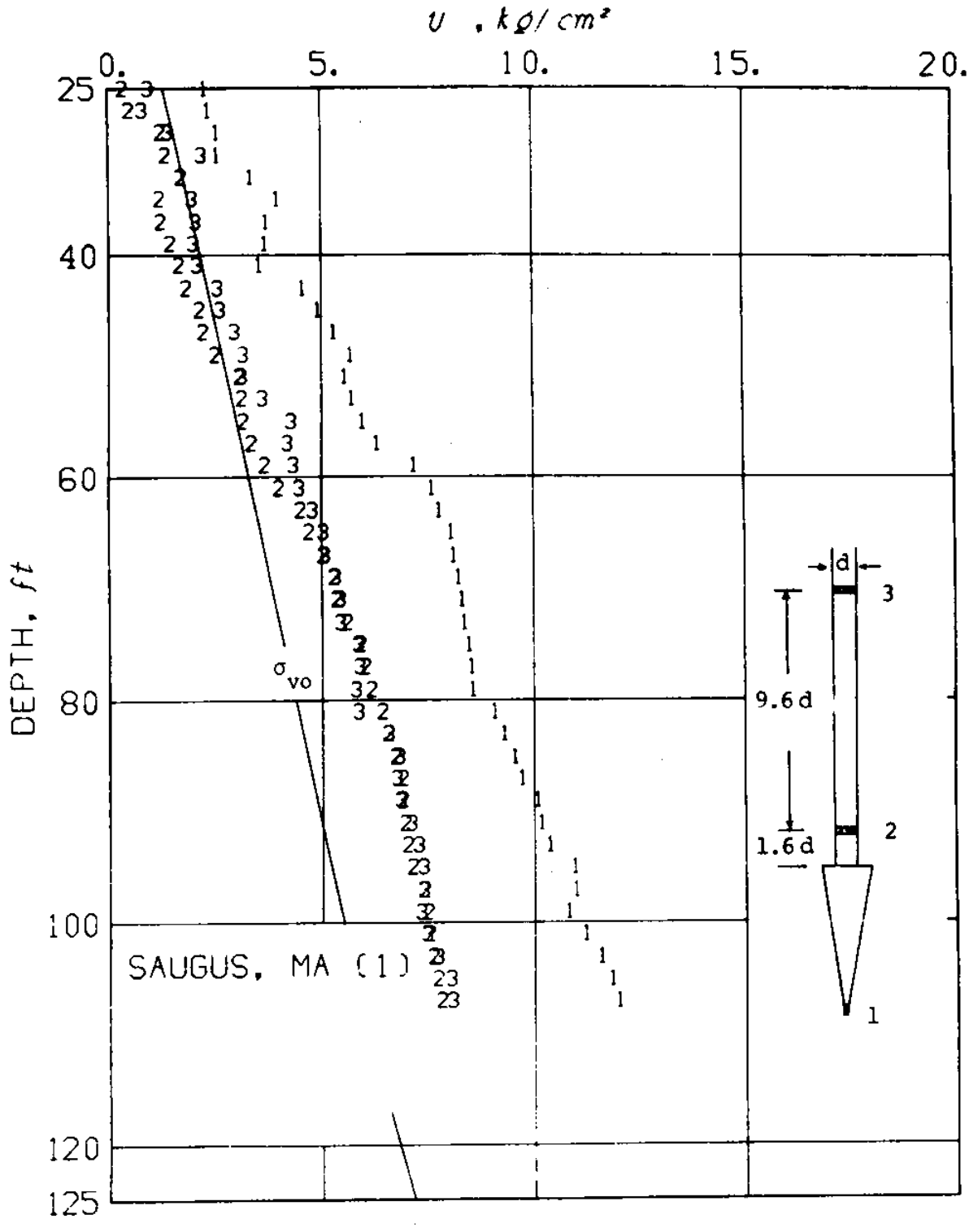

Figure 3.27 Pore pressures measured along an 18° enlarged cone during steady penetration.

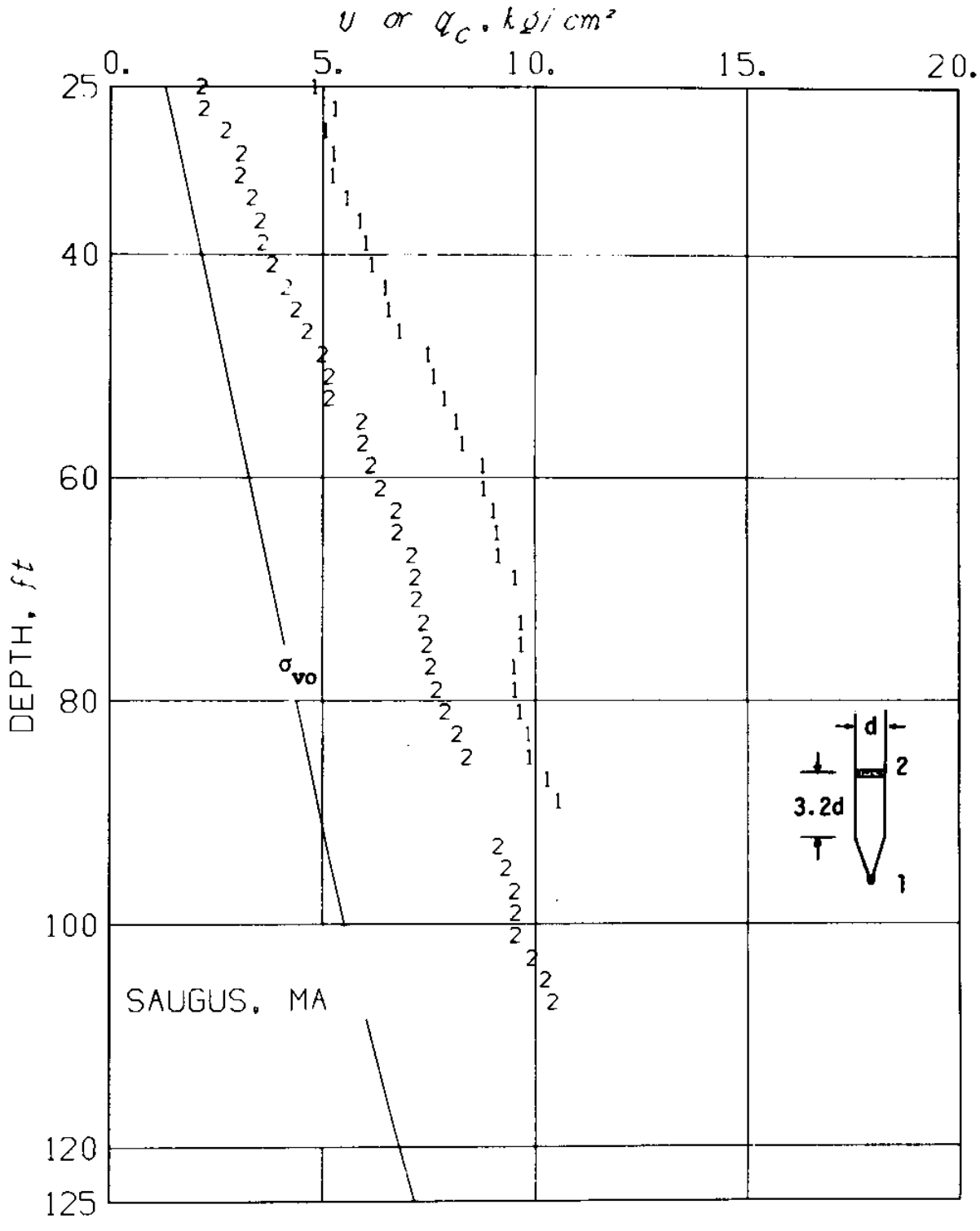

Figure 3.28 Pore pressures measured along a 60° unenlarged cone during steady penetration.

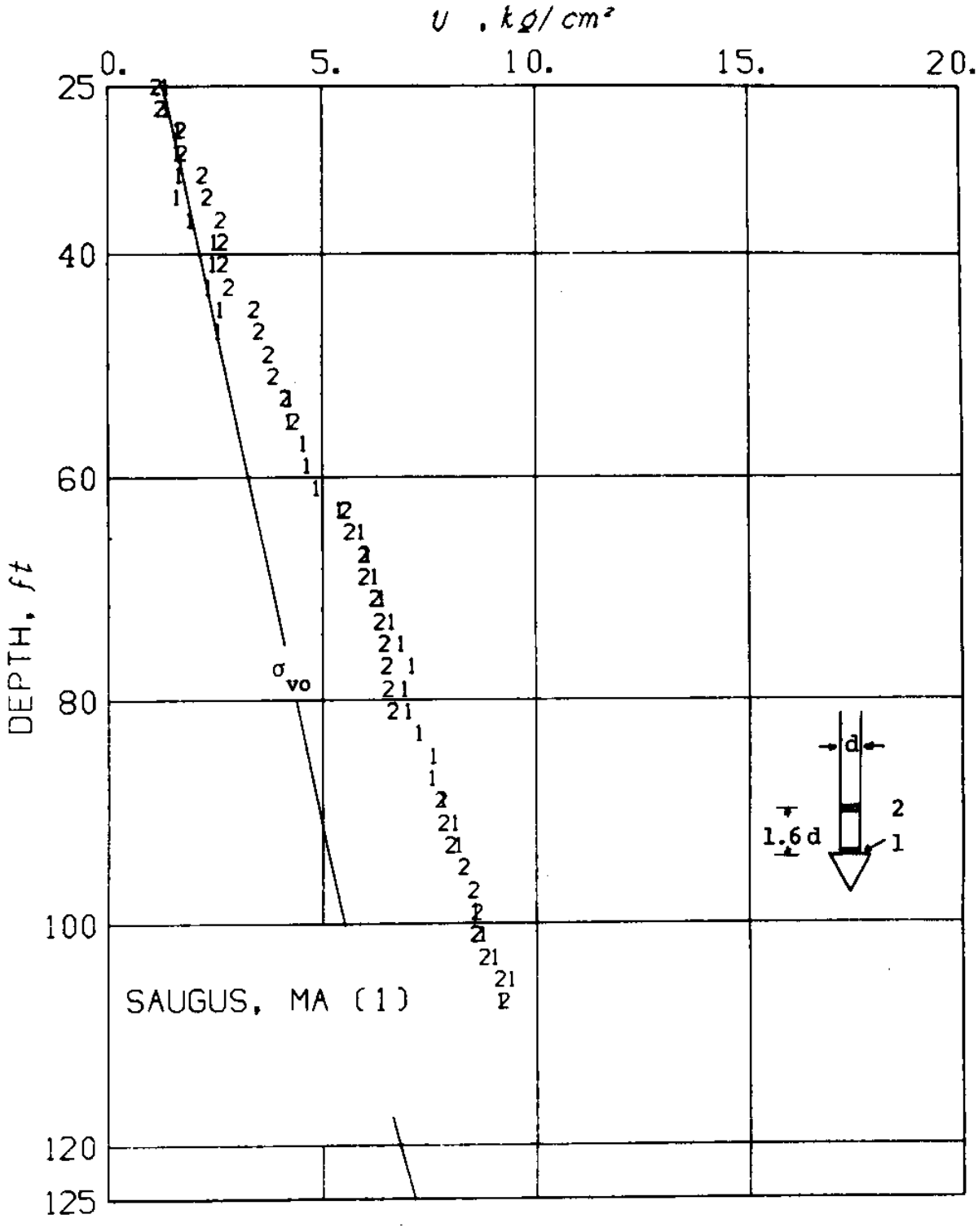

Figure 3.29 Pore pressures measured along a 60° enlarged cone during steady penetration.

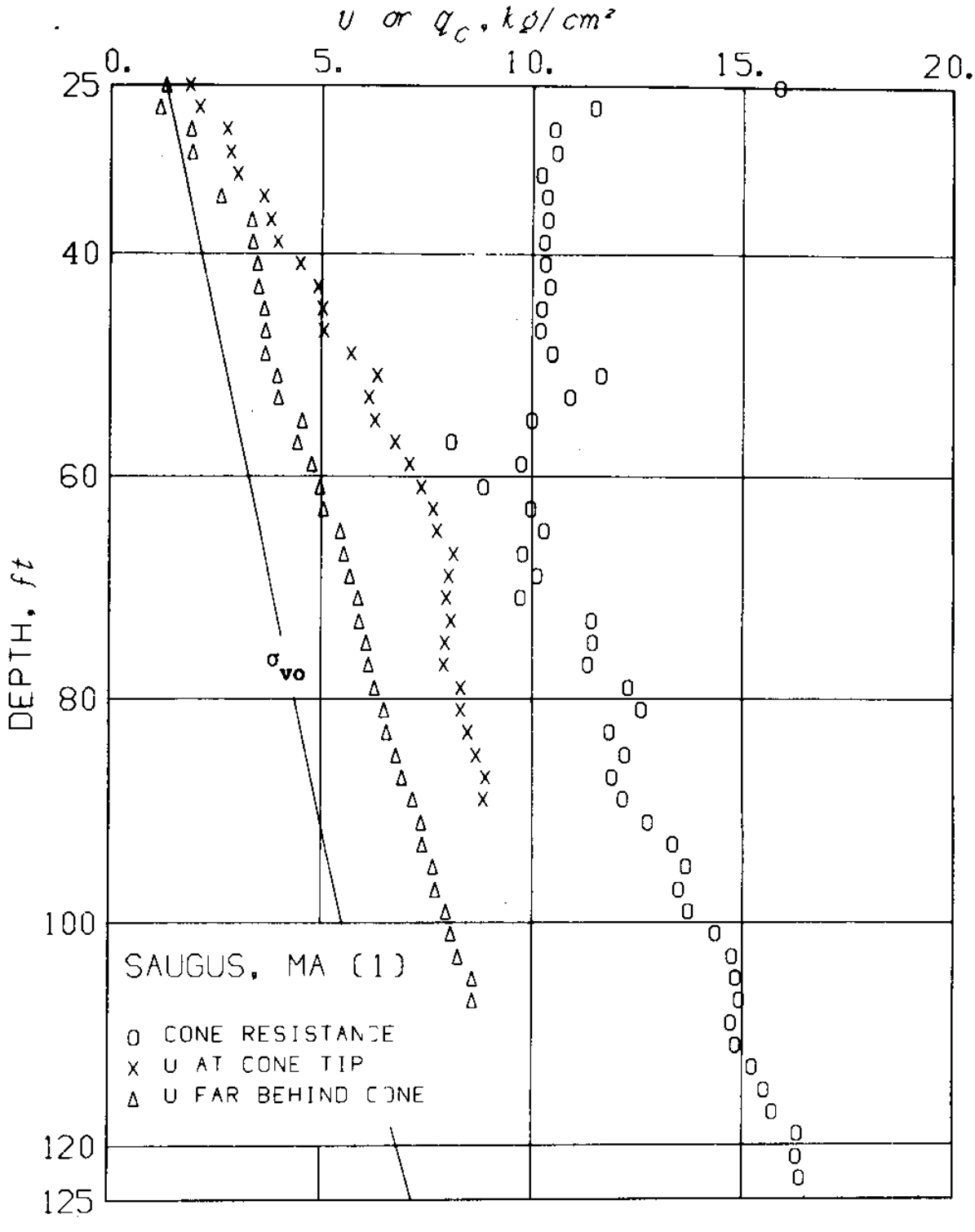

Figure 3.30 Cone resistance and pore pressures for an 18° unenlarged cone ($2\delta = 18°$, D/d = 1) in Boston Blue Clay.

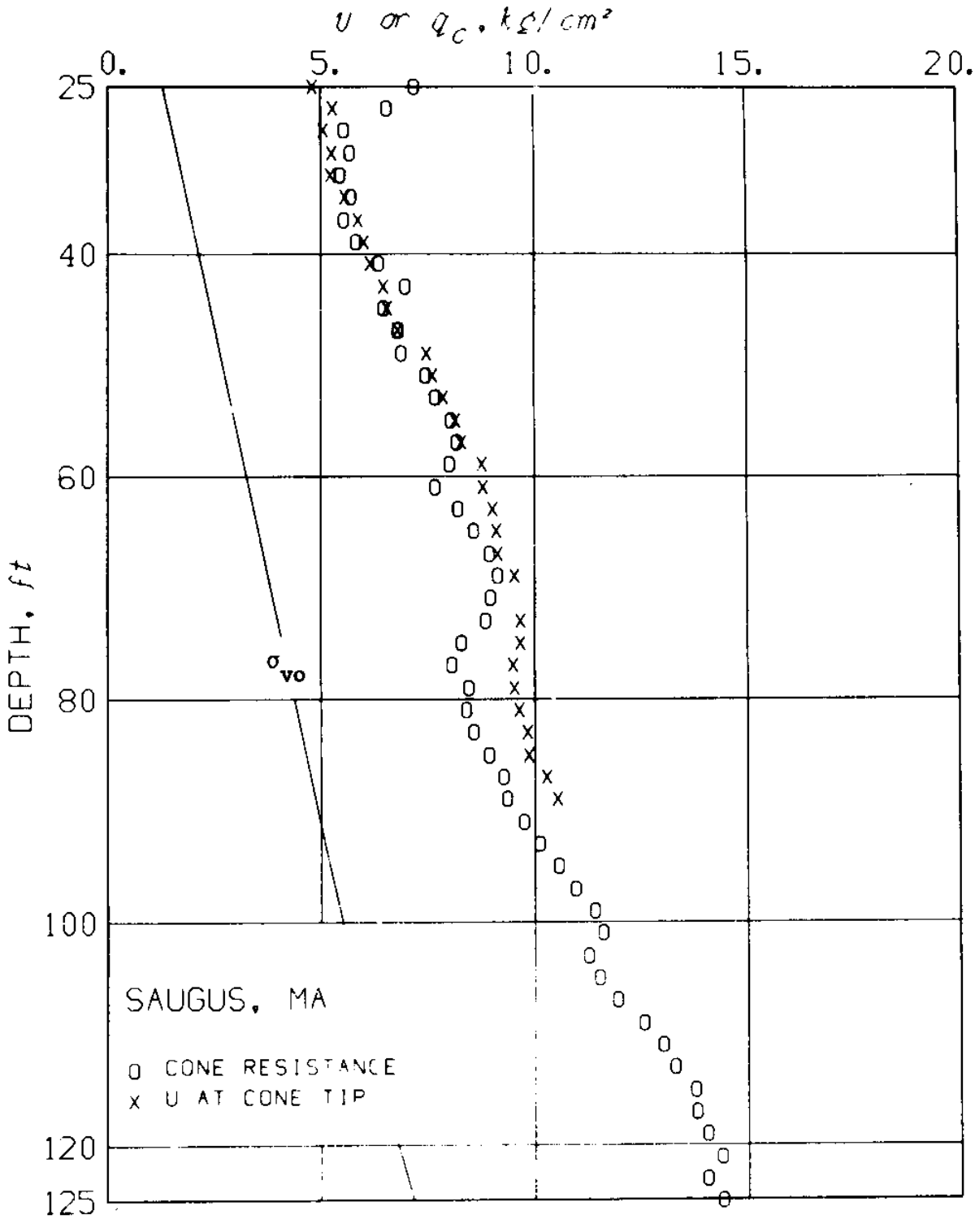

Figure 3.31 Cone resistance and pore pressures for a 60° unenlarged cone (2δ = 60°, D/d = 1) in Boston Blue Clay.

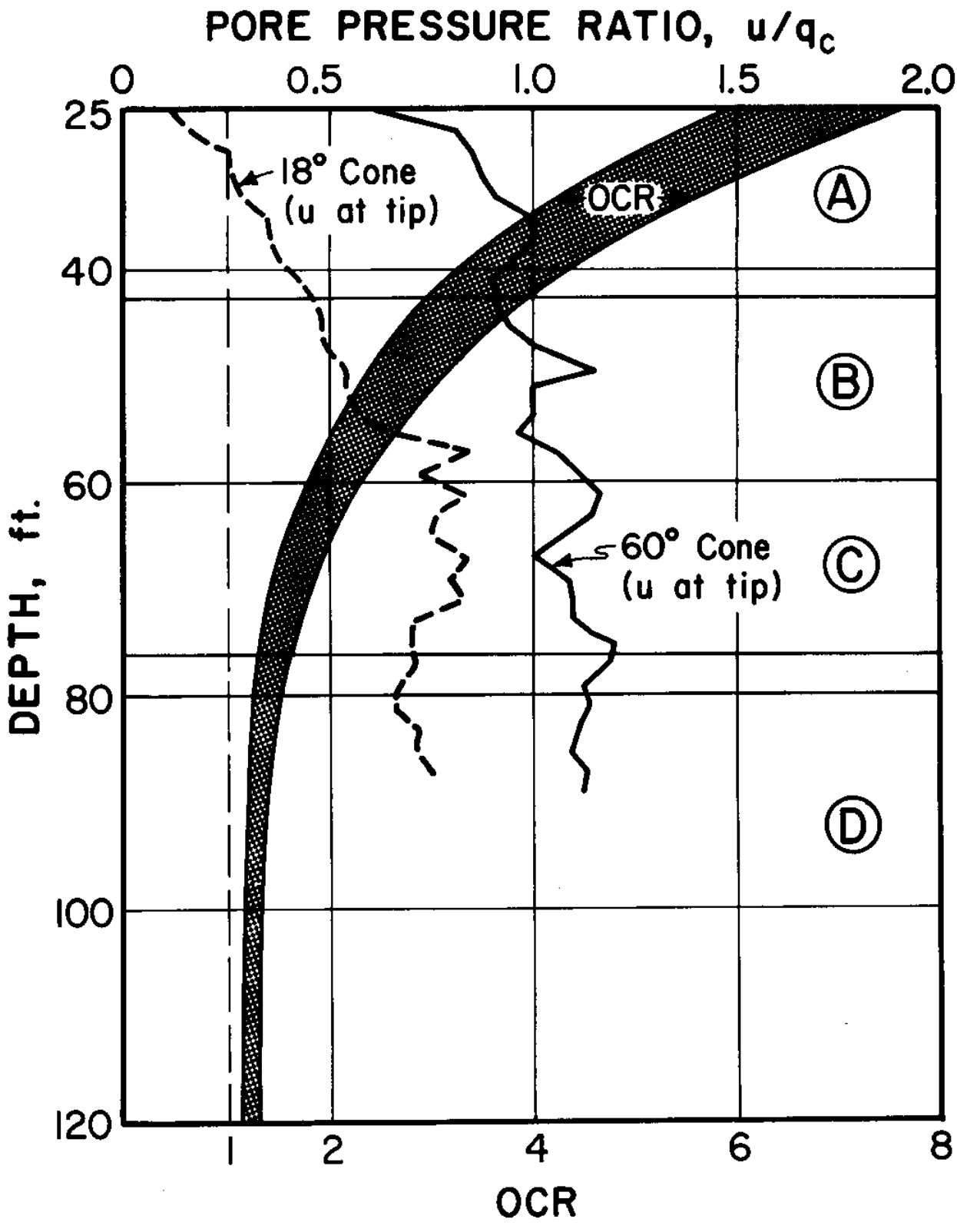

Penetration pore pressure to cone resistance ratio

Figure 3.32 Penetration pore pressure to cone resistance ratio in Boston Blue Clay.

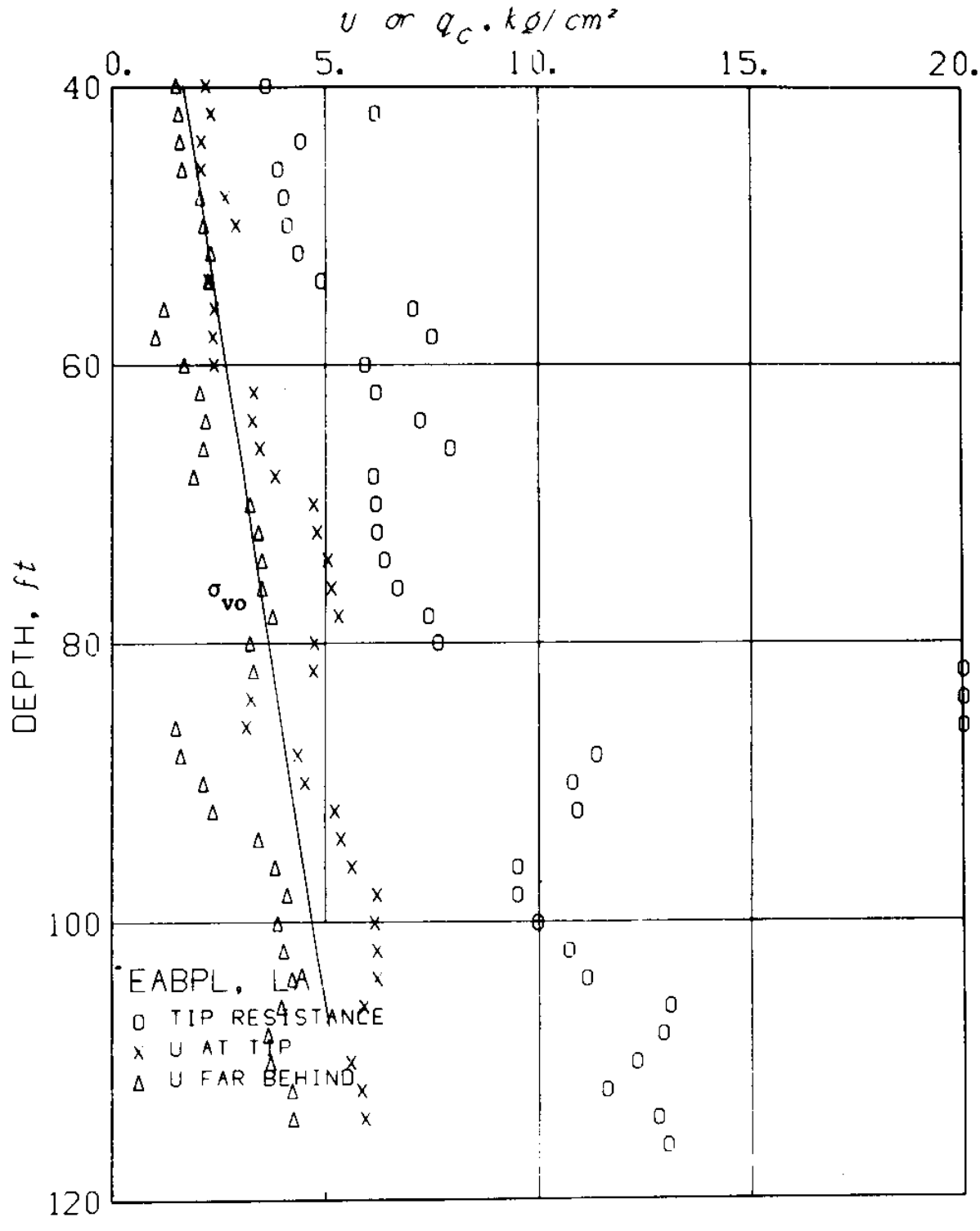

Figure 3.33 Cone resistance and pore pressure for an 18° unenlarged cone (2δ = 18°, D/d = 1) in EABPL clay.

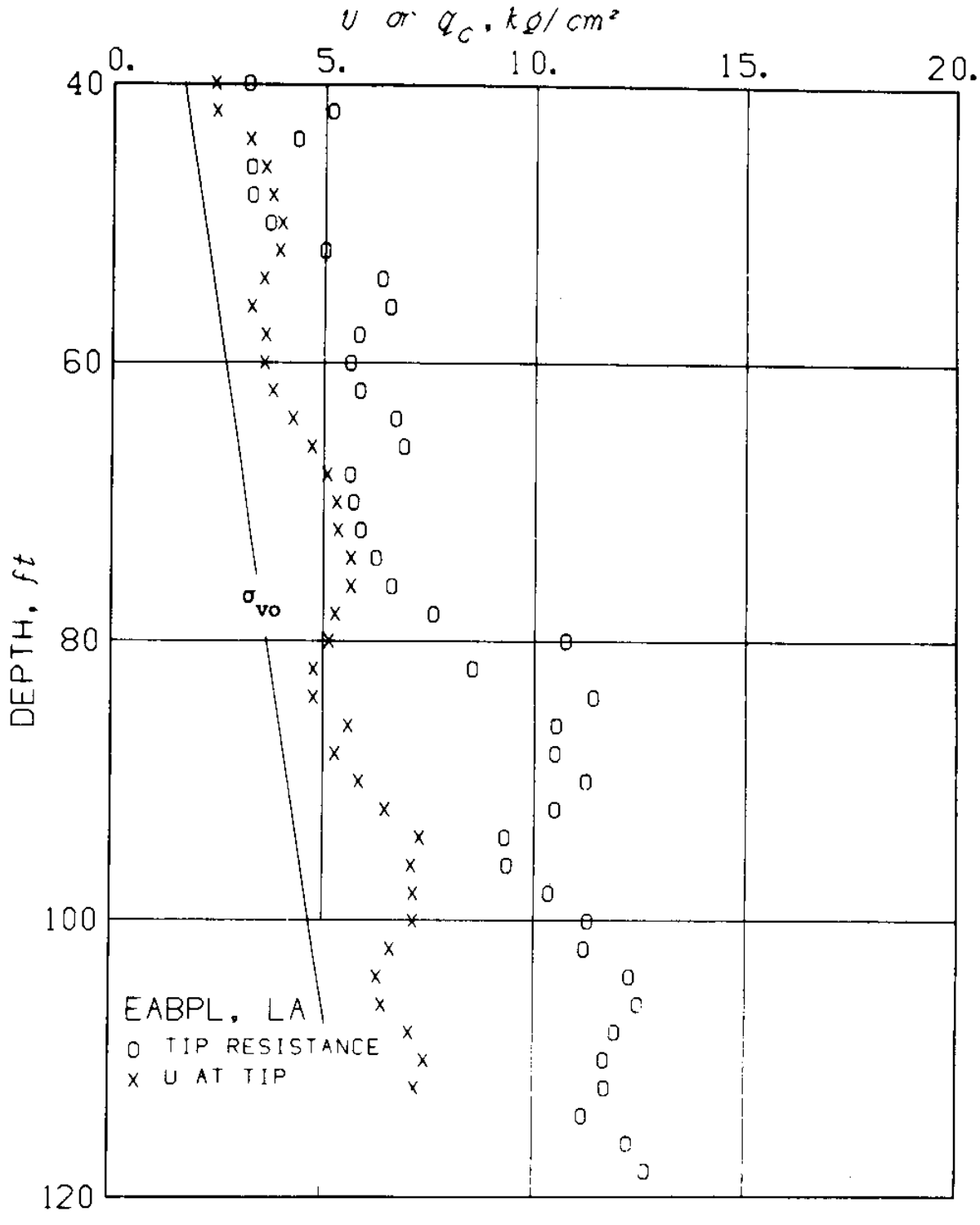

Figure 3.34 Cone resistance and pore pressure for a 60° unenlarged cone (2δ = 60°, D/d = 1) in EABPL clay.

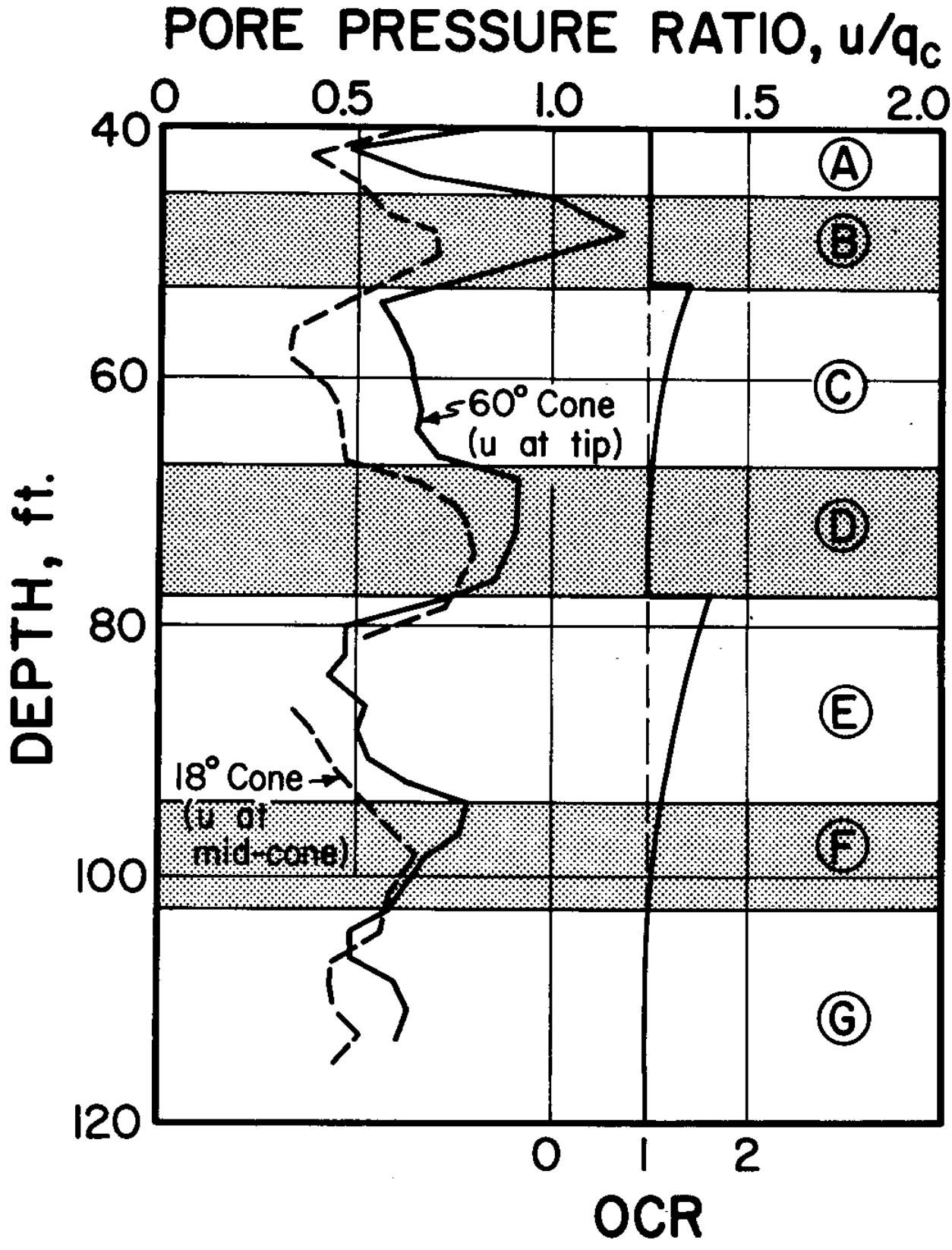

Penetration pore pressure to cone resistance ratio

Figure 3.35 Penetration pore pressure to cone resistance ratio in EABPL clay.

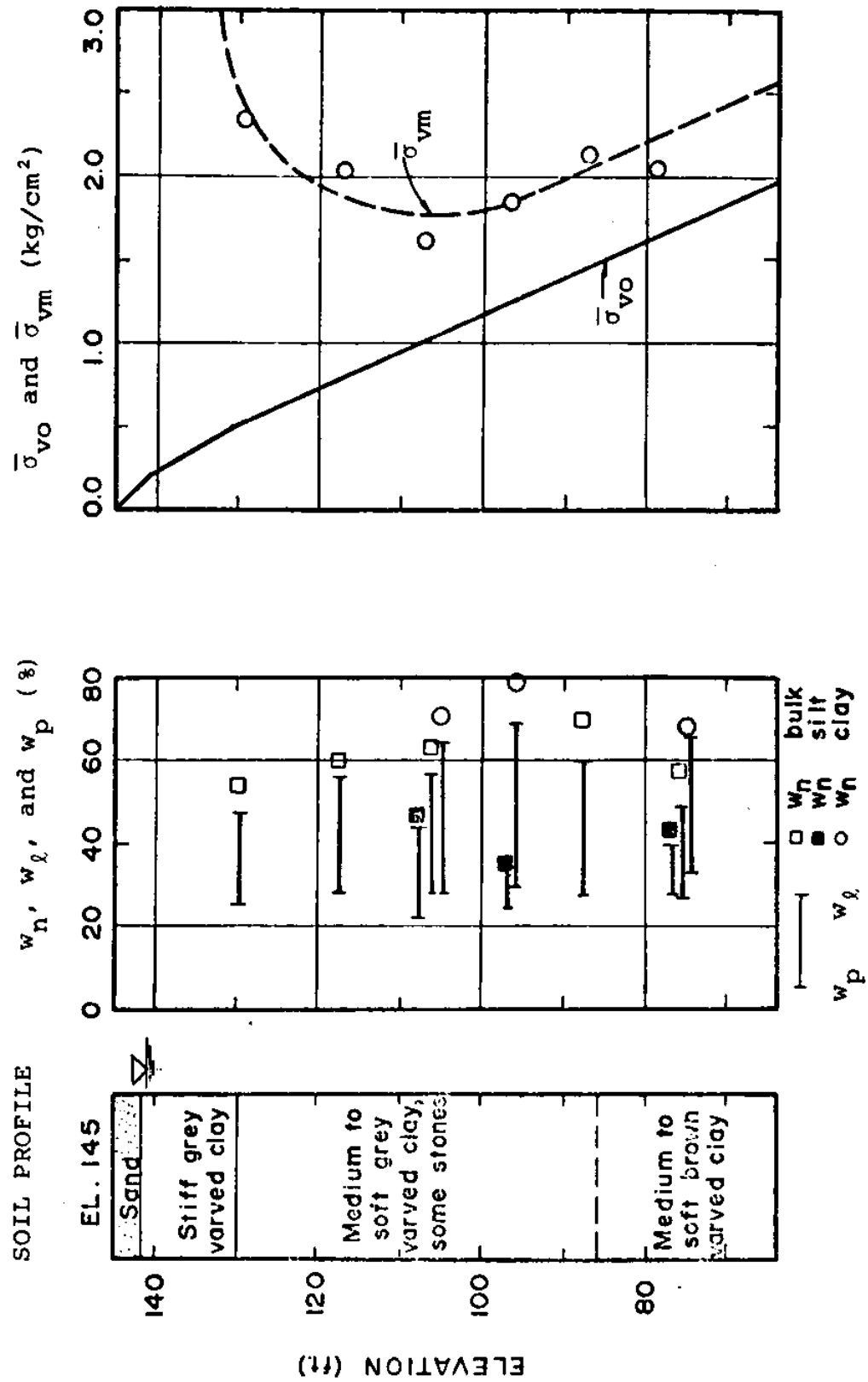

Figure 3.36 Soil conditions at the Amherst, MA, test site. (Route 116 Bypass and North Hadley Road; data from Ladd (1975); drawing courtesy of S.M. Lacasse).

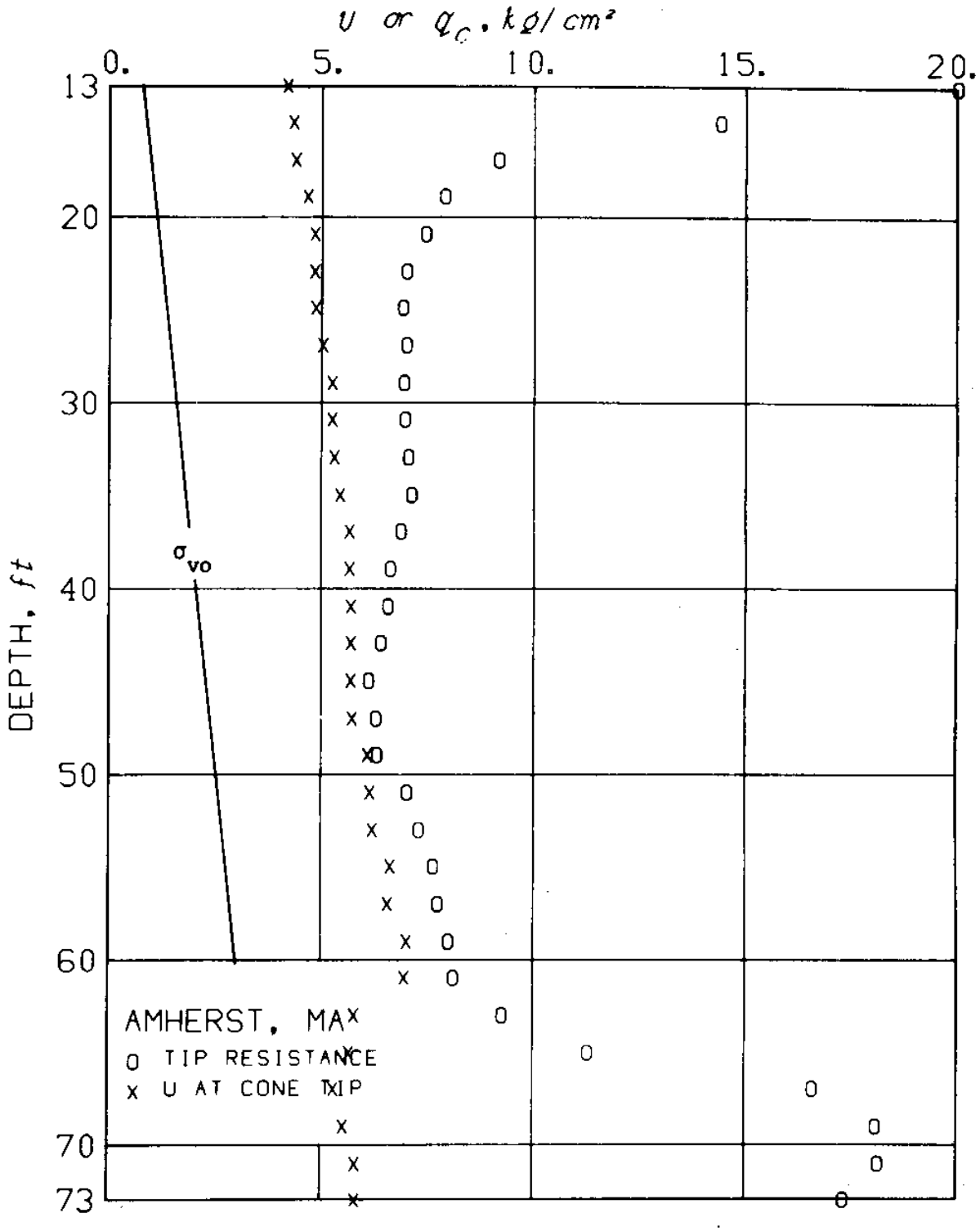

Figure 3.37 Cone resistance and pore pressure for an 18° unenlarged cone (2δ = 18°, D/d = 1) in Connecticut Valley Varved Clay.

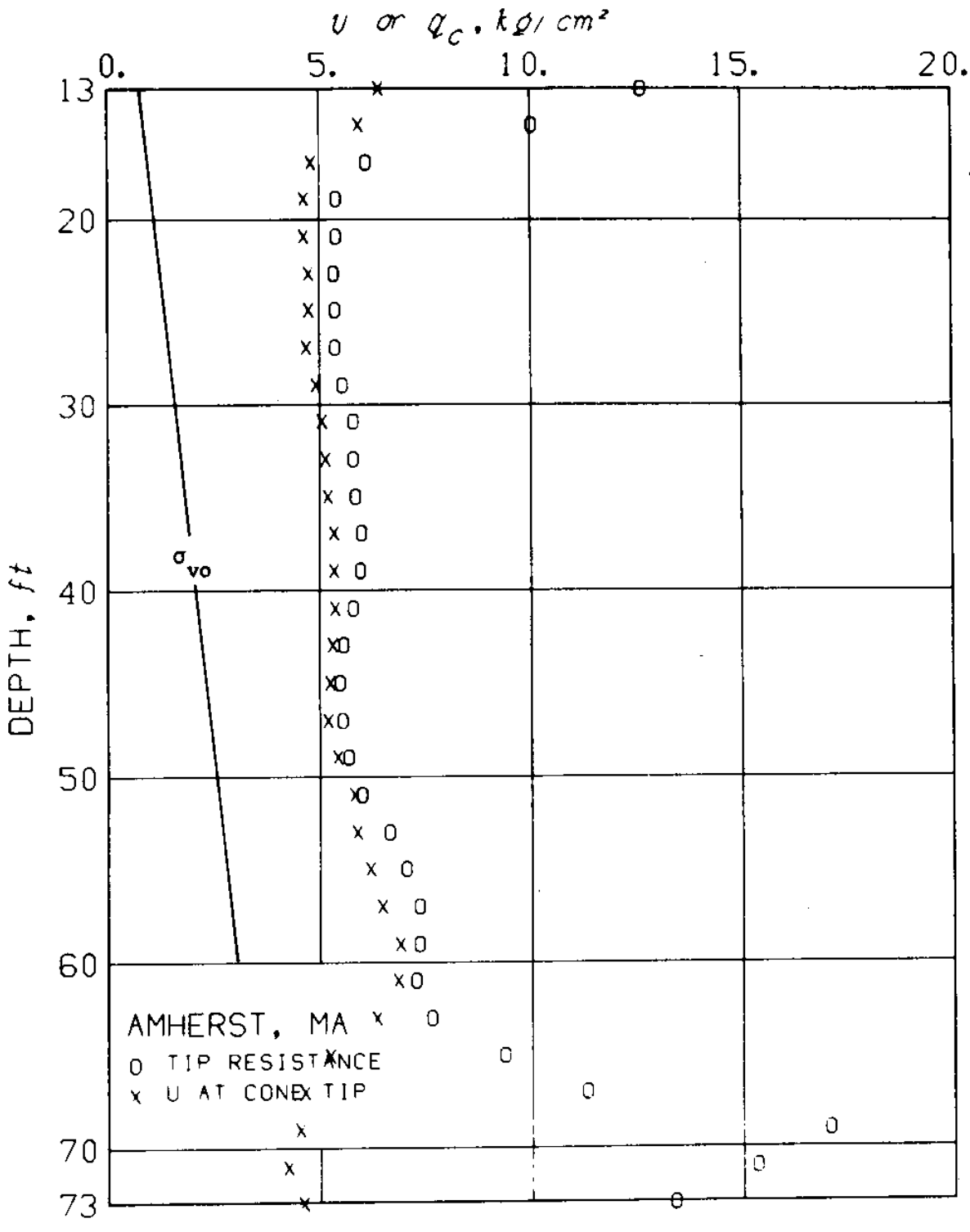

Figure 3.38 Cone resistance and pore pressure for a 60° unenlarged cone (2δ = 60°, D/d = 1) in Connecticut Valley Varved Clay.

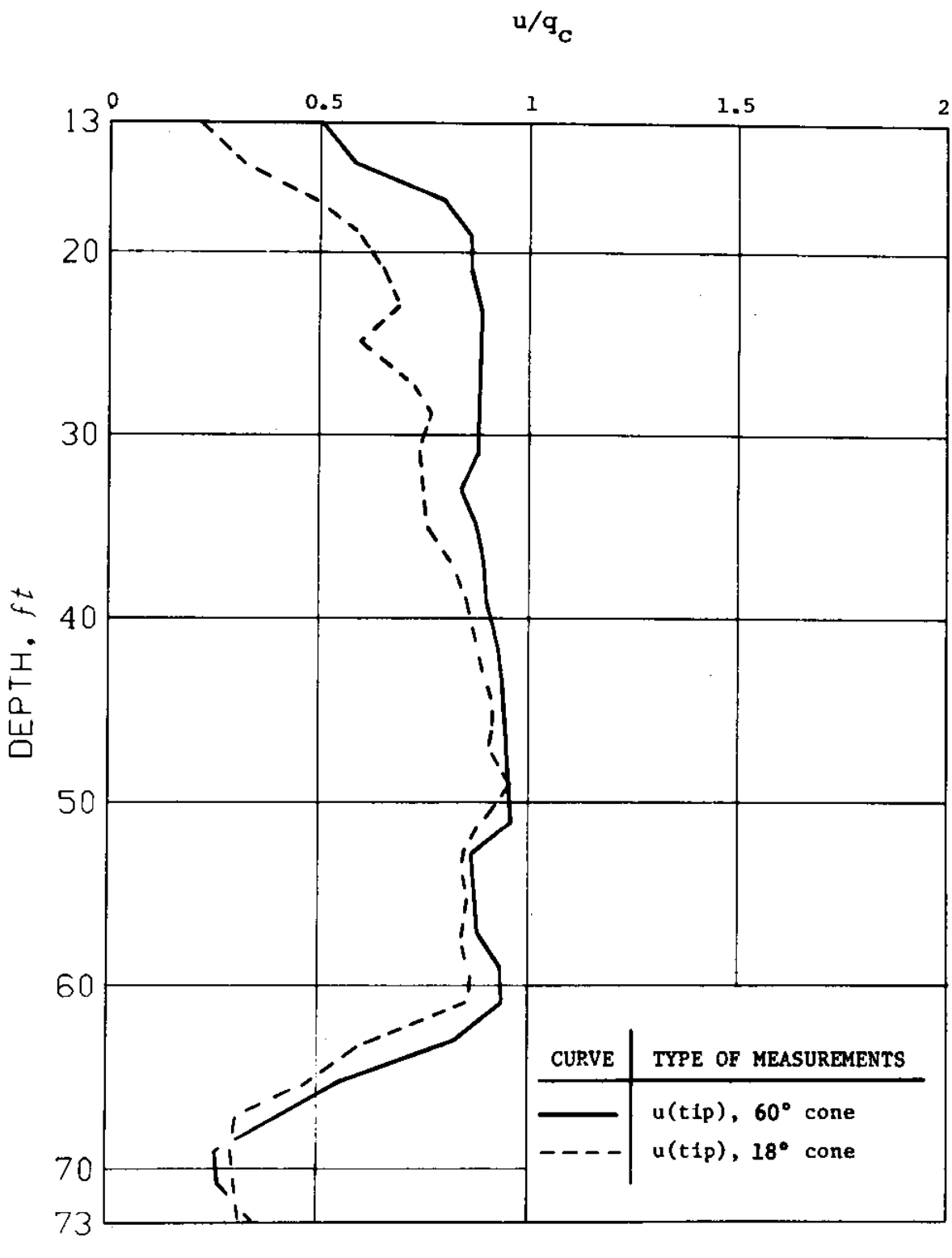

Figure 3.39 Pore pressure to cone resistance ratios in Connecticut Valley Varved Clay.

CHAPTER 4

OFFSHORE CONE PENETRATION RESULTS

4.1 INTRODUCTION

Instituto Tecnologico Venezolano del Petroleo (INTEVEP) is conducting a major geotechnical exploration program offshore the Venezuelan coast in order to determine the foundation soil conditions for proposed offshore structures. During the summer of 1979, drilling, sampling and in situ tests were conducted from the M/V SURVEYOR by FUGRO Gulf, Inc., acting as the geotechnical consultants. In situ pore pressure measurements were performed under the supervision of M.I.T. using piezometer probes manufactured by Geotechniques, Int.

According to FUGRO (1979a and b), the borings were drilled through a center well fabricated in the deck of the vessel using power tong rotary drilling techniques and a 5 inch OD IF drill pipe with an open-ended drill bit. The drill string was made up of the appropriate drilling subs and drill collars to enable using the push sampling and in situ tools. A heave compensator was used to control the vertical motion of the drill string during drilling, sampling, and in situ testing operations (see Fig. 2.1).

Cone penetration tests were conducted by means of the FUGRO/WISON equipment which is capable of pushing electrical cones and conical piezometer probes at a constant rate of

penetration of 2cm/sec. The WISON uses the weight of the drill string to provide the necessary reaction. A drill string anchor (packer) was used in some cases to provide the necessary additional reaction to penetrate hard soils. Cone resistance data, q_c , was measured by the FUGRO cone and penetration pore pressures, u, were measured by the special conical piezometer probes (see Chapter 2).

This chapter presents in situ cone penetration results at three sites where M.I.T. performed pore pressure measurements. Cone penetration data consisting of the cone resistance, q_c, and penetration pore pressures, u, are then correlated to soil properties determined from laboratory test results obtained by FUGRO onboard the vessel, Catholic University in Caracas, Venezuela, and by M.I.T.(Ladd et al., 1980).

Figure 4.1 shows the locations of the three sites investigated herein (E1, F1 and D2). At each site the following was done:

1) one boring to determine the soil stratigraphy and to obtain soil samples;

2) a second to perform cone penetrometer tests. At site D2, sampling and cone penetrometer tests were performed interchangeably in the same boring.

3) a third boring to conduct pore pressure measurements (pore pressure measurements were performed in two borings at site D2; the first to depth 108 ft below the mudline and the second to 46 ft);

4) in situ vane tests to depth 50 ft at site E1. This was performed in a separate boring adjacent to the cone penetrometer boring.

4.2 SOIL STRATIFICATION

Figure 4.2 shows the stratification at site E1 where the water depth was 85.5 ft. The first column represents the depth, in feet, below mudline. The second shows the location of samples retrieved from one boring carried out to a depth 428 ft below mudline. The sampling interval varied from 3 to 10 ft and the total number of samples was 59. The third column describes the sampling methods: Numbers identify driven samples and "WIP" denotes samples pushed by means of the WISON hydraulic equipment. The fourth column provides the soil description based on classification tests performed onboard the vessel and supplemented by tests at Catholic University. This classification indicates the presence of seven major soil strata as described in Table 4.1. Natural water contents and soil shear strength data obtained onboard the vessel and in situ by means of the field vane test (up to a depth of 50 ft) are presented in columns five and six, respectively. Also presented in column six is the direct simple shear strength obtained by Ladd et al., 1980, according to the SHANSEP* procedure (Ladd and Foott, 1974).

Figure 4.2 also shows the incremental cone resistance,

---

* An acronym for Stress History And Normalized Soil Engineering Properties

Δq_c,* and penetration pore pressure, u, measured during cone penetration. These plots represent the steady penetration data obtained after deleting the initial segments of the penetration records corresponding to unsteady and/or uncertain depth location at the beginning of each push. Appendix A presents plots of the complete records of Δq_c and u measurements.

We note from the cone penetration plots in Fig. 4.2 that:

1) The scale of Δq_c is 10 times larger than that of u. Furthermore, the maximum values of Δq_c and u on the graphs (500 and 50 kg/cm^2, respectively) roughly correspond to the maximum capacity of the two devices.
2) The plots of Δq_c and u are based on digitized data from FUGRO'S strip chart recorders available onboard. The scale of Δq_c was 1cm = 10kg/cm^2 in the upper 200 ft below the mudline and 1cm = 20kg/cm^2 below. This scale was selected to accomodate the large cone resistances encountered in dense and hard deposits without the use of zero suppressors to avoid complications in the data processing at the price of very limited resolutions in the upper soft clays. On the other hand, the scale of u was 1cm = 0.5kg/cm^2 in the upper 150 ft and 1cm = 1kg/cm^2 below.

---

* Cone penetration resistance data reported by FUGRO consists of the incremental cone resistance, Δq_c, in excess of the latch-zero reading down the drill string, i.e., $\Delta q_c = 0$ before pushing starts.

3) Δq_c measurements starts at a depth of 13 ft and are almost continuous to d = 423 ft. In the very dense sand below 320 ft, some penetration tests were discontinued because of the large resistance encountered without cone penetration. On the other hand, u measurements started at approximately 20 ft below the mudline in a separate boring (see Fig. 4.1). Because of economic considerations, continuous pore pressure records were only obtained in layers where the cone resistance data (available at the time u measurements were made) showed some variability (e.g., d =185 to 210 ft). Otherwise, they were made mostly at 5 ft intervals. Due to hardware problems, no pore pressure measurements were performed below d = 260 ft.

4) The estimated values of the total vertical stress, and hydrostatic pore pressure, u, are given by the expressions in Table 4.2.

In view of the penetration data (Δq_c and u) in Fig. 4.2, a more detailed stratigraphy can be observed. Table 4.1 describes the sublayers detected by Δq_c and u, where we note that:

a) Based on u, layer I can be possibly divided into four sublayers, I-1 through I-4:

(1) Sublayer I-2, at d = 60 to 65 ft, has a smaller penetration pore pressure in comparison with the layer above and below and is also marked by a

very slight increase in Δq_c. These features suggest that I-2 is a thin crust. Shallow seismic geophysical data reported by Mr. J. Butenko, formerly with INTEVEP, indicate the presence of a reflector at d ≃ 60 ft.

(2) Sublayer I-4, d = 90 to 151 ft, has a slightly different rate of increase of u with depth compared to layers I-1 and I-3. Laboratory test results (Ladd et al., 1980) show slightly different normalized strength characteristics between I-4 and the upper layers.

b) u and Δq_c measurements in the very stiff clay sublayer II-1 are consistent with sample classification data. On the other hand, the clean sand sublayer II-2 (d = 177-185 ft) was not detected by sampling. Clean sand is characterized by a high Δq_c and u is approximately equal to u_o, and hence, its drained friction angle, $\bar{\phi}$, can be estimated from q_c based on correlations established by Meyerhof (1976). For sublayer II-2, $\bar{\phi}$ is estimated to be equal to $38° \pm 2$.

c) Layer III is a transitional, highly variable layer where Δq_c decreases and u increases indicating the transition from sand to clay. Due to the significant value of excess pore pressure during penetration, the drained friction angle for this layer can not be directly estimated from Δq_c.

d) Layer IV (d = 198 - 299 ft), classified as very stiff to grey hard clay, can be further divided into four sublayers based on the Δq_c and u measurements:

(1) Sublayer IV-1 (d = 198 to 208 ft) is characterized by a very clear decrease in the mean value and variability of Δq_c, compared to Layer III, without a significant change in the u measurements. Note that the presence of silt seams and pockets within this clay layer was clearly detected by the pore pressure probe.

(2) In sublayer IV-2 (d = 208 to 250 ft), no significant change in the Δq_c data can be detected. However, the u data is characterized by a clear increase in the mean value accompanied by a reduction in the variability (scatter).

(3) Sublayer IV-3 (d = 250 to 260 ft) indicates a clear increase in the magnitude and variability of Δq_c as well as a very clear drop in u and its variability. Based on experience, these features of Δq_c and u correspond to a change from a uniform clay in sublayer IV-2 to a sand layer (IV-3).

(4) Unfortunately, no u measurements were obtained below layer IV-3 at a depth of approximately 260 ft. However, the small Δq_c measurements

between d = 260 to 299 ft indicate the presence of a uniform clay with the same features as sublayer IV-2.

Since no pore pressure measurements were made in layers V through VII (below d = 299 ft), and stratification in Table 4.1 was established by FUGRO on the basis of sampling and Δq_c data, no additional details on stratification can be provided. However, based on the Δq_c records, assuming that no significant excess pore pressures develop during penetration*, and using Meyerhof's correlations, $\bar{\phi}$ for both layers V and VII can be estimated at $\simeq 43^\circ \pm 2$. This information is very important in pile foundations design since it is used to estimate the point bearing capacity, and hence pile penetration and driveability. More reliable estimates of $\bar{\phi}$ and/or sand gradation, permeability and relative density could have been obtained had pore pressure measurements been made (especially in layer V, which represents the most likely layer to provide the point bearing of piles at this site).

Figure 4.3 presents cone resistance, q_c , and penetration pore pressure, u, data for site E1 between depths 0 to 260 ft. In this figure, both q_c and u are presented to the same scale for illustration. As mentioned earlier, u data is

---

* i.e., drained penetration in clean sands.

directly obtained from measurements. However, q_c is obtained from the expression:

$$q_c = \Delta q_c + \sigma_{vo} \qquad (4.1)$$

where Δq_c is the measured incremental cone resistance, presented in Figure 4.2, in excess of the latch-zero reading down the drill string, and σ_{vo} is estimated from the expressions and data given in Table 4.2.

Clearly the q_c and u data in Figure 4.3 are consistent with the stratification established above: q_c is "high" and u is "low" in sandy soils, and the inverse is true in "soft" clays.

Figure 4.4 presents the soil profile, stratification and cone penetration data at site F1 where the water depth was 78ft. We note the following from the results in this figure:

1) Δq_c measurements starts at a depth of 30 ft below the mudline and are almost continuous to d = 338 ft. In the very dense sand below 200 ft, some penetration tests were discontinued because of the large resistance encountered without cone penetration. The pore pressure measurements started at approximately 25 ft and are continuous to d = 134 ft. Due to hardware difficulties, no u measurements were made below this depth.

2) Based on samples, classification tests performed onboard the vessel, and cone penetration resistance data, the soil deposit at site F1 can be divided

into nine layers. However, as in the case of site E1, the scale of Δq_c records is not sufficient to provide detailed stratification information in the upper soft clay layer (layer I). Considering the u records, three sublayers I-1 through I-3 can be identified:

(a) Sublayer I-2, d = 75 to 130 ft, has a slightly different rate of increase of u with depth compared to I-1 and I-3.

(b) Sublayer I-3, d = 130 to 134 ft, is characterized by a clear drop in u which is accompanied by a very slight increase in Δq_c.

A transition sublayer between 75 and 85 ft could also have been added.

3) It appears, based on both u and Δq_c records, that the upper 134 ft at this site can be identified as basically the same clay observed in the upper 151 ft at site E1 (a more detailed discussion of this result is presented in Section 4.3.4).

4) Competent dense sand layers capable of providing the point bearing of piles (e.g., layer V) appear at a shallower depth at this site compared to site E1.

5) Assuming that no significant excess pore pressures develop during penetration, Meyerhof's correlations estimate $\overline{\phi}$ for layers V and IX to be around 45°.

Records of Δq_c and u at the third site D2 are shown in

Appendix A. Due to hardware difficulties encountered during the field work, the reliability of these records is questionable for research purposes and hence are not discussed herein. However, they might prove useful for the design engineer.

4.3 CORRELATIONS

4.3.1 General. A more detailed comparison of the u and q_c data can be provided by plotting the ratio u/q_c as was shown in Figs. 3.32, 3.35, and 3.39 for the three onshore sites described earlier, where the ground water table is at or near the surface.

However, in offshore deposits, this ratio is misleading because of the hydrostatic pore pressure u_o at the mudline. For example, two identical deposits under different water depths will have different values of u/q_c. A more representative ratio for offshore work is given by $R_1 = (u-u_o)/(q_c-u_o)$, where u_o is the hydrostatic pressure* at any depth. Noting that:

$$R_1 = \frac{u/q_c - u_o/q_c}{1 - u_o/q_c} \qquad (4.2)$$

Therefore $R_1 = 1$ when $u/q_c \simeq 1$, such that for practical purposes, the correlations established in Chapter 3 regarding u/q_c can be applied to R_1 in normally consolidated "soft" clays. Differences between R_1 and u/q_c are less than 10% in the Boston Blue Clay and the Amherst Varved Clay deposits.

---

*Given in Table 4.2 for sites E1 and F1.

For the Atchafalaya highly plastic clay deposit, u/q_c is relatively small, and hence u/q_c can overestimate R_1 by as much as 20%.

Another interesting correlation is the ratio $R_2 = \Delta q_c/\bar{\sigma}_{vo}$. This can be seen by writing the bearing capacity equations for deep foundations, where the effect of width is small compared to depth, and assuming that the ultimate capacity equals the cone resistance:

1) During undrained penetration in saturated clays we have:

$$q_c = s_u N_c + \sigma_{vo} \tag{4.3}$$

and hence:

$$\Delta q_c = s_u N_c \tag{4.4}$$

Assuming that:

$$s_u = \delta\, \bar{\sigma}_{vo} \tag{4.5}$$

we get:

$$\frac{\Delta q_c}{\bar{\sigma}_{vo}} = \delta\, N_c \tag{4.6}$$

The constant δ depends on the mode of shearing, overconsolidation ratio and the clay type. Typical average values of δ are given by the direct simple shear and field vane test results and are equal to $\delta = 0.20 \pm 0.02$ for normally consolidated, N.C., CL

clays (P.I. ≃ 20%) increasing to 0.28 ± 0.03 for N.C. CH clays (P.I. ± 80%). Ladd et al. (1977) indicate that δ increases with increasing the overconsolidation ratio, OCR, of the clay such that:

$$\delta_{O.C} = \delta_{N.C} \ (OCR)^{0.8} \qquad (4.7)$$

Furthermore, Chapter 3 (Fig. 3.24) shows that when the field vane shear strength is used, empirical cone factors, N_c, determined from eight sites have an average value of 14. Substituting N_c = 14 and the typical values of δ discussed above in Eq. (4.6) we get that $\Delta q_c/\bar{\sigma}_{vo}$ = 2.8 ± 0.30 for normally consolidated CL clays and 4.0 ± 0.40 for normally consolidated CH clays.

2) On the other hand, during <u>drained</u> penetration in uncemented sands:

$$q_c = N_q \bar{\sigma}_{vo} + u_o \qquad (4.8)$$

Noting that $\Delta q_c = q_c - \sigma_{vo}$ and that $\sigma_{vo} = \bar{\sigma}_{vo} + u_o$, we get:

$$\frac{\Delta q_c}{\bar{\sigma}_{vo}} = N_q - 1 \qquad (4.9)$$

However, in view of the approximations in deriving Eq. (4.9), and the large values of N_q encountered in sands, it is practically reasonable to write:

$$\frac{\Delta q_c}{\bar{\sigma}_{vo}} \simeq N_q \qquad (4.10)$$

Correlations based on the ratios R_1 and R_2 discussed above will now be presented for the soil deposits at sites E1 and F1.

4.3.2 General Correlations at Site E1. Figure 4.5 presents the ratio R_1 for site E1, where we note:

1) Generally when R_1 approaches unity, the soil is a normally consolidated "soft" clay and when it approaches zero, the soil is a clean sand. Therefore, the clay layer I with $R_1 = 0.80 \pm 0.1$ is close to being normally consolidated, except for the clay crust I-2 with $R_1 = 0.40 \pm 0.10$. The large scatter of R_1 in I-1 is mainly caused by the poor resolution in the q_c measurements.
2) The overconsolidated layer II-1 has $R_1 = 0.30 \pm 0.1$.
3) The clean sand layer II-2 has $R_1 \simeq 0$.
4) In the transitional layer III, R_1 increases from 0 to 0.30 and exhibits significant scatter in layer IV-1.
5) The ratio R_1 in layer IV-2, classified as very stiff to hard clay, is high: $R_1 = 1.1 \pm 0.1$. Theoretically, Baligh et al. (1978) argue that u cannot exceed q_c, i.e., R_1 cannot exceed unity unless significant pore pressure gradients exist around the cone tip during penetration. Levadoux and Baligh (1980) show that for 60° tips, which were used in obtaining the data in Fig. 4.5, such gradients do not exist (see results in Chapter 3). Values of

$R_1 > 1$ are therefore believed to be caused by equipment inaccuracies caused by pore pressure acting over a portion of the base of the cone tip, which in turn reduces the measured values of q_c.

6) Finally, in the sand layer IV-3, $R_1 = 0.10 \pm 0.10$.

Figure 4.6 shows a plot of $R_2 = \Delta q_c/\bar{\sigma}_{vo}$ for site E1 up to a depth of 423 ft below the mudline, where we note that:

1) In the uniform clay layers I, IV-2 and IV-4, $\Delta q_c/\bar{\sigma}_{vo}$ is "small" in the range of 3 ± 1. The information presented in the previous section suggest that these clays are probably normally to slightly overconsolidated.
2) Layer II-1 has a higher value of $\Delta q_c/\bar{\sigma}_{vo}$, equal to 6, thus indicating an increase in the over-consolidation ratio of this clay compared to layer I.
3) The clean sand layers II-2, V and VII have high values of $\Delta q_c/\bar{\sigma}_{vo} = N_q = 30$ to 40.
4) The N_q values in transitional layers vary significantly.

In view of the limited accuracy of the cone resistance measurements in the soft clay deposits, as discussed in Section 4.1, a normalized excess pore pressures plot is shown in Fig. 4.7, where $R_3 = (u-u_o)/\bar{\sigma}_{vo}$ is plotted versus depth.

The results in this figure show:

1) A clear picture of the stratigraphy at the site. For example, in the upper clay deposit (layer I), R_3 is generally between 2.5 and 3, except for the crust sublayer I-2 where R_3 is mostly between 1.0 and 2.5. In the lower layers, R_3 detects the same layers as R_2 (Fig. 4.6), except that as R_2 increases in the clean sands, R_3 approaches zero.
2) In normally consolidated deposits, where u/q_c is close to unity, R_2 and R_3 have roughly the same magnitude. However, due to limited accuracy of the cone resistance measurements in clays, R_3 provides more reliable data especially regarding soil variability.

4.3.3 General Correlations at Site F1. Figure 4.8 presents the ratio $R_2 (=\Delta q_c/\bar{\sigma}_{vo})$ for site F1 up to a depth of 338 ft below the mudline, where we note that:

1) The R_2 values in layers I and VI are "small", in the range of 3 ± 1. This suggests that these clays are mostly normally to slightly overconsolidated. It also indicates that probably the same clay layer overlies the soil deposits at sites E1 and F1 (compare Figs. 4.6 and 4.8).
2) Assuming that no significant excess pore pressures develop during penetration in layers II, V, VIII and IX, the corresponding $\Delta q_c/\bar{\sigma}_{vo}$ values thus represent

the bearing capacity factors, N_q (see Eq. 4.10) for these layers. On the average, the N_q values in this site are significantly higher than those reported for site E1.

3) As in the case of site E1, the R_2 values in the transitional layers vary significantly.

As mentioned previously, no pore pressure measurements were made below the clay layer I (d = 134 ft) at site F1. Hence, the normalized pore pressure ratio, $R_3 = (u-u_o)/\bar{\sigma}_{vo}$, calculated on the basis of the limited data obtained will be discussed in the following section which addresses general correlations in the soft clay deposit.

4.3.4 Correlations in the Orinoco Clay. The Orinoco Clay designates the very extensive "mud wedge" encountered over a vast area throughout the Gulf of Paria and Orinoco Delta based on geophysical survey data, drop core samples and the results of an extensive laboratory testing program at M.I.T. (discussed subsequently). The mud wedge is important in providing the lateral support of piles and in shallow foundation problems involving pipe lines, jacked-up platforms and anchors.

An extensive experimental testing program involving the Orinoco Clay has just been completed at MIT. (Ladd et al., 1980). The objectives of this program was to: (1) perform compositional analysis in order to identify unusual clay

minerals and potential testing problems; and (2) conduct SHANSEP type testing to establish the stress history of the deep clay deposit, its consolidation characteristics and "normalized soil parameters" for determining in situ stress-strain-strength properties required for the design of offshore structures.

This section presents detailed cone penetration data with the objective of:

(1) Establishing detailed stratigraphy within the mud wedge;

(2) Correlating properties obtained from penetration tests with laboratory test results determined by Ladd et al. (1980); and

(3) Establishing correlations between sites E1 and F1. If successful, such correlations will practically reduce the scope and cost of future soil exploration programs to be conducted within the vast area covered by the mud wedge.

According to the results of the detailed laboratory testing program performed at MIT, as reported by Ladd et al. (1980), the Orinoco Clay is a soft, highly plastic CH-OH soil. Its Atterberg limits straddle the A-line (Fig. 4.9) with a typical plasticity index, P.I., equal to 40 ± 10% at site E1 and 55 ± 10% at site F1. The pore fluid salt concentration decreases slightly with depth (from about 30 to 25 g/l), while the organic content remains essentially constant at about 2%. X-ray diffraction analyses indicate

the same basic mineralogical composition at both sites, the principal clay minerals being kaolinite, illite and an interstratified phase ranging from chlorite (non-swelling) to smectite (highly swelling). Some of the shallower clay samples (d < 85 ft) contained calcite, the deeper ones contained a greater proportion of swelling minerals and all had substantial quartz and feldspar contents.

Figure 4.10 presents the maximum past pressures, $\bar{\sigma}_{vm}$, data obtained by Ladd et al. (1980). The results show that the same $\bar{\sigma}_{vm}$ profile exists at the two widely separated E1 and F1 sites* and that $\bar{\sigma}_{vm}$ increases linearly with depth and exhibits very little scatter amongst those tests judged of excellent to good quality. The data in Fig. 4.10 indicate that the clay at site E1 is essentially normally consolidated (OCR ≈ 1.0), as would be expected based on geological considerations, whereas the deposit at site F1 is slightly overconsolidated** (OCR ≈ 1.2 at F1), perhaps due to wave action. If the same $\bar{\sigma}_{vm}$ profile exists throughout most of the Orinoco Clay, which appears reasonable for locations between and around sites E1 and F1, then the in situ engineering properties should also be reasonably constant.

Figure 4.11 summarizes compressibility and coefficient of consolidation data obtained from the oedometer test program. The Orinoco Clay is highly compressible, especially

---

*Sites E1 and F1 are about 125 km apart.

**Note that the $\bar{\sigma}_{vo}$ values used by Ladd et al. are slightly different from those given in Table 4.2.

at depths exceeding about 75 ft, and has a very low normally consolidated coefficient of consolidation.

The results of the CK_oU direct simple shear, DSS, test program reported by Ladd et al. (1980) indicate that the Orinoco Clay exhibits normalized behavior, i.e., $s_u/\bar{\sigma}_{vc}$ is uniquely related to OCR independent of the actual values of $\bar{\sigma}_{vc}$ or $\bar{\sigma}_{vm}$ (see Fig. 4.12). However, the magnitude of the normally consolidated s_u (DSS)$/\bar{\sigma}_{vc}$, and to a lesser extent the ratio of the undrained Young's modulus to the undrained shear strength, E_u/s_u, vary with depth. Specifically, data from nine tests run on normally consolidated samples from site E1 and F1 show (see Figs. 4.13 and 4.14):

$s_u(DSS)/\bar{\sigma}_{vc}$ = 0.235 ± 0.01 for d less than 75 ft

$s_u(DSS)/\bar{\sigma}_{vc}$ = 0.200 ± 0.005 for d greater than 75 ft

Figure 4.15 shows the variation of s_u (DSS)$/\bar{\sigma}_{vc}$ with the overconsolidation ratio, OCR, of the Orinoco Clay, along with data on three other clays (Ladd et al., 1977). The Orinoco Clay data were determined from tests performed on shallow samples (d < 75 ft), where the normally consolidated $s_u/\bar{\sigma}_{vc}$ is believed to be equal to 0.200. The limited results show that the variation of $s_u/\bar{\sigma}_{vc}$ vs. OCR of the Orinoco Clay can be reasonably estimated by the following expression developed by Ladd et al. (1977) based on the results collected on several clays:

$$\frac{s_u\ (DSS)}{\bar{\sigma}_{vc}} = \left[\frac{s_u(DSS)}{\bar{\sigma}_{vc}} \text{ for OCR = 1}\right] (OCR)^{0.8} \qquad (4.11)$$

In summary, the results of the extensive testing program

performed at MIT show that:

1) For all practical purposes, the Orinoco Clay at sites E1 and F1 has similar in situ engineering properties.
2) The in situ engineering properties (e.g., compressibility and normalized strength) vary slightly with depth.

The remaining of this chapter will now attempt to correlate the cone penetration data with the laboratory test results.

Figures 4.16 and 4.17 present the penetration pore pressure data measured at site E1 and F1, respectively. The data between d = 0 to 140 ft suggest that two zones with different rates of pore pressure increase with depth can be established at both sites. At E1, the clay above d = 90 ft has a higher rate of increase in comparison with the lower clay. Similarly, the clay above d = 75 ft at site F1 has a higher rate of pore pressure increase with depth with respect to that of the lower clay.

Figure 4.18 presents $R_3 = (u-u_o)/\bar{\sigma}_{vo}$ data for the clay in sites E1 (Fig. 4.18a) and F1 (Fig. 4.18b) from which we note:

1) With the exception of sublayer I-2, the $(u-u_o)/\bar{\sigma}_{vo}$ values at site E1 are essentially constant with depth and are in the range of 2.5 to 3 (see Fig. 4.18a). For I-2, this ratio is between 1 to 2.5.
2) On the other hand, at site F1 (Fig. 4.18b),

variation in the R_3 values with depth can be observed. For d < 75 ft, $(u - u_o)/\bar{\sigma}_{vo}$ is in the range of 3 to 3.5, except from d = 25 - 35 ft where it ranges from 3.5 to 6. For d = 75 - 125 ft, $(u - u_o)/\bar{\sigma}_{vo}$ ranges between 2.5 to 3.

Figure 4.19 presents the cone factor, N_c (= $\Delta q_c/s_u$, see Eq. 4.4) at sites E1 (Fig. 4.19a) and F1 (Fig. 4.19b). The s_u values used in this figure (and also in Fig. 4.20) are those obtained by means of the direct simple shear test (Ladd et al., 1980) and illustrated in Figs. 4.13 and 4.14. The data in Fig. 4.19 show that:

1) The N_c values are quite erratic, especially at site F1. As mentioned previously, this is due to the poor q_c resolution in the soft clays.
2) At site E1, N_c is essentially constant with depth at 12 ± 2. At F1, N_c is equal to about 15 ± 3 down to d ≈ 110 ft and decreases to about 13 ± 1 below.

Using the penetration pore pressure data, a pore pressure probe factor, $N_u = (u-u_o)/s_u$, is illustrated in Fig. 4.20a and b for sites E1 and F1, respectively. The data in Fig. 4.20 show that:

1) The N_u values at site E1 vary with depth. In sublayer I-1, the average N_u value is equal to 11 ± 1. In sublayers I-3 and I-4, N_u = 12 ± 1 and 14 ± 1, respectively. In the crust I-2, N_u varies significantly and has a value of 8 ± 4.

2) Similarly, the N_u values at site F1 vary with depth. For d = 45 - 85 ft, N_u = 13 ± 1 and decreases to about 11 ± 1 for d = 85 - 125 ft.

Based on the results presented in Figs. 4.16 through 4.20, the following conclusions regarding the correlations in the Orinoco Clay can be drawn:

1) Ladd et al., 1980, concluded, based on the results of their experimental testing program, that the clays at sites E1 and F1 have similar engineering properties. The pore pressure data normalized with respect to $\bar{\sigma}_{vo}$ (to avoid uncertainties associated with the determination of the undrained shear strength) confirm this result for the clay below a depth of 75 ft, as the clay at both sites exhibit similar $(u-u_o)/\bar{\sigma}_{vo}$ values. The same could not be established for the clays above 75 ft (especially for d = 20 - 40 ft and 60 - 65 ft). However, it should be mentioned that the laboratory testing program carried out by Ladd et al., 1980, included only one shallow (d < 75 ft) sample from site E1 (sample S15, d = 55 - 57 ft). The other available sample (S12, d = 37 - 40 ft) was highly disturbed.
2) The results at site F1 show, more or less, a variation in properties between the "upper" and "lower" clays as detected by a difference in the

rate of pore pressure increase with depth (Fig. 4.17) and the $(u-u_o)/\bar{\sigma}_{vo}$ values (Fig. 4.18b). This is in agreement with the results reported by Ladd et al. (1980). At site E1, although a difference in the rate of pore pressure increase with depth can be observed (see Fig. 4.16), such a trend could not be substantiated by the normalized pore pressure data $(u-u_o)/\bar{\sigma}_{vo}$.

3) Empirical cone factors correlating the cone resistance data and the undrained shear strength (determined by the direct simple shear test) are equal to 12 ± 2 and 15 ± 3 for the clays in sites E1 and F1, respectively (see Fig. 4.19). However, due to the poor resolution in the q_c measurements in soft clay deposits, these correlation factors are quite erratic and are thus subject to a large degree of variability and uncertainty.

4) In view of this limited accuracy of the cone resistance measurements in soft clay deposits, a new pore pressure factor, N_u $[=(u-u_o)/s_u]$ is introduced. In soft clay deposits, N_u provides more reliable data especially regarding stratigraphy and soil variability.

Table 4.1 Soil layering data at site E1

SAMPLE CLASSIFICATION DATA			CONE PENETRATION DATA					
Layer	Depth (ft)	Description	Layer	Depth (ft)	q_c	u	Description	Notes
I	0-151	very soft to stiff grey clay	I-1	0-60	start at 13 ft	start at 20 ft	very soft to soft clay	poor q_c resolution
			I-2	60-65	very slight increase	clear drop	possible thin crust	
			I-3	65-90		clear increase	soft to medium clay	
			I-4	90-151		slight slope change	medium to stiff clay	
II	151-185	very stiff olive green clay	II-1	151-177	some increase	very large variability and drop in mean value	highly variable, very stiff clay	poor q_c resolution
			II-2	177-185	very clear increase in mean value	very clear drop	dense clean sand	$\bar{\phi}$ = 38° ± 2 based on q_c*
III	185-198	medium dense olive grey silty fine sand to clayey sand	III	185-198	very clear decrease	very clear gradual increase in mean value	transition: variable dirty sands	partially drained, $\bar{\phi}$ = ?
IV	198-299	very stiff to hard grey clay	IV-1	198-208	very clear decrease in mean value and variability	no significant change	transition: sandy clays	
			IV-2	208-250	no significant change	clear increase in mean value and decrease in variability	uniform clay	different from clays in layers I and II
			IV-3	250-260	very clear increase in mean value and variability	very clear drop in mean value and increase in variability	medium sands with some fines	partially drained, $\bar{\phi}$ = ?
			IV-4	260-299	very clear drop in mean value and variability	no measurements	uniform clay	as in IV-2
V	299-368	dense grey fine sand	V	299-368	clear increase	no measurements	very dense below 320 ft.	$\bar{\phi}^* \geq 43°(\pm 2)$
VI	368-386	very stiff dark grey clay and sandy clay	VI	368-386	clear decrease	no measurements	very stiff clay with sandy pockets	
VII	386-428	very dense light grey clay and brown fine sand	VII	386-428	clear increase	no measurements	very dense sand	$\bar{\phi}^* \geq 43°(\pm 2)$

*According to Meyerhof (1976)

TABLE 4.2 Unit Weights, Pore Pressures, Effective and Total Stresses

Site	Water depth (ft.)	Depth (ft.)	Assumed		Parameters for u_o (2)		Parameters for σ_{vo} (2)		Parameters for $\bar{\sigma}_{vo}$ (2,3)	
			w_N (%)	γ_t (1) (pcf)	a_o	a_1	a_o	a_1	a_o	a_1
E1	85.5	0 - 140	55	107	2.673	0.0312	2.673	0.0522	0	0.0210
		below 140	30	123			1.567	0.0601	-1.106	0.0289
F1	78	0 - 140	65	103	2.438	0.0312	2.438	0.0503	0	0.0191
		below 140	25	128			0.730	0.0625	-1.708	0.0313

(1) Based on $G_s = 2.72$, $\gamma_w = 64$pcf and 100% degree of saturation.

(2) $\left.\begin{matrix} u_o(kg/cm^2) \\ \sigma_{vo}(kg/cm^2) \\ \bar{\sigma}_{vo}(kg/cm^2) \end{matrix}\right\} = a_o + a_1 \, z(ft)$

(3) Assuming hydrostatic pore pressure.

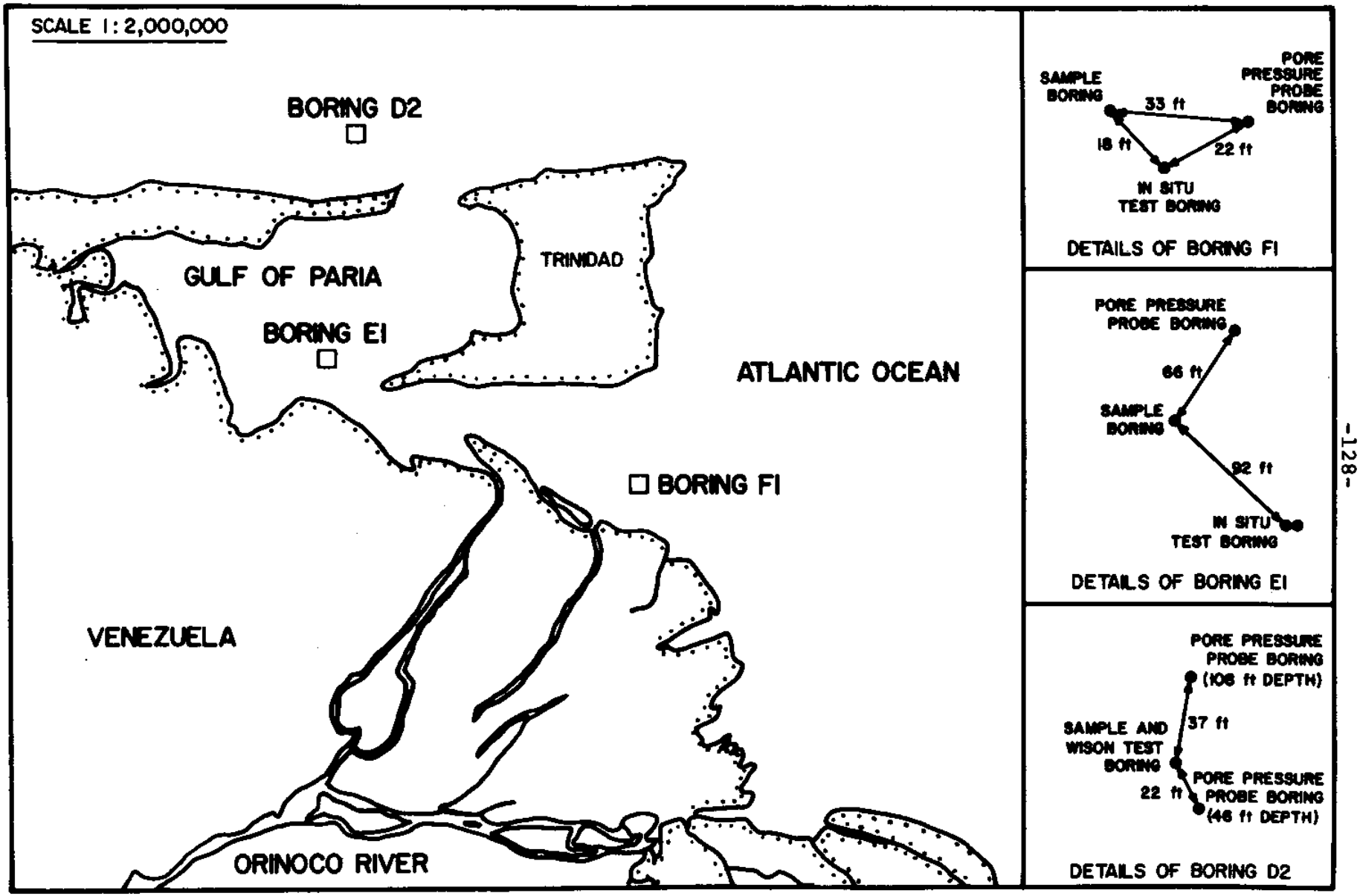

Figure 4.1 Boring locations.

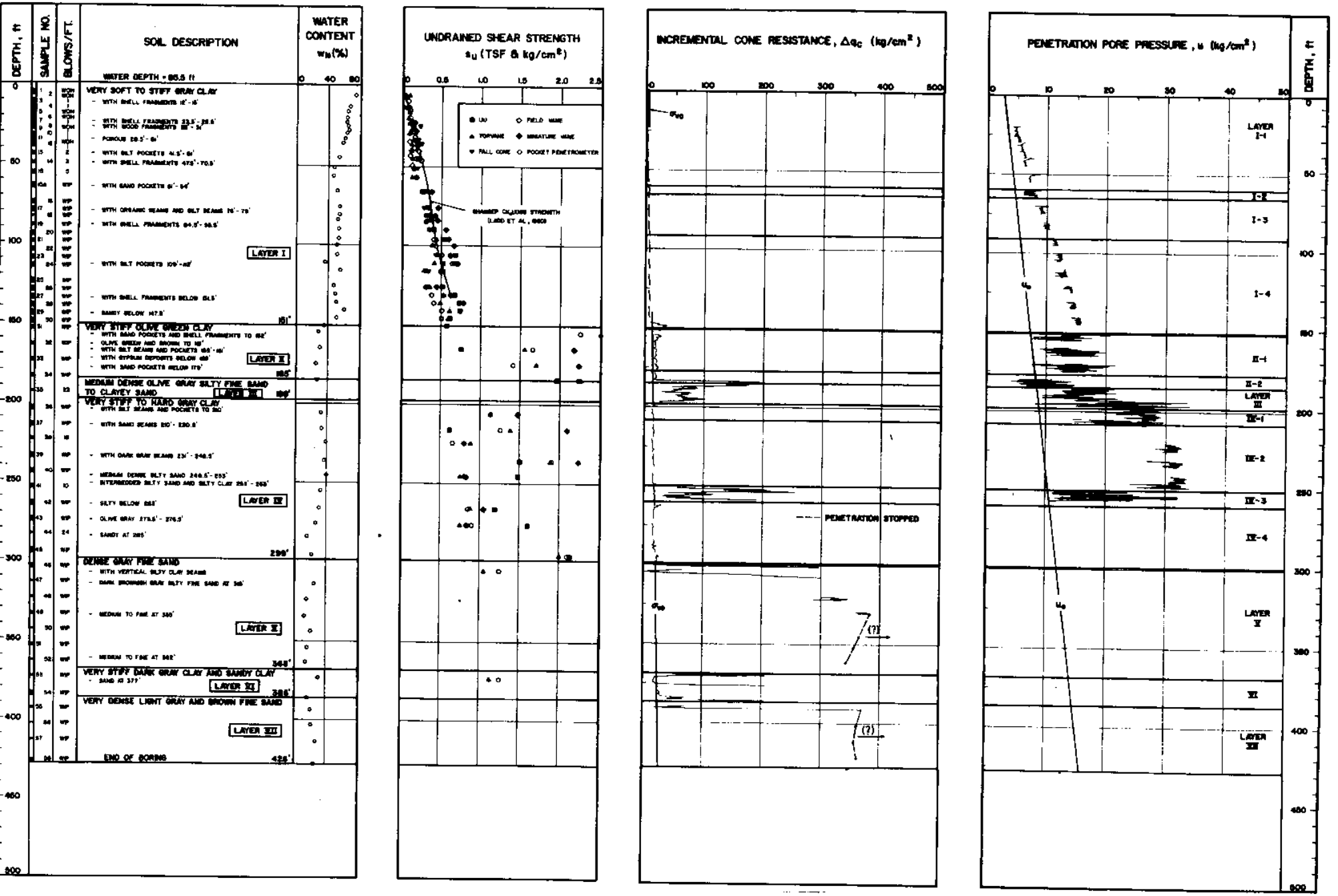

FIGURE 9.2 SOIL PROFILE AND STRATIFICATION DETAILS

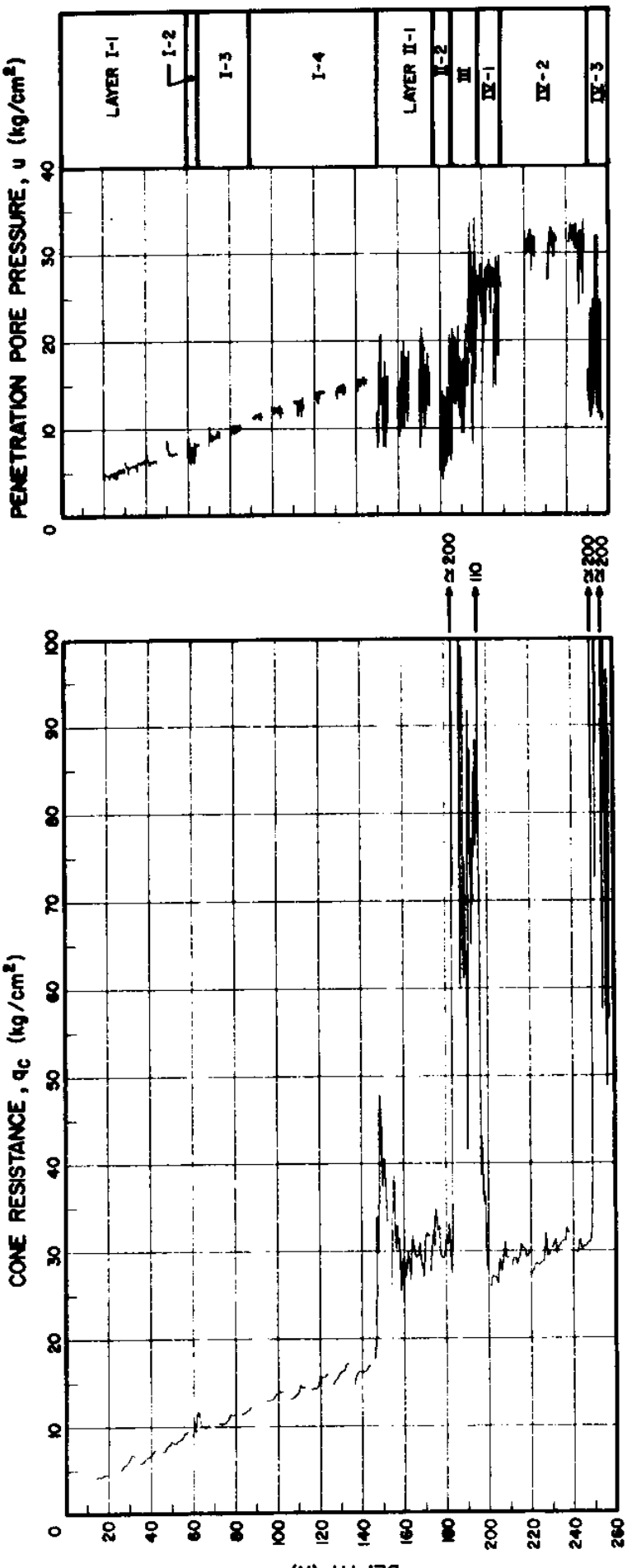

Figure 4.3 Cone resistance and pore pressure at site E1.

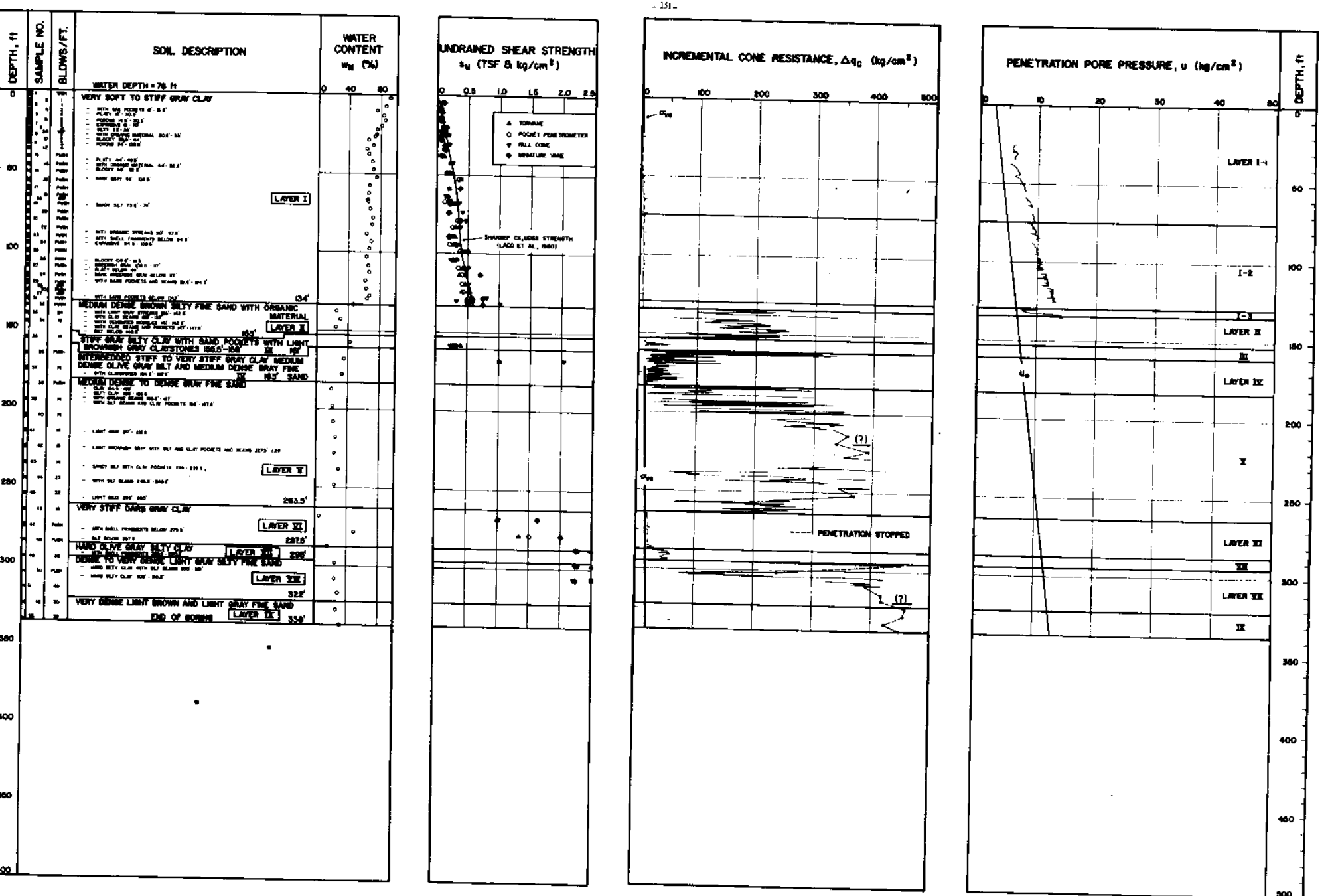

FIGURE B.9 SOIL PROFILE AND STRATIFICATION DATA AT SITE F1.

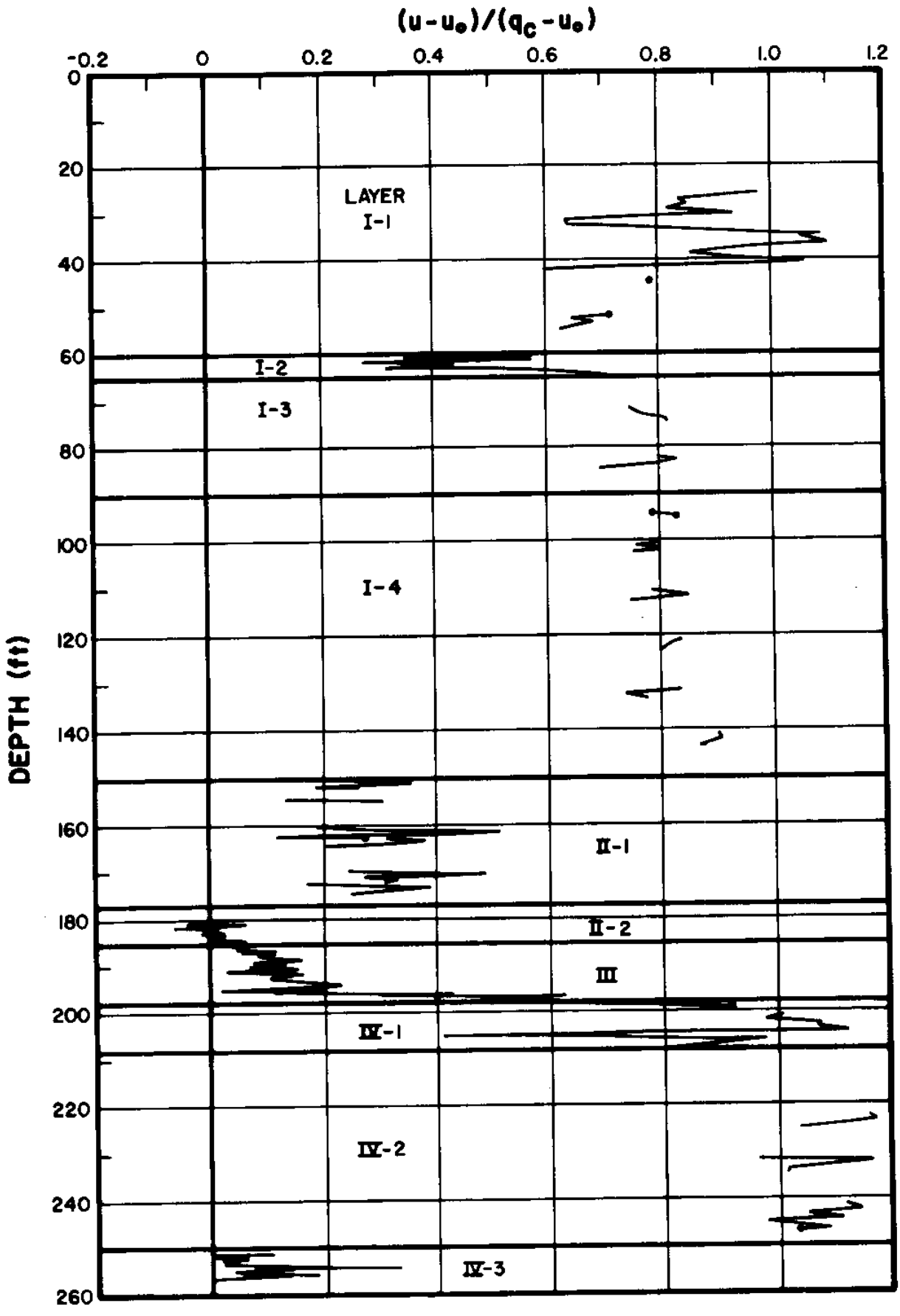

Figure 4.5 Pore pressure to cone resistance ratios at site E1.

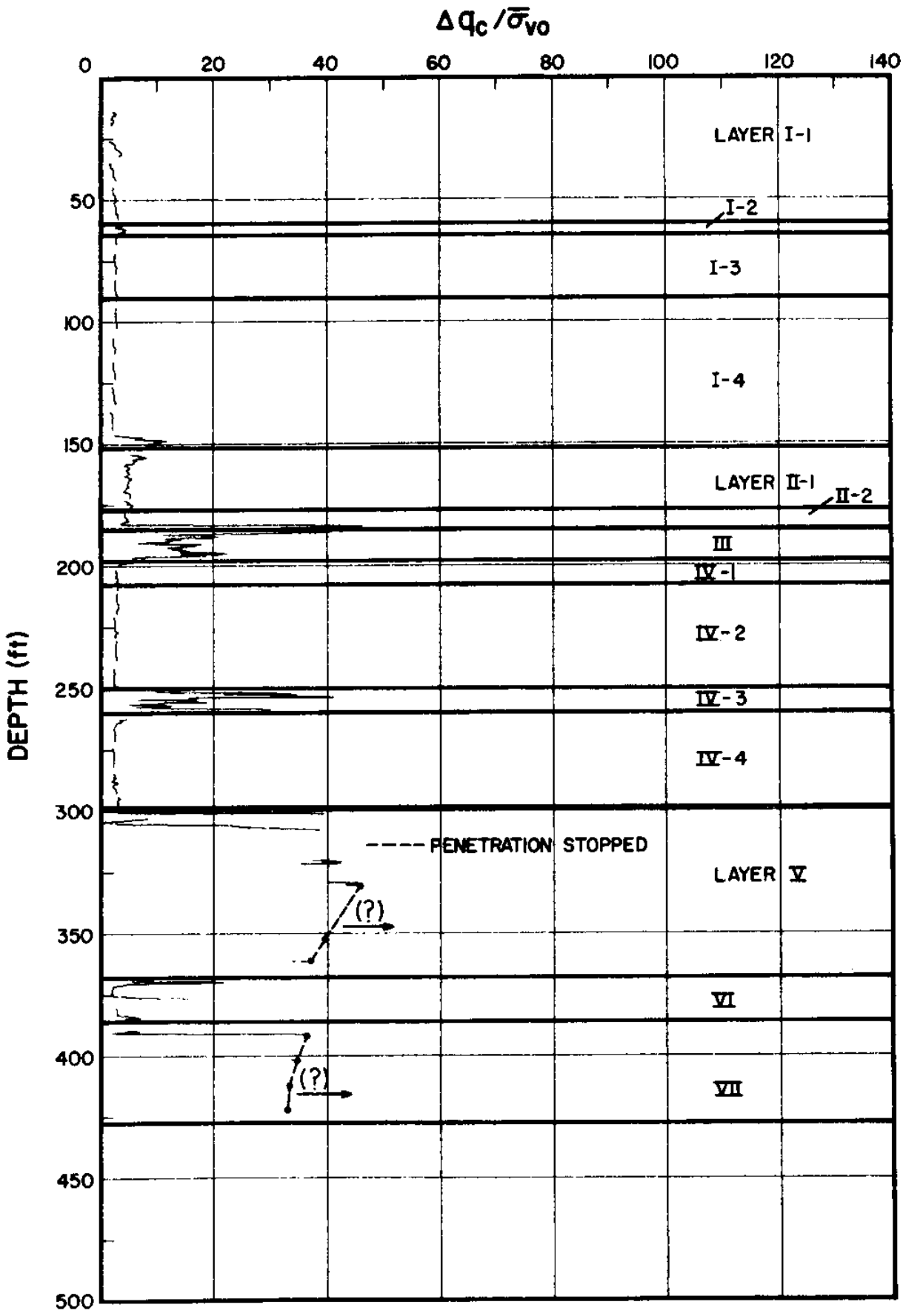

Figure 4.6 $\Delta q_c/\bar{\sigma}_{vo}$ at site El.

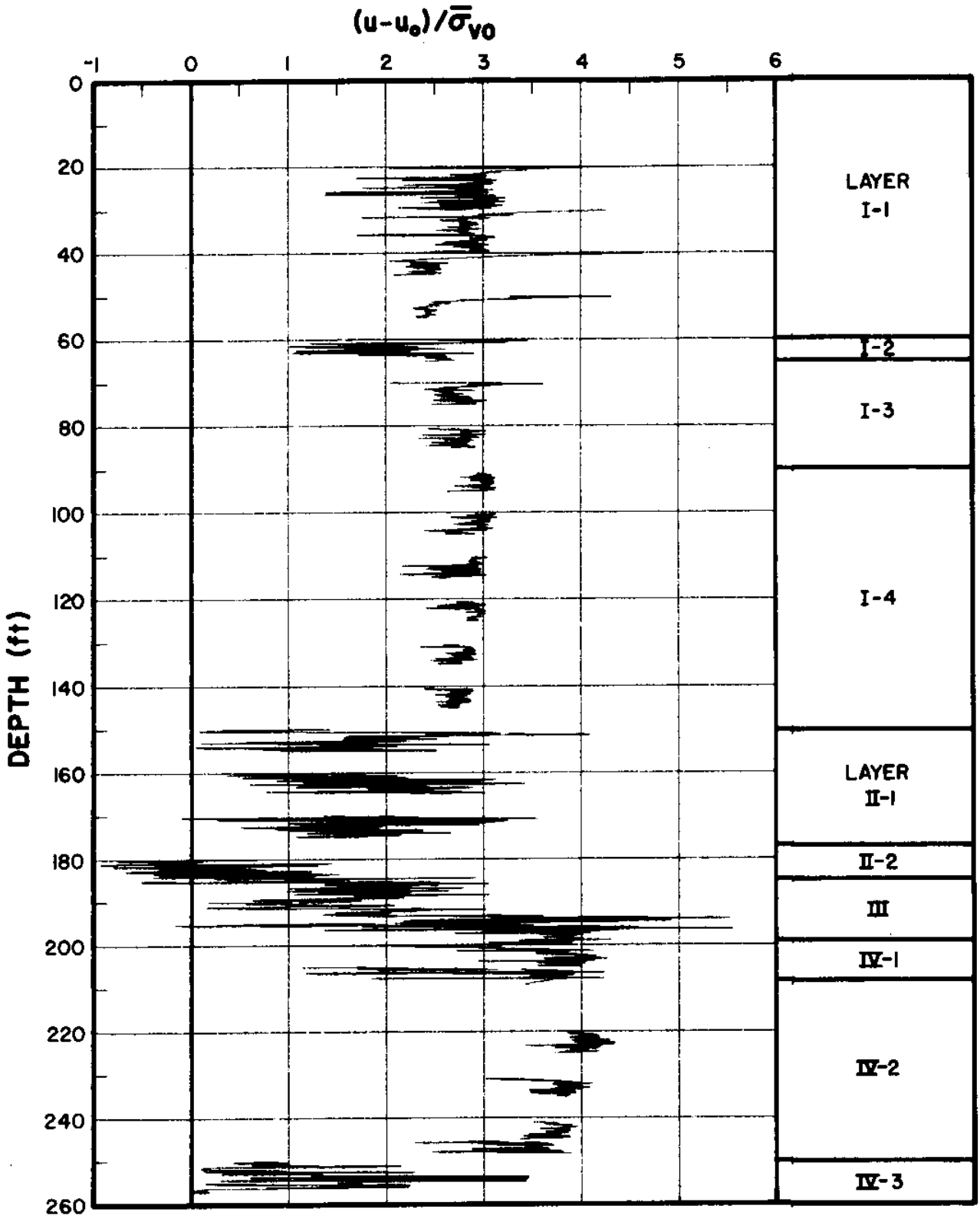

Figure 4.7 $(u-u_o)/\bar{\sigma}_{vo}$ at site El.

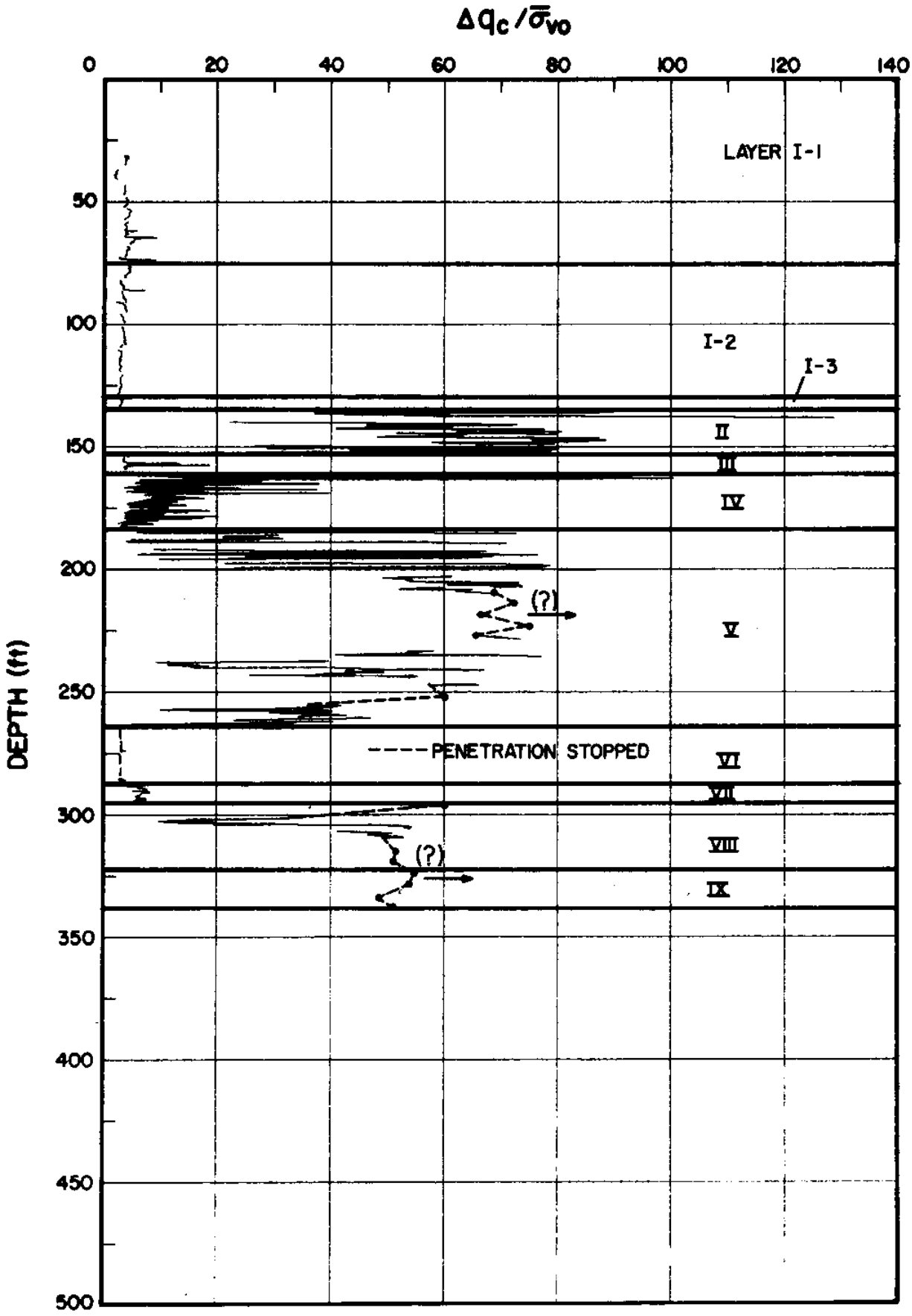

Figure 4.8 $\Delta q_c / \bar{\sigma}_{vo}$ at site F1.

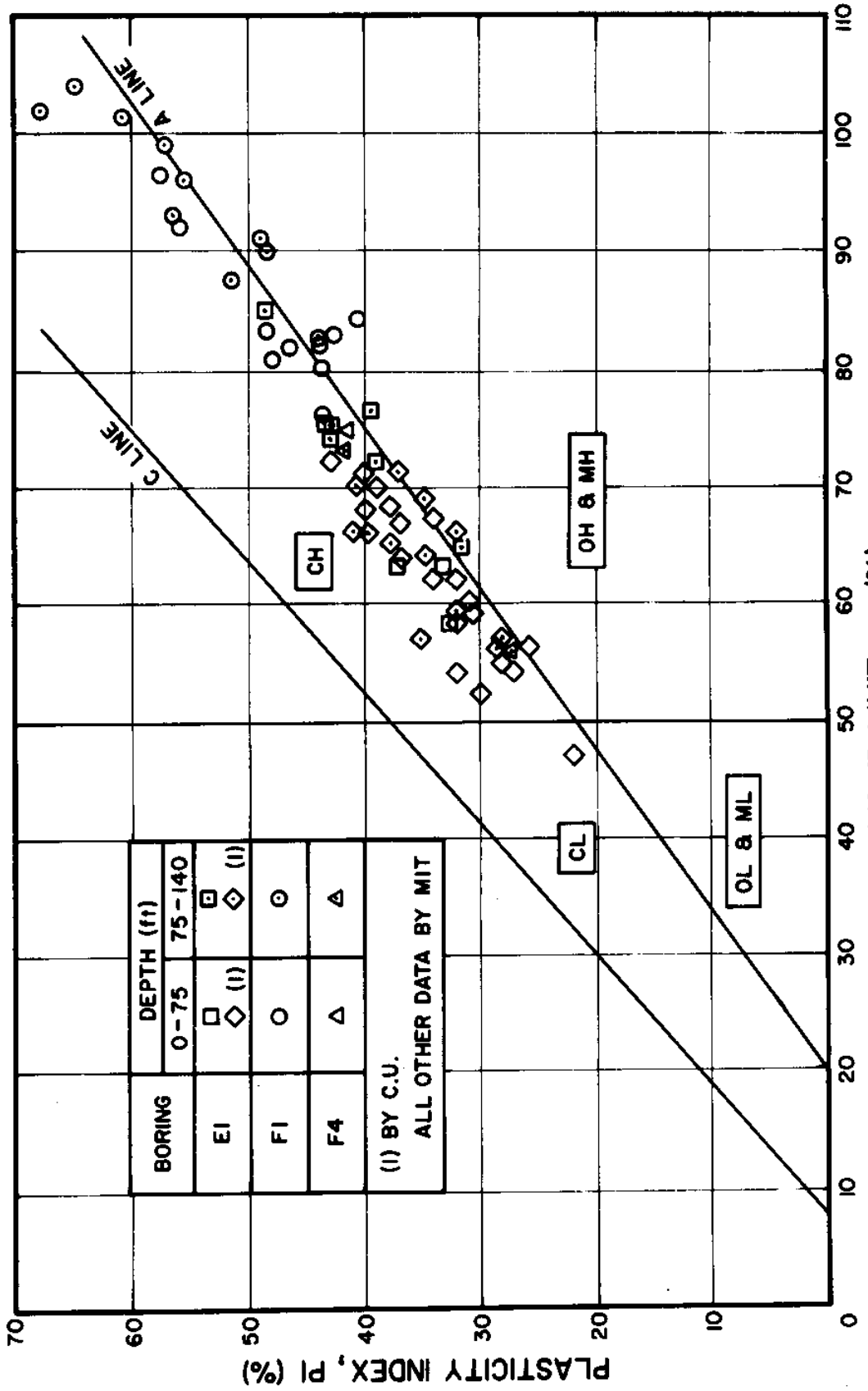

Figure 4.9 Plasticity chart: Orinoco clay (from Ladd et. al., 1980)

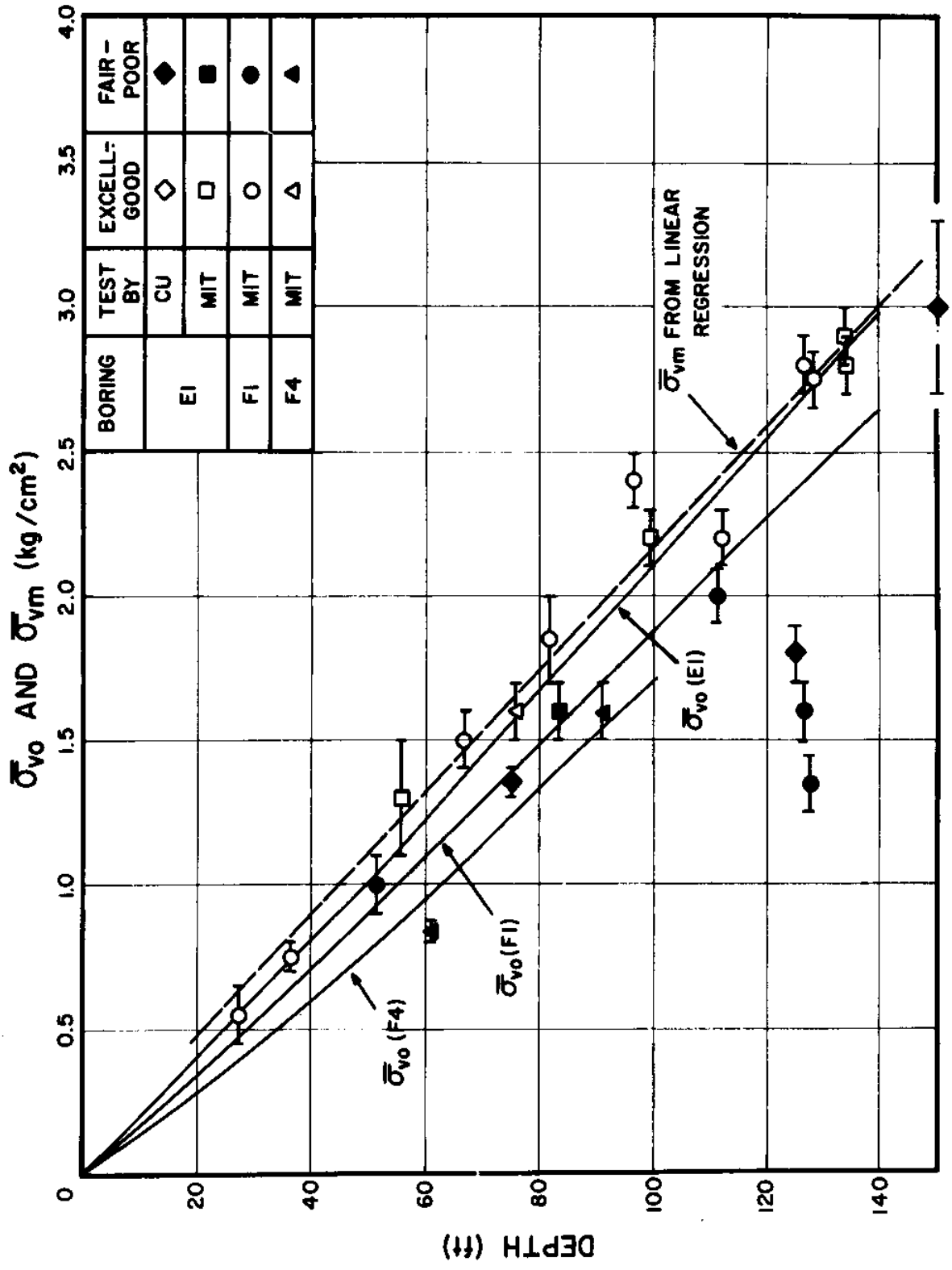

Figure 4.10 Stress history: Orinoco clay (from Ladd et. al., 1980)

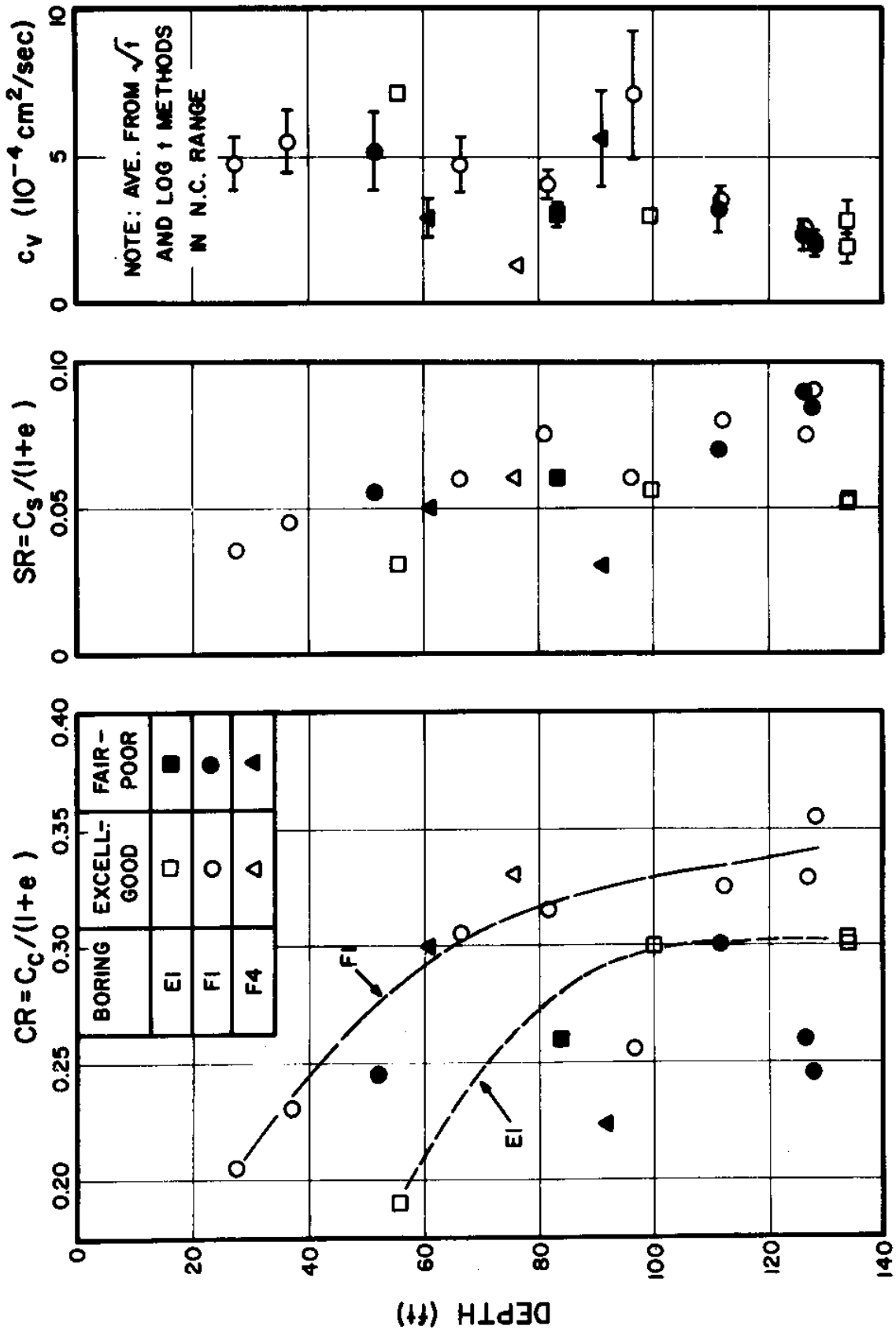

Figure 4.11 Compressibility and coefficient of consolidation: Orinoco clay (from Ladd et. al., 1980)

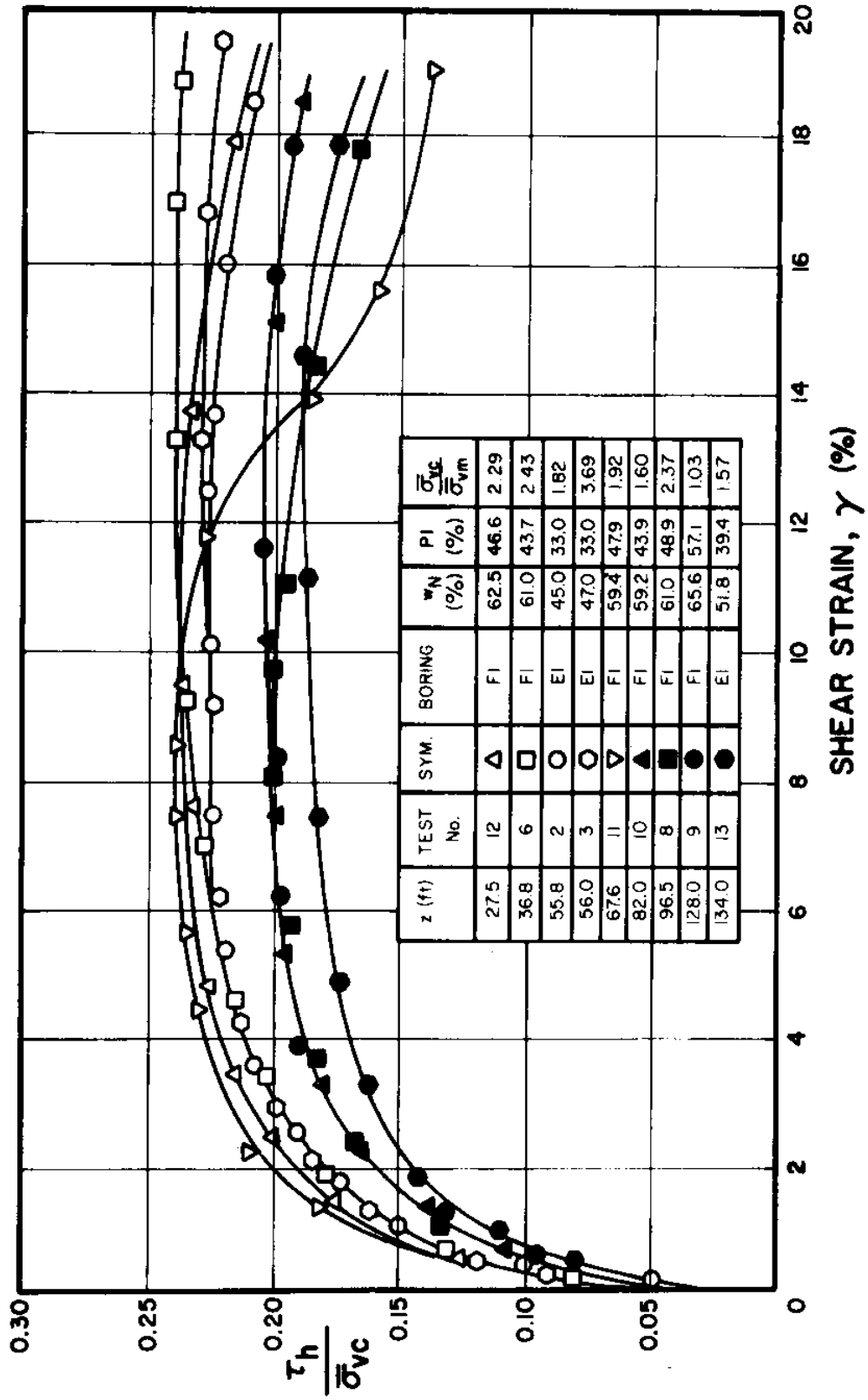

Figure 4.12 Normalized stress vs. strain from direct simple shear tests: N.C. Orinoco clay (from Ladd et. al., 1980)

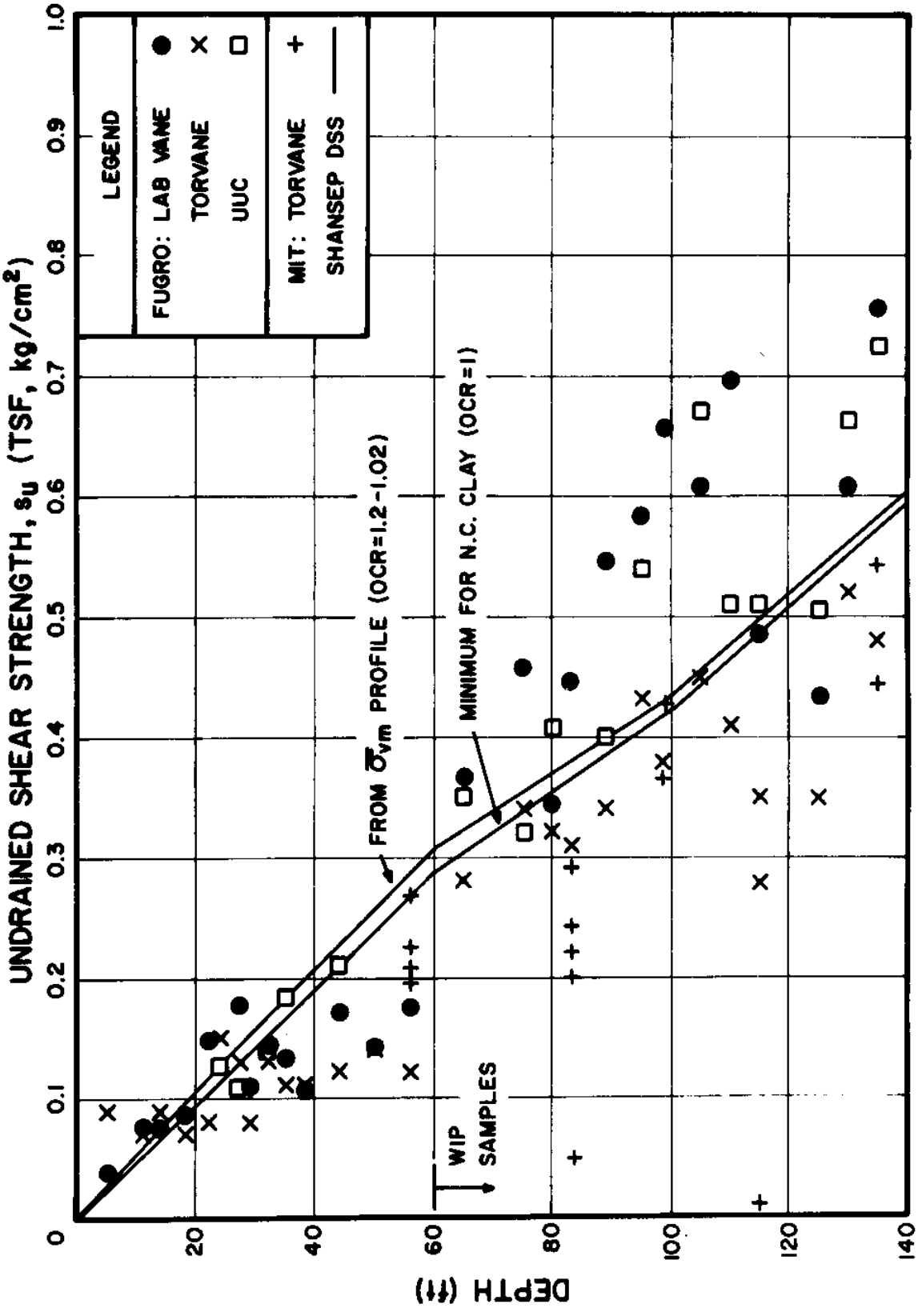

Figure 4.13 Undrained shear strength data at site E1 (from Ladd et. al., 1980)

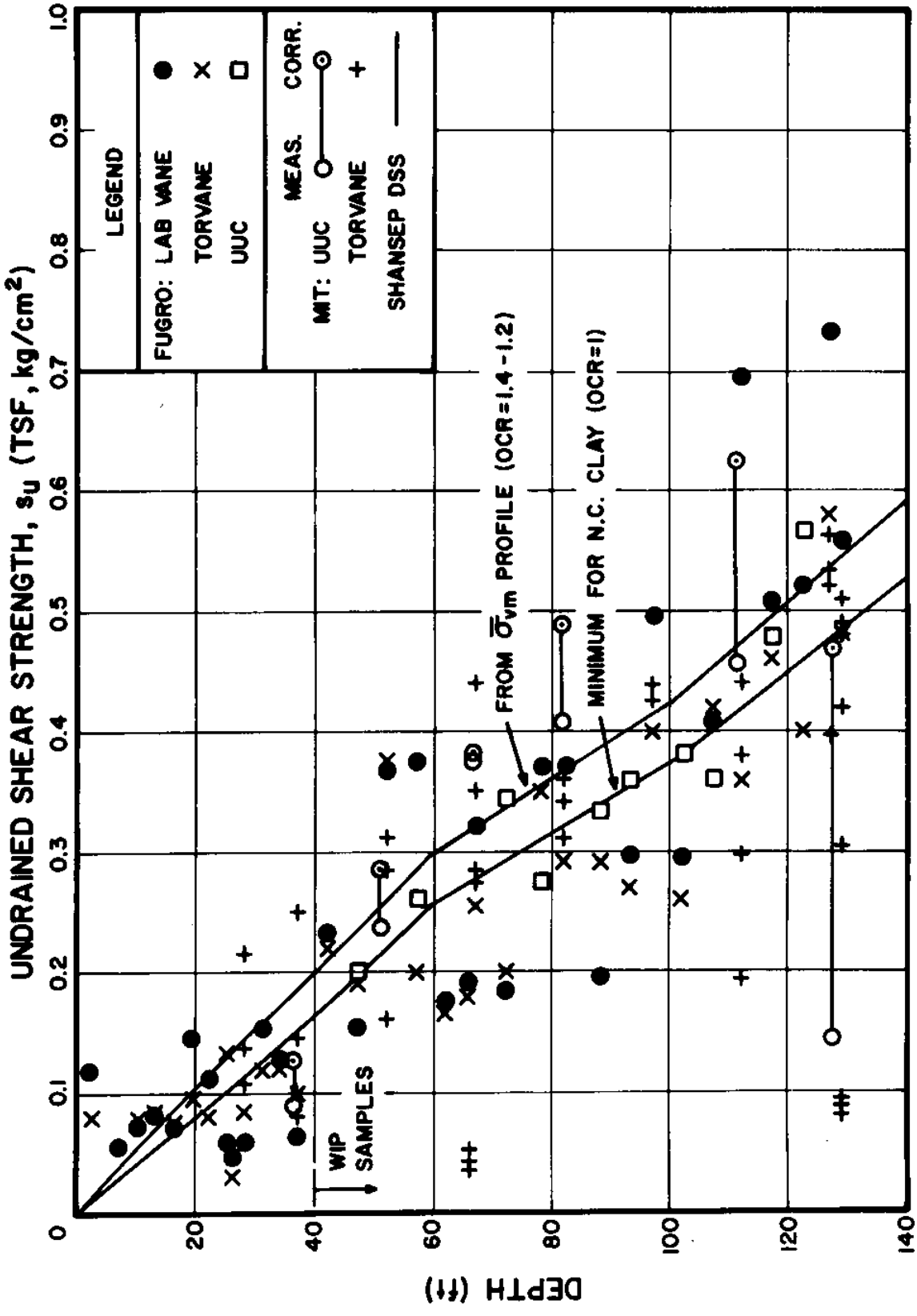

Figure 4.14 Undrained shear strength data at site F1 (from Ladd et. al., 1980)

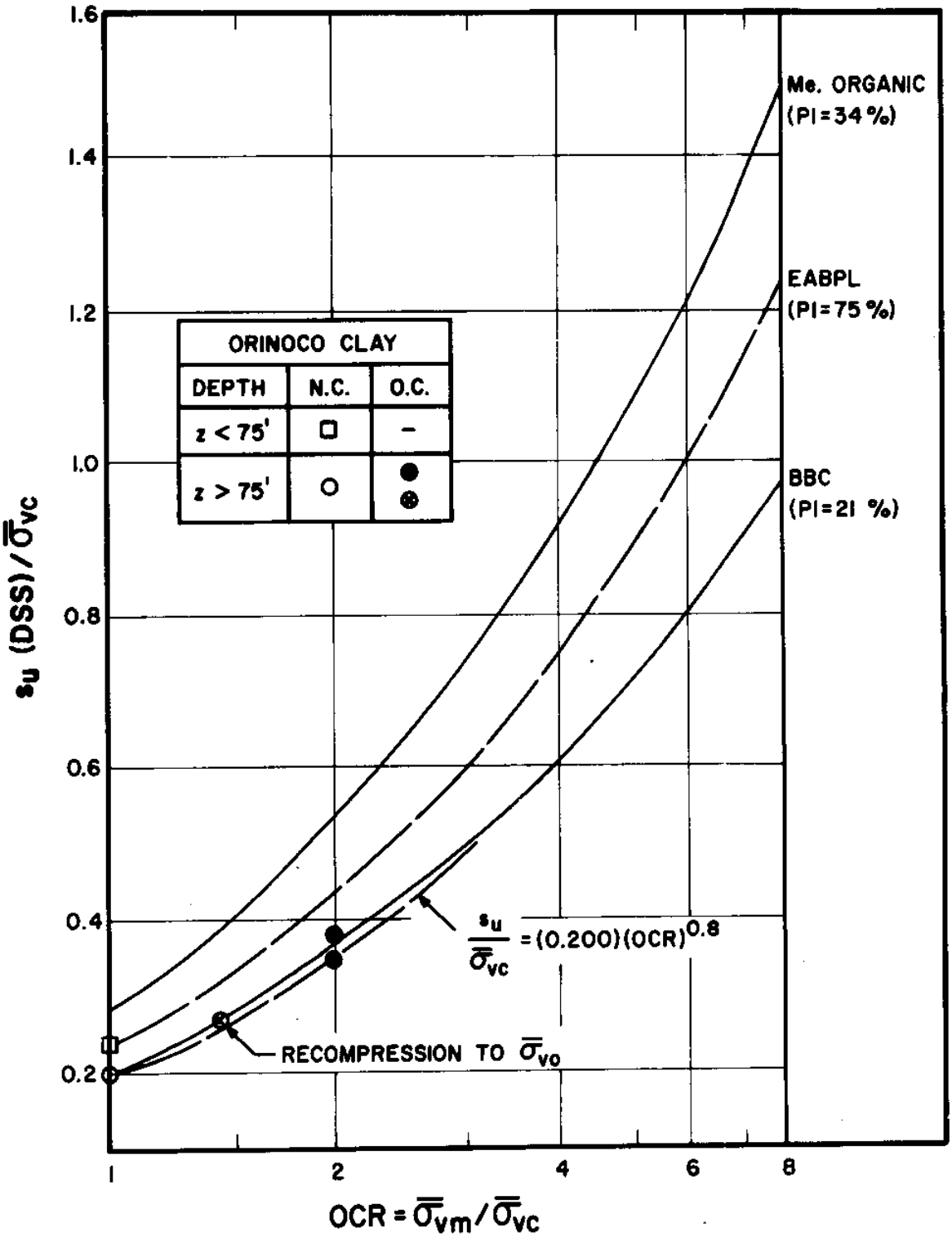

Figure 4.15 Effect of OCR on s_u (DSS/$\bar{\sigma}_{vc}$): Orinoco clay (from Ladd et. al., 1980)

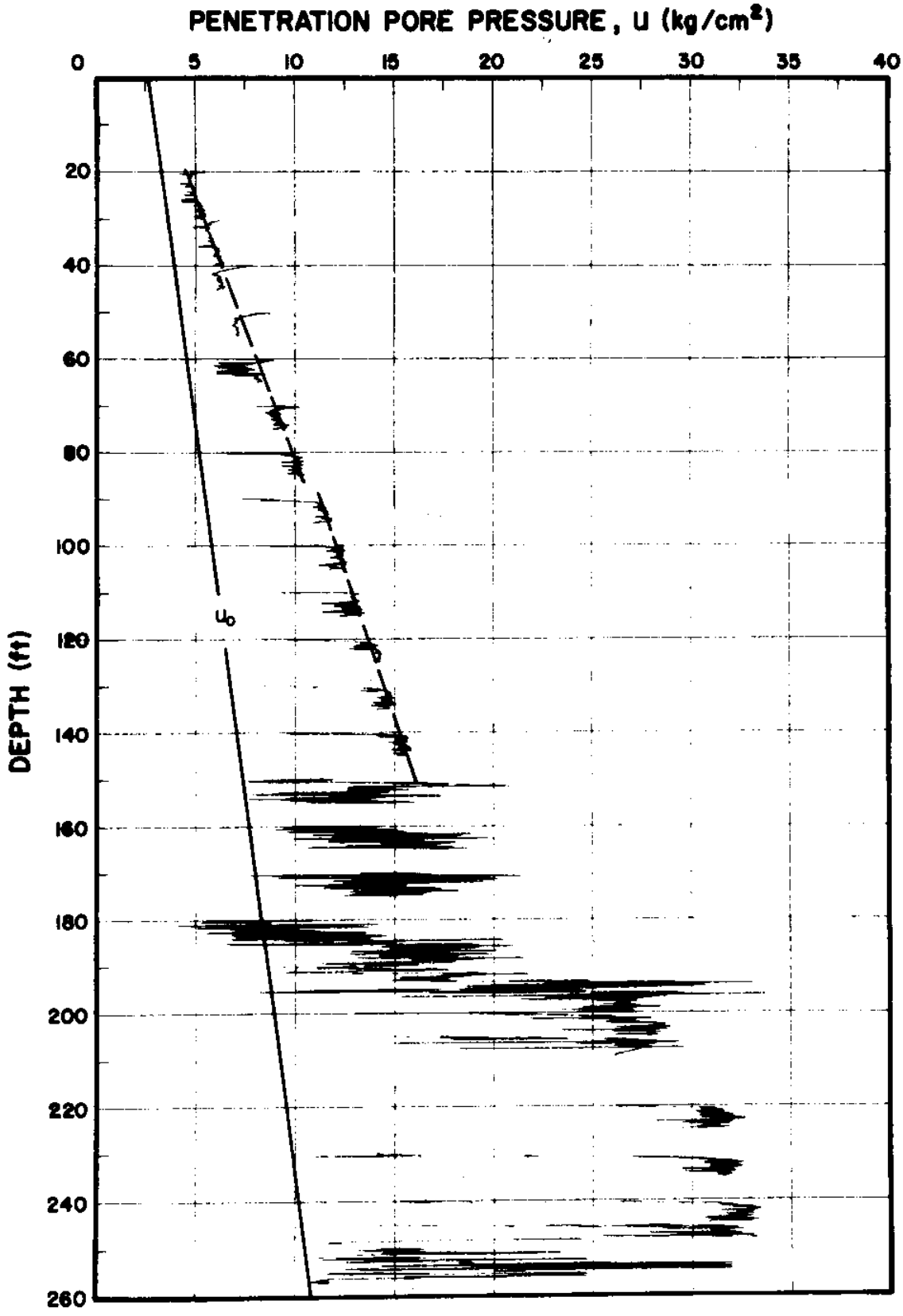

Figure 4.16 Penetration pore pressure data at site E1.

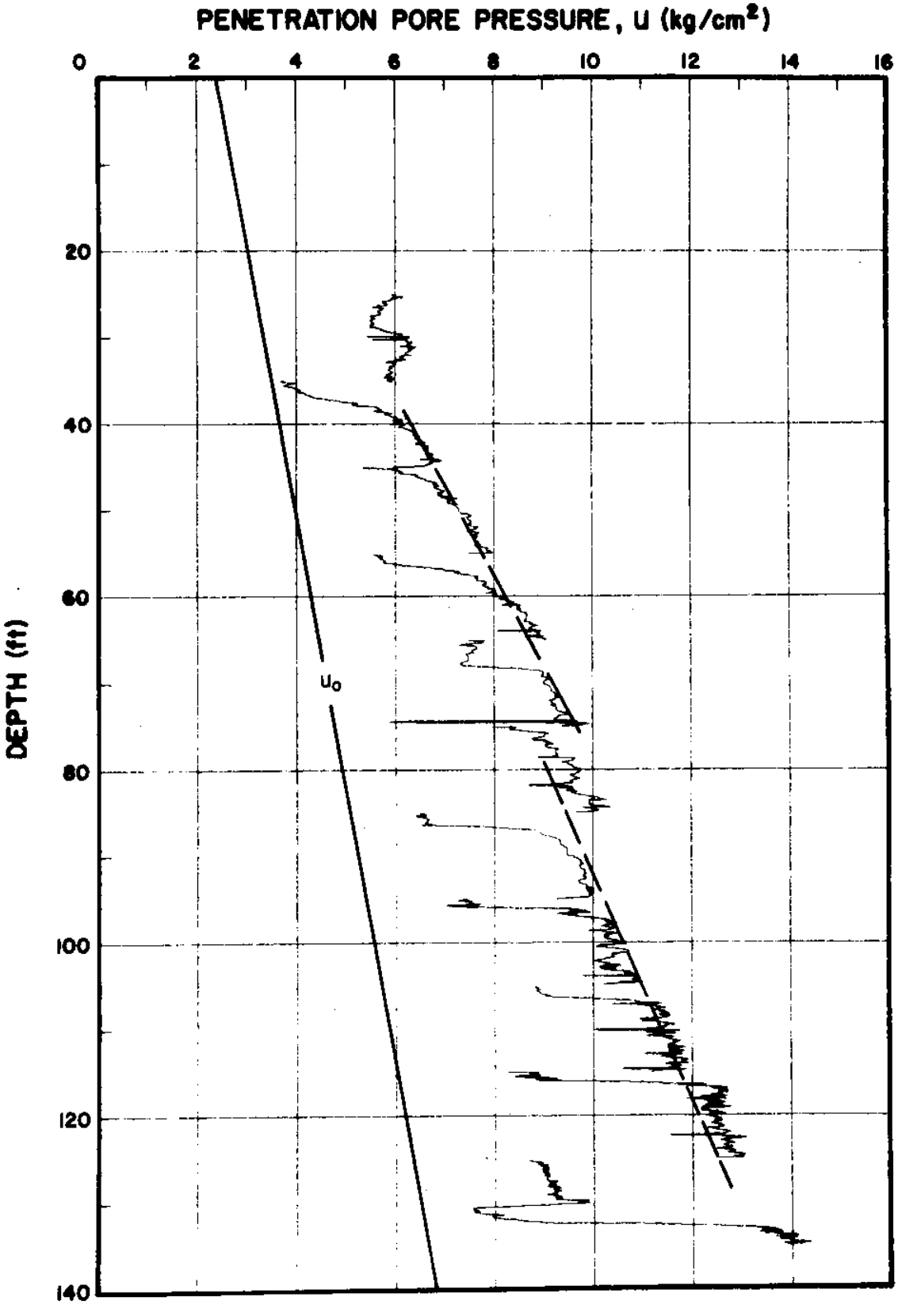

Figure 4.17 Penetration pore pressure data at site F1.

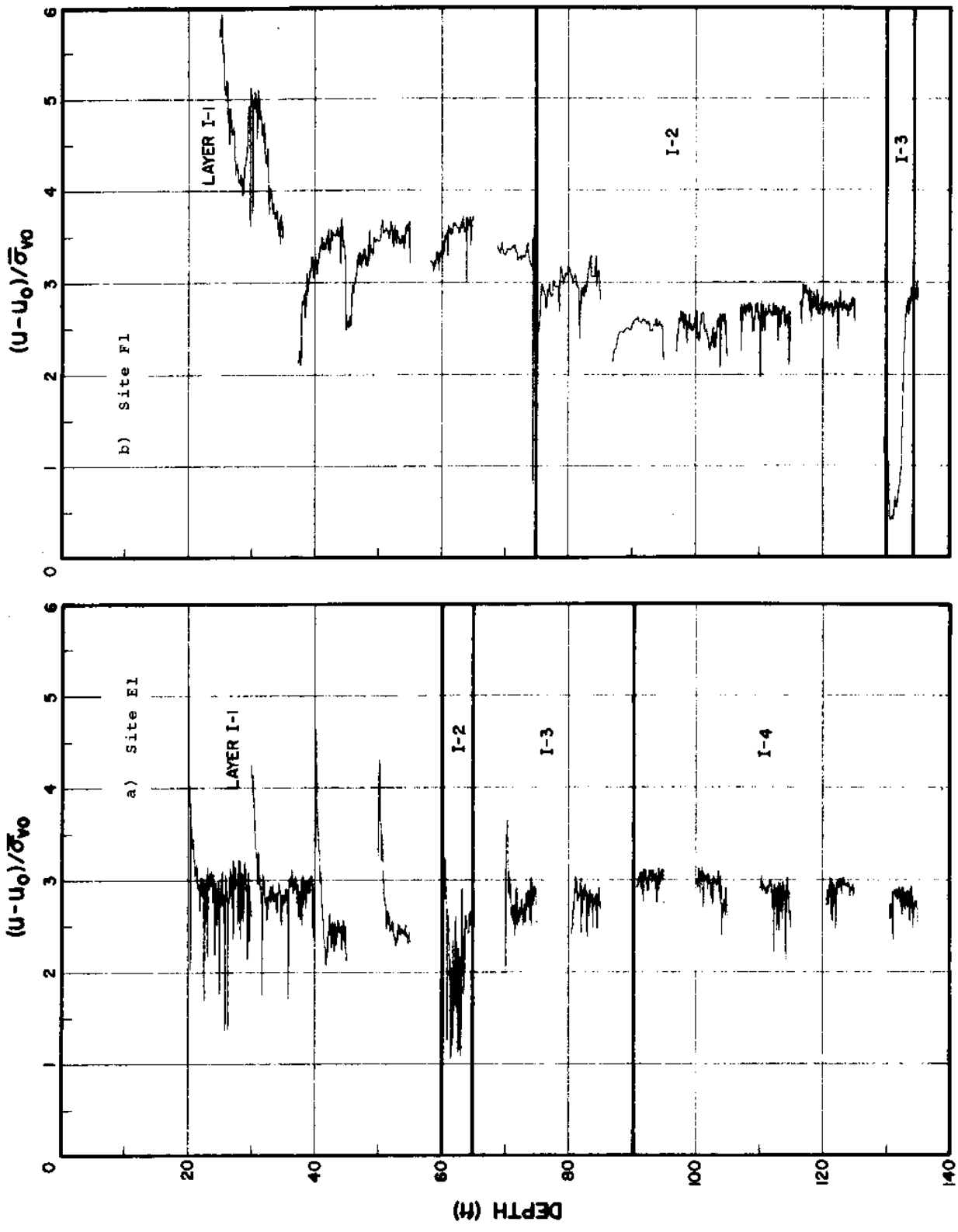

Figure 4.18 $(u-u_o)/\bar{\sigma}_{vo}$ data: Orinoco Clay.

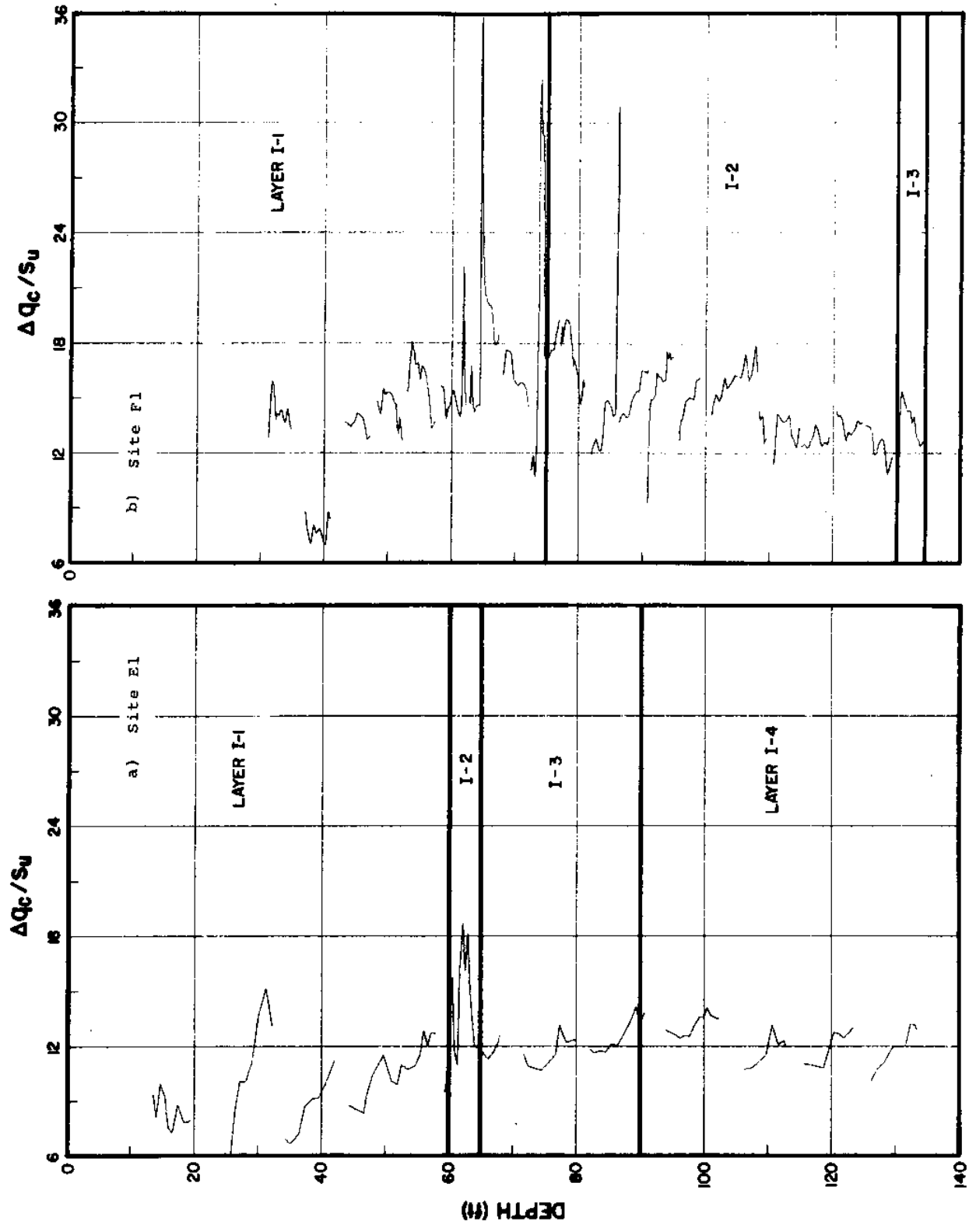

Figure 4.19 $\Delta q_c/s_u$ data: Orinoco Clay

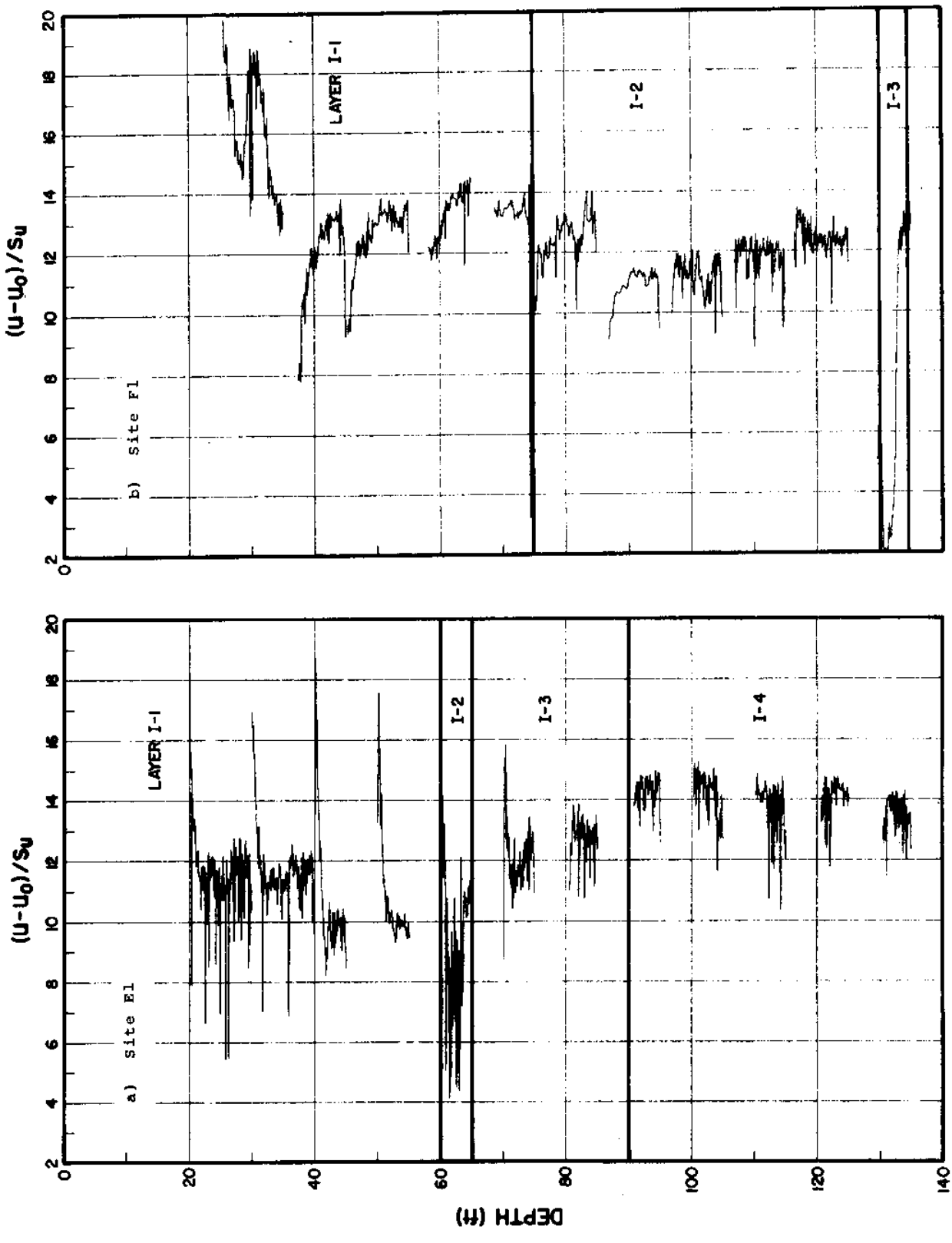

Figure 4.20 $(u - u_o)/s_u$ data: Orinoco Clay

CHAPTER 5

CONCLUSIONS

In situ soil testing is gaining importance in site investigation and in the determination of the necessary soil properties for foundation engineering design. This results from: (a) a growing concern over the escalating cost and the reliability of traditional exploration techniques based on boring, sampling and laboratory testing; (b) the increasingly difficult and unfamiliar environments in which engineering structures are founded; and (c) the necessity to assess soil conditions, in situ properties, and their variability in more detail to complement the development in analytical capability of the geotechnical profession.

The electric cone penetrometer and the pore pressure probe represent a new generation of in situ testing devices combining wide applicability with simplicity, consistency and economy. Both have no mechanically moving parts and are readily amenable to remote control and automated data recording and processing, and are thus ideal instruments for difficult locations with no easy access, e.g., in deep water. They provide continuous measurements, allowing better identification of soil stratigraphy and variability than discrete field measurements, e.g., the field vane test, or laboratory tests on selected samples.

This report presents cone penetration measurements in marine sediments offshore the Venezuelan coast which marks

the first time pore pressure measurements were performed offshore. The results of this study show that measurements of cone resistance, q_c, by means of electrical cones are very valuable to: (a) detect the presence of thin soft layers and more previous layers which might strongly affect stability and drainage, respectively; (b) distinguish between different strata even in the difficult case of consecutive layers of slightly different clays having different OCR and/or frequencies of sand lenses; (c) provide a good description of soil variability (scatter) affecting design reliability; and (d) provide useful information regarding the point bearing capacity of piles, and hence pile penetration and driveability.

Conical piezometer probes used in this study have very rapid response time (essentially instantaneous) and thus can be used for identification and stratification of soil deposits by means of the pore pressures developed during steady cone penetration and their subsequent decay after penetration stops. Measurements of penetration pore pressure, are as repeatable, and provide the same advantages (mentioned above) as q_c in soil stratification. Furthermore, the pore pressure decay data can be used along with the methodology recently developed at MIT (Baligh and Levadoux, 1980) to estimate the consolidation and permeability characteristics of soils. Hence, the pore pressure probe is a very promising soil exploration tool and, whenever possible, should be used, along with the electric cone penetrometer, in future soil investigation programs.

REFERENCES

Note: ASCE = American Society of Civil Engineers
BOSS = Behavior of Off-Shore Structures
ICSMFE = International Conference on Soil Mechanics and Foundation Engineering
MIT = Massachusetts Institute of Technology

Al-Awkati, Z. (1975), "On Problems of Soil Bearing Capacity at Depth," Ph.D. Dissertation to the Dept. of Civil Engineering, Duke University, 204 p.

Azzouz, A.S. and Baligh, M.M. (1978), "Three-Dimensional Stability of Slopes," Research Report R78-8, Order No. 595, Department of Civil Engineering, MIT, Cambridge, Mass., 249 p.

Baguelin, F., Jezequel, J.F., Le Mee, H. and Le Mehaute, A. (1972), "Expansion of Cylindrical Probes in Cohesive Soils," Journal of the Soil Mechanics and Foundation Division, ASCE, Vol. 98, No. SM11, pp. 1129-1142.

Baligh, M.M. (1972), "Application of Plasticity Theory to Selected Problems in Soil Mechanics," Soil Mechanics Lab. Report, California Institute of Technology, 228 p.

Baligh, M.M. (1975), "Theory of Deep Site Static Cone Penetration Resistance," Research Report R75-56, Order No. 517, Department of Civil Engineering, MIT, Cambridge, Mass., 133 p.

Baligh, M.M. and Levadoux, J.N. (1980), "Pore Pressure Dissipation after Cone Penetration," Research Report R80-11, Order No. 662, Department of Civil Engineering, MIT, Cambridge, Mass., 368 p.

Baligh, M.M. and Scott, R.F. (1976), "Wedge Penetration in Clays," Geotechnique, Vol. 26, No. 1, pp. 185-208.

Baligh, M.M., Vivatrat, V., and Ladd, C.C. (1978), "Exploration and Evaluation of Engineering Properties for Foundation Design of Offshore Structures," Research Report R78-40, Order No. 607, Department of Civil Engineering, MIT, Cambridge, Mass.

Baligh, M.M., Vivatrat, V., and Ladd, C.C. (1980), "Cone Penetration in Soil Profiling," Journal of the Geotechnical Engineering Division, ASCE, Vol. 106, No. GT4, pp. 447-461.

Bishop, R.F., Hill, R. and Mott, N.F. (1945), "Theory of Indentation and Hardness Tests," Proceedings, Physical Society of London, Vol. 57, Part 3, No. 321, pp. 147-159.

Bjerrum, L. (1972), "Embankments on Soft Ground," State-of-the Art Report, Proceedings, ASCE Specialty Conference on Performance of Earth and Earth-Supported Structures, Lafayette, Vol. 2, pp. 1-54.

Bjerrum, L. (1973), "Problems of Soil Mechanics and Construction on Soft Clays," State-of-the-Art Report, Session 4, Proceedings, 8th ICSMFE, Moscow, Vol. 3, pp. 109-159.

Brinch-Hansen, J. (1961), "A General Formula for Bearing Capacity," Bulletin No. 11, Danish Geotehcnical Institute, Copenhagen, pp. 8-13.

Brinch-Hansen, J. (1970), "A Revised and Extended Formula for Bearing Capacity," Bulletin No. 28, Danish Geotechnical Institute, Copenhagen, Denmark, pp. 5-11.

Buisman, A.S.K. (1935), "De Weerstand van Paalpunten in Zand," De Ingenieur 50, pp. Bt. 25-28, 31-35.

Caquot, A. (1934), "Equilibre des Massifs a Frottement Interne," Paris, (Gauthier-Villars).

Chadwick, P., Cox, A.D. and Hopkins, H.G. (1963), "Mechanics of Deep Underground Explosions," Philosophical Trans., Royal Society of London, Series A, Vol. 256, pp. 235-300.

Davis, E.H. and Christian, J.T. (1971), "Bearing Capacity of Anisotropic Cohesive Soil," Journal of the Soil Mechanics and Foundations Division, ASCE, Vol. 97, No. SM5, pp. 753-769.

de Ruiter, J. (1971), "Electric Penetrometer for Site Investigation," Journal of the Soil Mechanics and Foundations Division, ASCE, Vol. 97, No. SM2, pp. 457-472.

de Ruiter, J. (1976), "North Sea Site Investigations - The Role of the Geotechnical Consultant," Offshore Soil Mechanics, Ed. by Philip George and David Wood, Cambridge University Engineering Department, pp. 62-78.

Dn V (1976), "Foundation Investigation for Offshore Structures," Det Norske Veritas, Fixed Offshore Structures, Technical Note.

Doyle, E.N., McClelland, B. and Ferguson, G.H. (1971), "Wire-Line Vane Probe for Deep Penetration Measurements of Ocean Sediment Strength," Proceedings, 3rd Offshore Technology Conference, Houston, Vol. 1, pp. 21-32.

ESOPT (1974), "Proceedings of the European Symposium on Penetration Testing," Swedish Geotechnical Society, Stockholm, 2 Vol.

Fugro Gulf, Inc. (1979a), "Description of Field Techniques M/V SURVEYOR, Offshore Venezuela," Report to INTEVEP in Venezuela, April, 23 p.

Fugro Gulf, Inc. (1979b),"Geotechnical Investigation Golfo de Paria, Offshore Venezuela," Report to INTEVEP in Venezuela, Report No. 79-005-5, December, 82 p.

Gibson, R.E. (1950), Discussion of G. Wilson, "The Bearing Capacity of Screw Piles and Screwcrete Cylinders," Journal of the Institution of Civil Engineers, Vol. 34, No. 4, pp. 382.

Hedberg, J., Urzua, A., and Marr, A. (1978), "Exploration Methods for Offshore Foundations," Research Report R78-42, Order No. 610, Department of Civil Engineering, MIT, Cambridge, Mass., 278 p.

Høeg, K. (1976), "Foundation Engineering for Fixed Offshore Structures," Proceedings, BOSS '76, Vol. 1, Trondheim, pp. 39-69.

Kraft, L.M. Jr., Ahmad, N. and Focht, J.A. Jr. (1976), "Application of Remote Vane Results to Offshore Geotechnical Problems," Proceedings, 8th Offshore Technology Conference, Houston, p. 75-96.

Ladanyi, B. (1967), "Deep Punching of Sensitive Clays," Proceedings, 3rd Panamerican Conference on Soil Mechanics and Foundation Engineering, Caracas, Vol. 1, pp. 533-546.

Ladanyi, B. (1972), "In Situ Determination of Undrained Stress-Strain Behavior of Sensitive Clays with the Pressurementer," Canadian Geotechnical Journal, Vol. 9, No. 3, pp. 313-319.

Ladd, C.C. (1975), "Foundation Design of Embankments Constructed on Connecticut Valley Varved Clays," Research Report R75-7, Order No. 343, Department of Civil Engineering, MIT, Cambridge, Mass., 439 p.

Ladd, C.C., and Edgers, L. (1972), "Consolidated-Undrained Direct Simple Shear Test on Saturated Clays," Research Report R72-82, Order No. 284, Department of Civil Engineering, MIT, Cambridge, Mass.

Ladd, C.C. and Foott, R. (1974), "New Design Procedure for Stability of Soft Clays," Journal of the Geotechnical Engineering Division, ASCE, Vol. 100, No. GT7, pp. 763-786.

Ladd, C.C. et al. (1971), "Consolidated-Undrained Plane-Strain Shear tests on Boston Blue Clay," Research Report R71-13, Order No. 272, Department of Civil Engineering, MIT, Cambridge, Mass.

Ladd, C.C. et al. (1977), "Stress-Deformation and Strength Characteristics," State-of-the-Art Report for Session I, Proceedings, 9th ICSMFE, Tokyo, Vol. 2, pp. 421-494.

Ladd, C.C. et al. (1979), "Evaluation of Self-Boring Pressure-meter Tests in Boston Blue Clay," Research Report R79-4, Order No. 640, Department of Civil Engineering, MIT, Cambridge, Mass.

Ladd, C.C. et al. (1980), "Evaluation of Compositional and Engineering Properties of Offshore Venezuelan Soils - Volume 1: Orinoco Clay (Gulf of Paria and Orinoco Delta), "Research Report R80-14, Order No. 665, Department of Civil Engineering, MIT, Cambridge, Mass., 286 p.

Lambe, T.W. (1967), "Stress Path Method," Journal of the Soil Mechanics and Foundation Division, ASCE, Vol. 93, No. SM6, pp. 309-331.

Levadoux, J.N., and Baligh, M.M. (1980), "Pore Pressures During Cone Penetration in Clays," Research Report R80-15, Order No. 666, Department of Civil Engineering, MIT, Cambridge, Mass., 310 p.

Lunne, T., Eide, O. and de Ruiter, J. (1976), "Correlations between Cone Resistance and Vane Shear Strength in Some Scandinavian Soft to Medium Stiff Clays," Canadian Geotechnical Journal, Vol. 13, pp. 430-441.

Marsland, A., and Powell, J.J.M. (1979), "Evaluating the Large Scale Properties of Glacial Clays for Foundation Design," Proceedings, BOSS '79, Vol. 1, pp. 193-214.

Meyerhof, G.G. (1951), "The Ultimate Bearing Capacity of Foundations," Geotechnique, Vol. II, No. 4, pp. 301-332.

Meyerhof, G.G. (1961), "The Ultimate Bearing Capacity of Wedge-Shaped Foundations," Proceedings, 5th ICSMFE, Paris, Vol. 2, pp. 103-109.

Meyerhof, G.G. (1976), "Bearing Capacity and Settlement of Pile Foundations," Journal of Geotechnical Engineering Division, ASCE, Vol. 102, No. GT3, pp. 195-228.

Mitchell, J.K. and Durgunoglu, H.T. (1973), "In Situ Strength by Static Cone Penetration Test," Proceedings, 8th ICSMFE, Moscow, Vol. 1, pp. 279-286.

Mitchell, J.K. and Gardner, W.S. (1975), "In Situ Measurement of Volume Change Characteristics," State-of-the-Art Paper, Proceedings, ASCE Speciality Conf. on In Situ Measurement of Soil Properties, Raleigh, Vol. II, pp. 279-345.

Norwegian Geotechnical Institute (1973), "Condeep Drilling Production Platform - Recommended Soil Investigation Program," Internal Report.

Norwegian Geotechnical Institute (1975), "A Comparision between Cone Resistance and Vane Shear Strength in Some Scandinavian Clays, Part A: Soft Clays, Part B: Overconsolidated Clays," Internal Reports 52155-2 and -3.

Palmer, A.C. (1972), "Undrained Plane Strain Expansion of a Cylindrical Cavity in Clay: A Simple Interpretation of the Pressuremeter Test," Geotechnique, Vol. 22, No. 3, pp. 451-457.

Prandtl, L. (1920), "Uber die Harte Plastischer Korper" (concerning the Hardness of Plastic Bodies), Nachr. Kgl, Ges. Wiss, Göttingen, Math. phys. Klasse.

Prevost, J.H. and Høeg, K. (1975a), "Soil Mechanics and Plasticity Analysis of Strain-Softening," Geotechnique, Vol. 25, No. 2, pp. 279-297.

Prevost, J.H. and Høeg, K. (1975b), "Analysis of Pressuremeter in Strain-Softening Soil," Journal of the Goetechnical Engineering Division, ASCE, Vol. 101, No. GT8, pp. 717-732.

Reissner, H. (1924), "Zum Erddruckproblem," Proceedings, First International Congress of Applied Mechanics, Delft, pp. 295-311.

Robinsky, E.I. and Morrison, C.F. (1964), "Sand Displacement and Compaction Around Model Friction Piles," Canadian Geotechnical Journal, Vol. 1, pp. 81-93.

Rourk, T.L. (1961), "Model Studies of a Pile Failure Surface in a Cohesive Soil," M.S. Thesis, Civil Engineering Dept., Georgia Institute of Technology, Atlanta, 56 p.

Sanglerat, G. (1972), The Penetrometer and Soil Exploration, Elsevier Publishing Co., Amsterdam.

Sangrey, D.A. (1977), "Marine Geotechnology, State-of-the-Art, Marine Geotechnology, Vol. 2, Crane, Russak and Co., Inc., New York.

Schmertmann, J.H. (1975), "Measurement of In Situ Shear Strength," State-of-the-Art Report, Proceedings, ASCE Specialty Conference on In Situ Measurement of Soil Properties, Raleigh, N.C., Vol. II, pp. 57-138.

Schmertmann, J.H. (1978a), "Study of Feasibility of Using Wissa-Type Piezometer Probe to Identify Liquefaction Potential of Saturated Find Sands," Technical Report S-78-2, Waterways Experiment Station, U.S. Army Corps of Engineers, Vicksburg, Miss., 73 p.

Schmertmann, J.H. (1978b), "Guidelines for Cone Penetration Test Performance and Design," U.S. Department of Transportation, Federal Highway Administration, Report No. FHWA-TS-78-209, Washington, D.C., 145 p.

Semple, R.M., and Johnston, J.W. (1979), "Performance of 'Stingray' in Soil Sampling and In Situ Testing," Preprint of a paper submitted to a Conference on Offshore Site Investigation, London, England.

Skempton, A.W. (1951), "The Bearing Capacity of Clays," Building Reserach Congress, London, The Institute of Civil Engineering, Division I, London, pp. 180-189.

Sullivan, R. (1978), "Platform Site Investigation," Civil Engineering and Public Works Review, London, pp. 26-34.

Szechy, K. (1968), "Deformations Around and Below Driven and Vibrated Test Tubes," Acta Technica Acad. Sci., Hungary, Vol. 62, pp. 97-113.

Terzaghi, K. (1943), Theoretical Soil Mechanics, John Wiley and Sons, New York, 1943.

Torstensson, B.A. (1975), "Pore Pressure Sounding Instrument," Discussion, Session I, Proceedings, ASCE Specialty Conference on In Situ Measurement of Soil Properties, Raleigh, North Carolina, Vol. II, pp. 48-54.

Vesic, A.S. (1963), "Bearing Capacity of Deep Foundations in Sands," Stresses in Soils and Layered Systems, Highway Research Board Record No. 39, pp. 112-153.

Vesic, A.S. (1967), "Ultimate Loads and Settlements of Deep Foundations in Sand," Proceedings, Symposium on Bearing Capacity and Settlement of Foundations, Duke University, Durham, N.C., 53 p.

Vesic, A.S. (1975), "Principles of Pile Design," Lecture Series on Deep Foundations Sponsored by the Geotechnical Group, BSCES/ASCE.

Vesic, A.S. (1977), "Design of Pile Foundation," Systhesis of Highway Practice 42, Transportation Research Board, National Research Council, Washington, D.C. 68 p.

Vivatrat, V. (1978), "Cone Penetration in Clays," thesis presented to Massachusetts Institute of Technology, at Cambridge, Mass., in partial fulfillment of the requirements for the degree of Doctor of Science.

Wissa, A.E.Z., Martin, R.T. and Garlanger, J.E. (1975), "The Piezometer Probe," Proceedings, ASCE Specialty Conference on In Situ Measurement of Soil Properties, Raleigh, N.C., Vol. I, pp. 536-545.

Zuidberg, H.M. (1974), "Use of Static Cone Penetrometer Testing in the North sea," Proceedings, European Symposium on Penetration Testing, Stockholm, Vol. 2.2, pp. 433-436.

APPENDIX A

CONE PENETRATION DATA

Figures A-1 through A-3 present the incremental cone resistance data, Δq_c, at sites E1, F1 and D2, respectively, and Figs. A-4 through A-6 illustrate the penetration pore pressure data at the same sites.

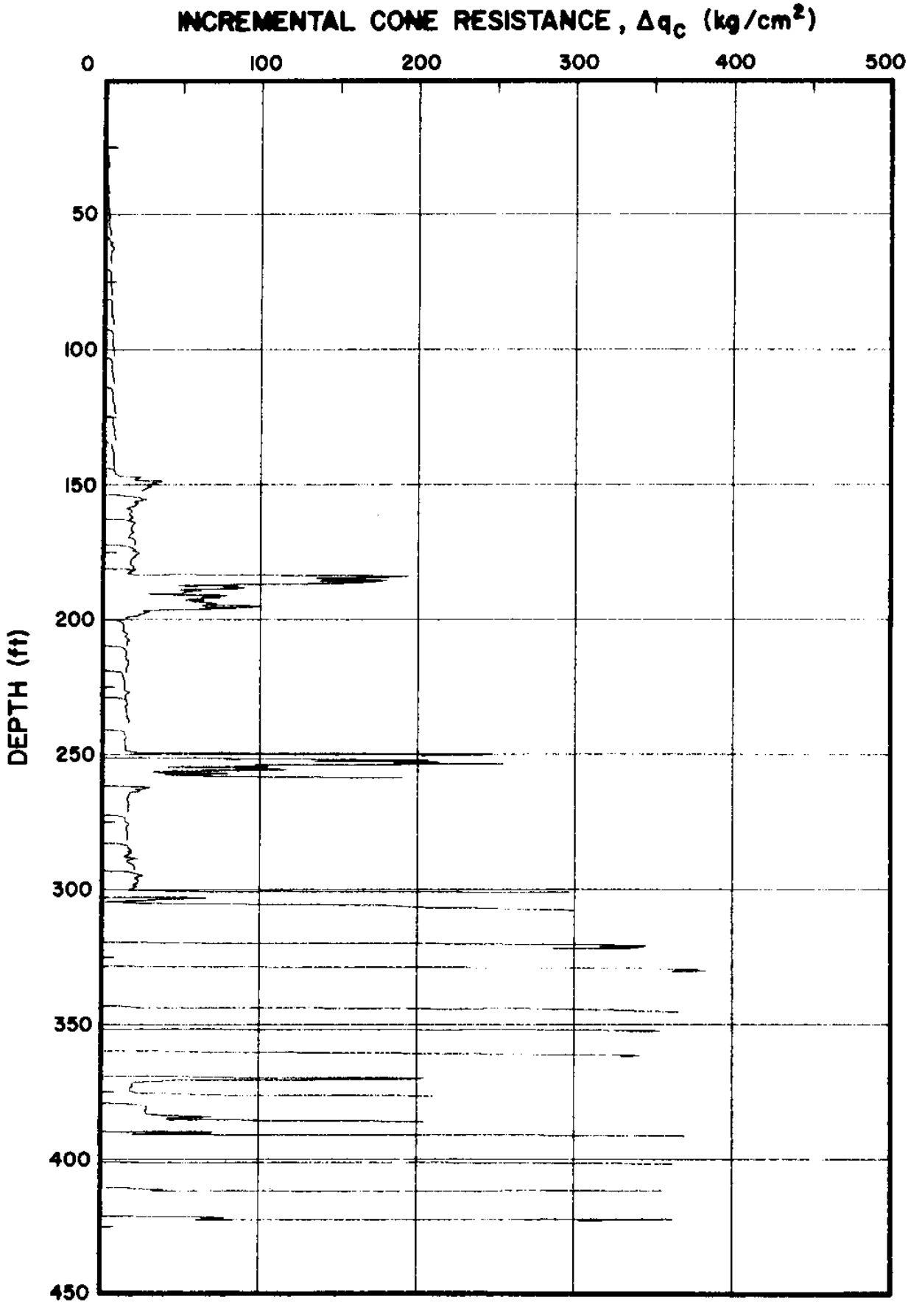

Figure A-1 Δq_c data for Site E1

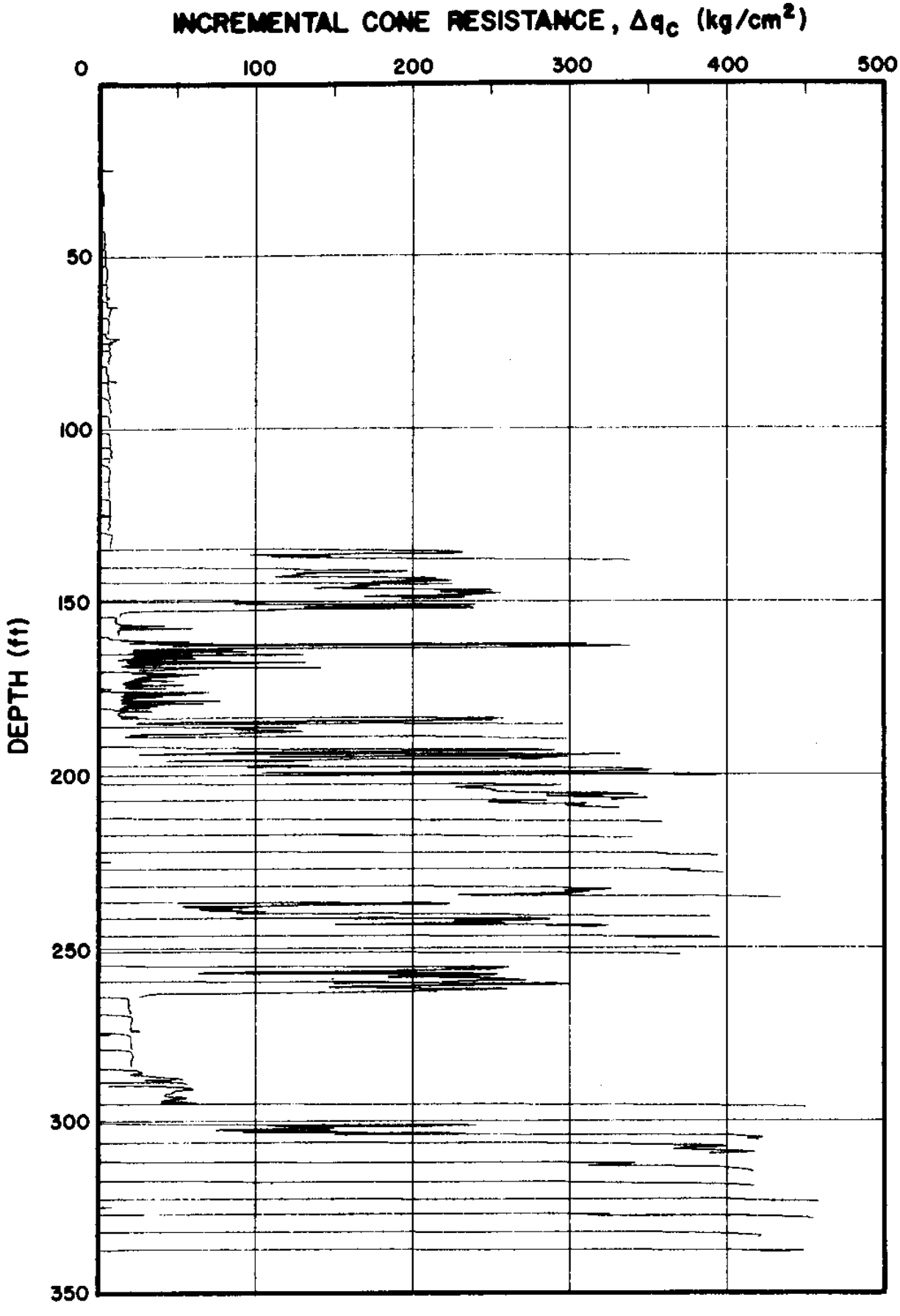

Figure A-2 Δq_c data for Site F1

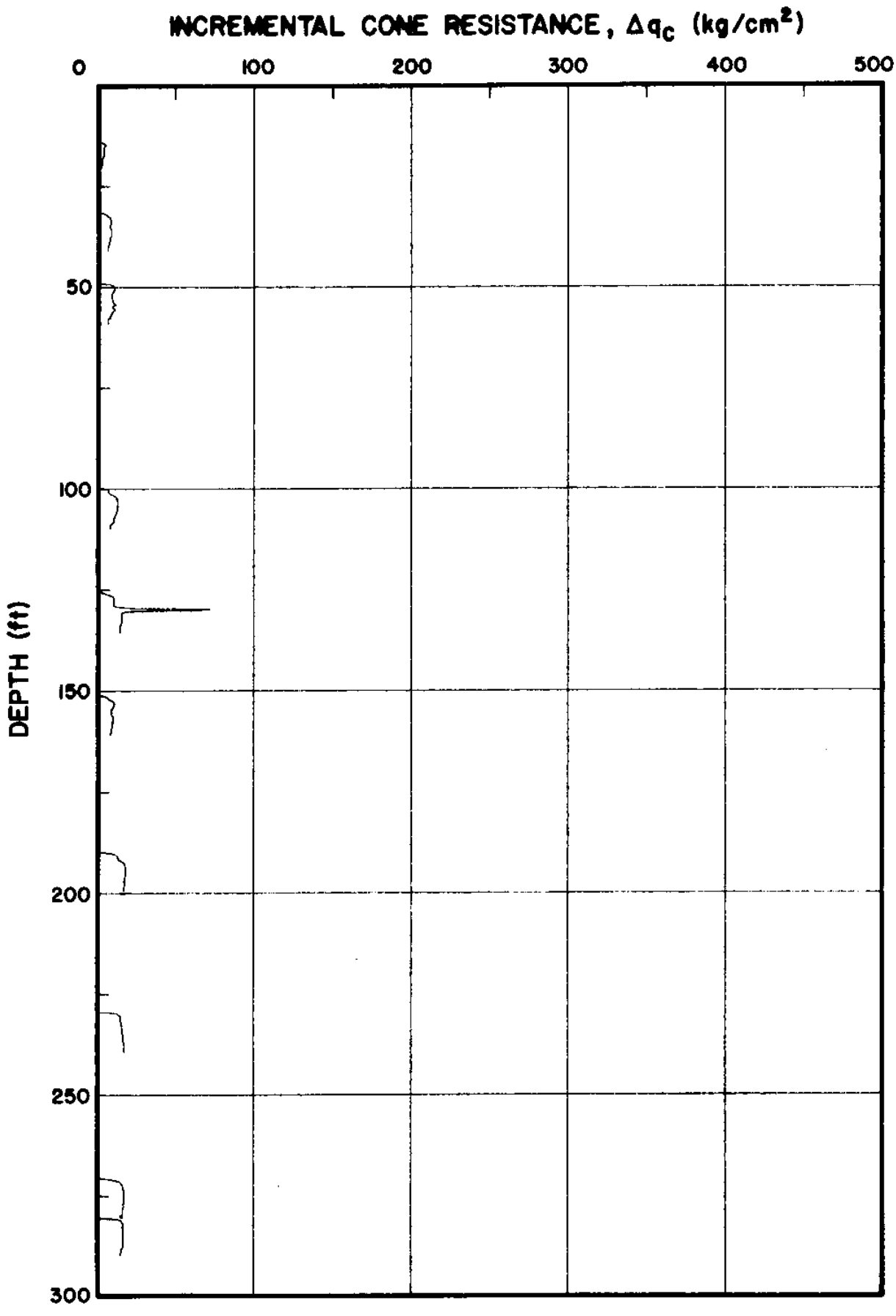

Figure A-3 Δq_c data for Site D1

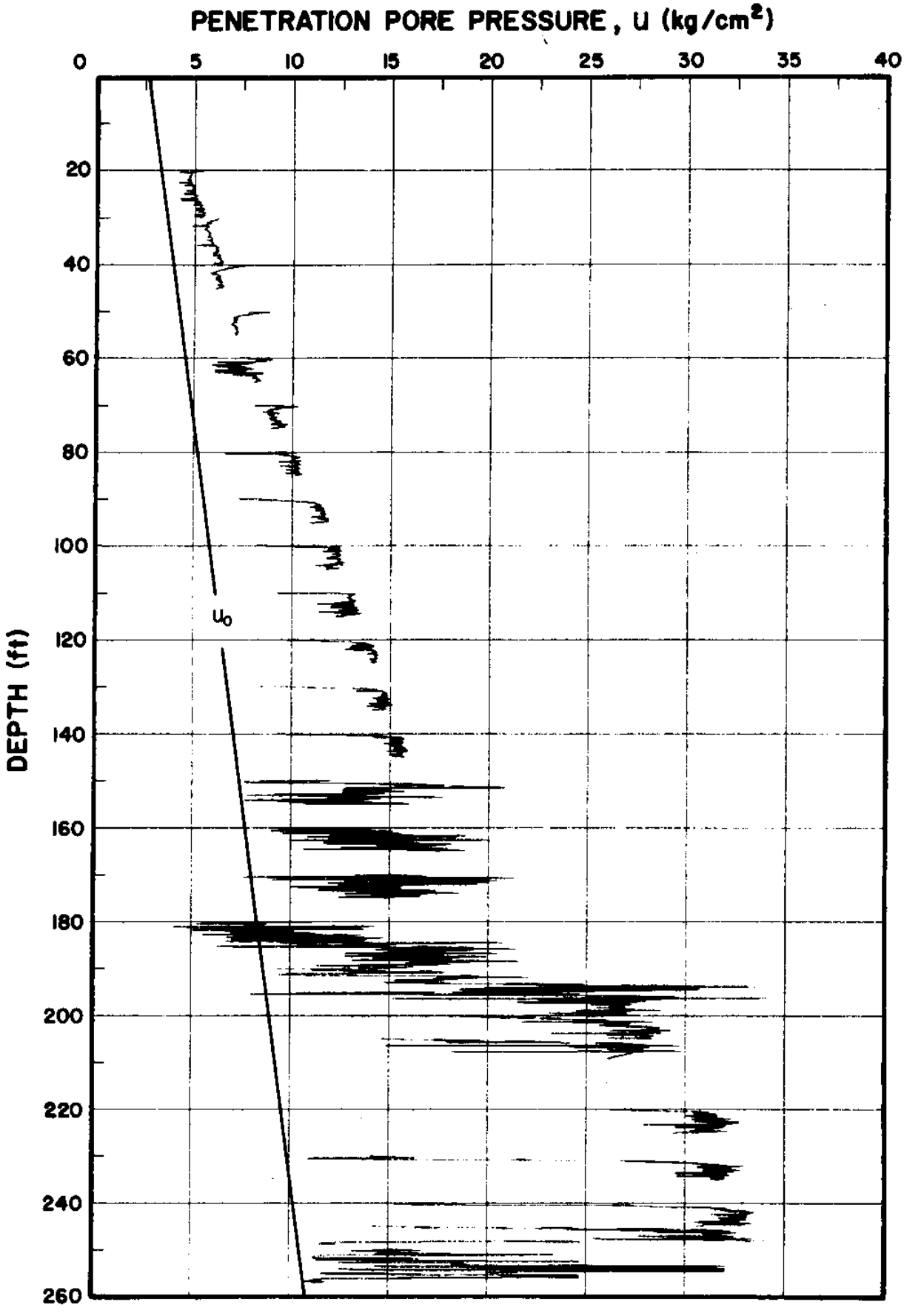

Figure A-4 u data for Site E1

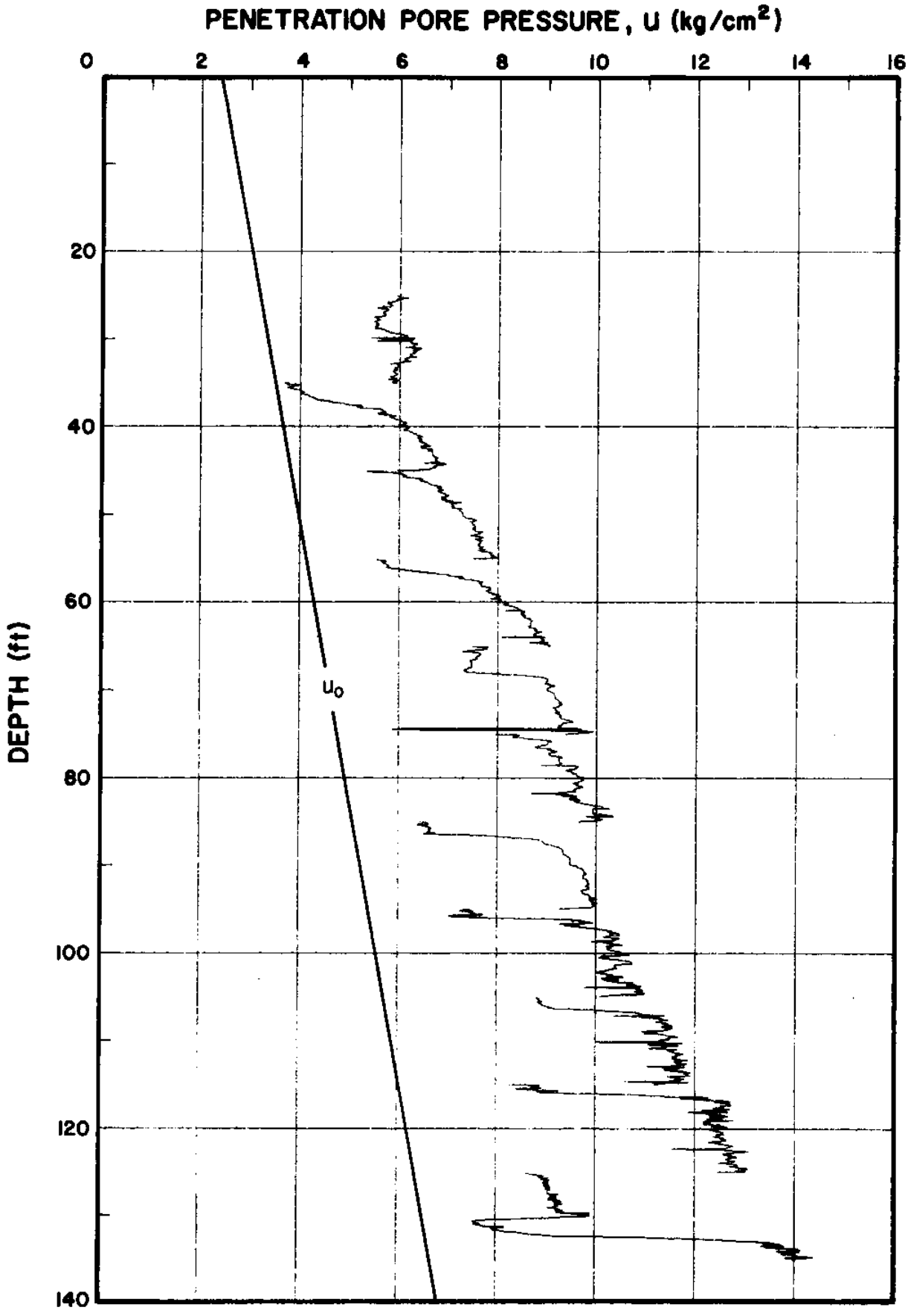

Figure A-5 u data for Site F1

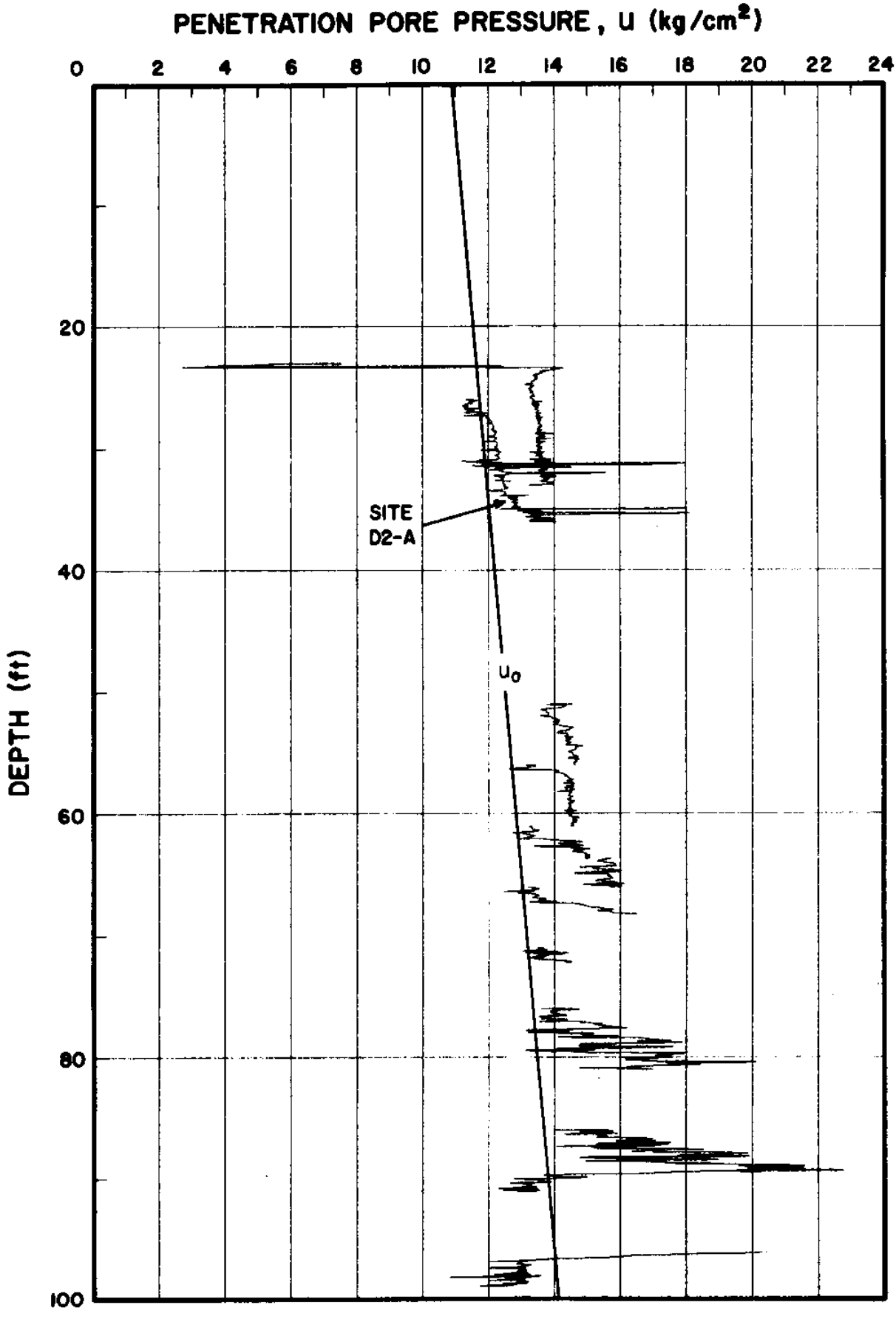

Figure A-6 u data for Site D1